5-10-2013

Functional carbon nanotubes for electrical conductors

Christopher Schauerman

FUNCTIONAL CARBON NANOTUBES FOR ELECTRICAL CONDUCTORS

by

Christopher Mark Schauerman

DISSERTATION

For the degree of Doctor of Philosophy in Sustainability

at the

Rochester Institute of Technology

Department of Sustainability

In the Golisano Institute for Sustainability

May 10th 2013

Dissertation Advisor

Dr. Brian Landi

Dissertation Committee Members

Dr. Callie Babbitt

Dr. Gabrielle Gaustad

Dr. Ryne Raffaelle

I would like to dedicate this dissertation to everyone that has contributed directly and indirectly to my personal and professional development. Especially my friends over the years in NanoPower Research Labs including Dr. Matt Ganter, Dr. Roberta DiLeo, Dr. Cory Cress, Dr. Annick Anctil, Andrew Bucossi, Jack Alvarenga, Jamie Ellis, Andrew Merrill, Nate Cox, Tom Mastrangelo, Dr. Chris Bailey, Steve Polly, and Zac Bittner. I would like to thank all the support staff at RIT. I would like to specifically acknowledge the help of Jim Smith and Catherine Washington whom have helped make my research and education possible.

I would like to thank my committee members for all their support and help over the last 5 years. I would especially like to acknowledge my advisor, Dr Brian Landi, who has been a source of knowledge, guidance, and inspiration. He has shaped my experience in the PhD program and changed the way I see both problems and solutions. I will be forever grateful for the time and effort you've expended to make me a better student. I would also like to thank Dr. Ryne Raffaelle who first introduced me the world of nanotechnology and encouraged me to pursue my PhD. Thank you for believing in me and pushing me to the next level.

Finally, I would like to thank my family, my girlfriend Jenn, my sister Anne, and my parents Mark and Ellen who have loved and supported me. I thank you all for the examples you set and how you have motivated me to become the person I am today.

Executive Summary of the Dissertation Subject and Scope

Carbon nanotube (CNT) conductors are an enabling technology for advancing the efficacy of sustainable energy systems. In parallel, proactive consideration for each of the phases in the material life cycle can enhance device performance while minimizing unwanted impacts. Increasing the yield of CNTs through advances in synthesis will help reduce the electricity, chemicals, and costs associated with their production. Modifications to the nanoscale morphology (alignment, bundling, density and lower contact resistances) are needed to improve the CNT material properties to meet or exceed those of conventional metallic conductors. Also, a robust evaluation of methods for contacting carbon-based wires is needed when interfacing with metallic contacts. Finally, it's important to begin looking at upstream options for proper treatment of waste streams containing CNT conductors when they reach the end of their useable life.

Therefore, the subject of this dissertation focuses on the development of functional CNT conductors and considers approaches to improve each phase of their life cycle. Specifically, progress towards using more efficient catalysts in the laser vaporization process has led to a 50% increase in SWCNT yield and simplified the purification procedure. The use of chemical dopants such as $KAuCl_4$ has increased the electrical conductivity up to $1x10^6$ S/m which is over an order of magnitude higher than the pre-doping baseline value. Alternatively, chlorosulfonic acid was used to disperse high weight loadings of SWCNTs and modify the nanoscale morphology through the use of selective coagulation and mechanical extrusions of binder free SWCNT wires. The highly dense and aligned wires have electrical conductivities as high as $4.9x10^6$ S/m and are in agreement with the highest CNT conductivities reported. The ability to contact bulk CNT conductors through ultrasonic welding was demonstrated for the first time and exhibit low

carbon-copper contact resistances of 4.3 mΩ-cm^2. Finally, a refunctionalization procedure was developed for upcycling end-of-life CNT electrodes from lithium ion anodes. This is the first reported recycling procedure developed for CNT materials and was successful in reducing the direct electricity consumption by 75 % and the volumetric waste generation by 66 % compared to synthesizing new CNT materials.

Overall, CNT based conductors have been enhanced at each point in their life cycle (see Figure 1) and the results presented in this dissertation represent a significant step forward towards manufacturing of next generation carbon conductors.

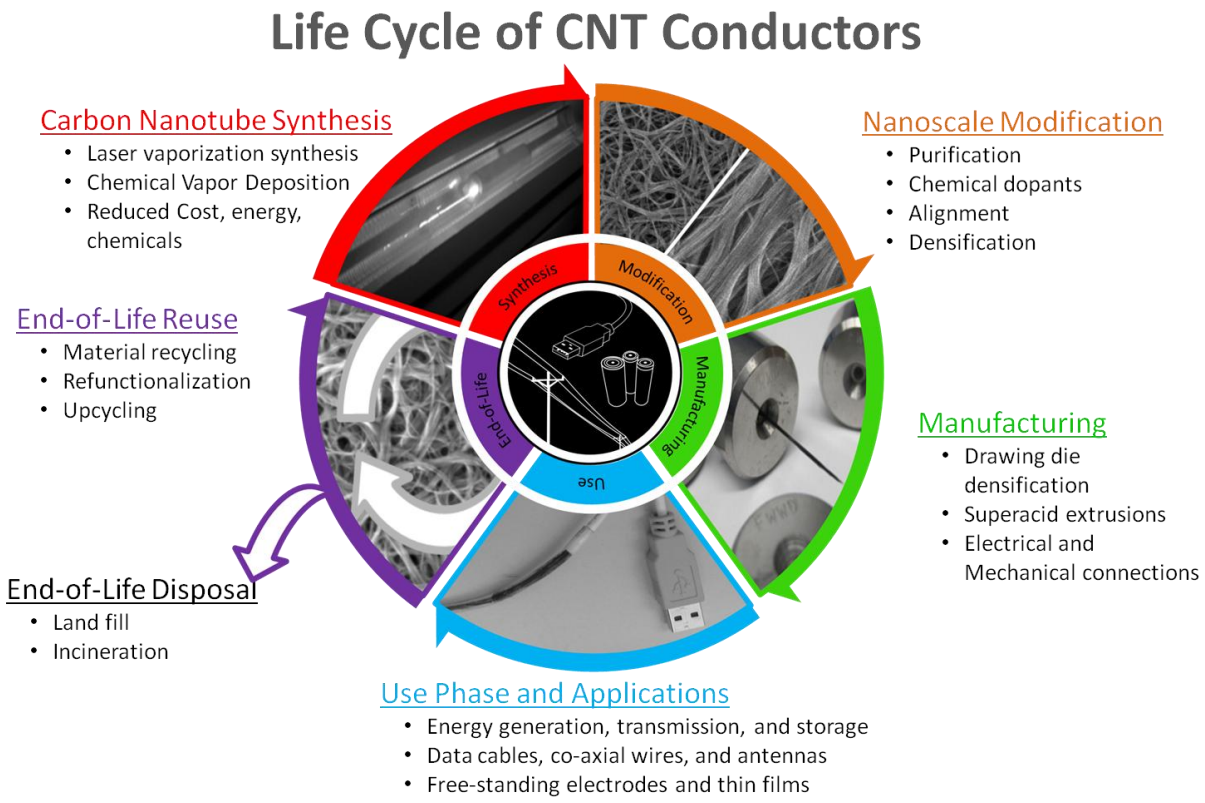

Figure 1. Schematic flow diagram of the relationship between developmental stages for carbon nanotube conductors. Original figure created by author.

Table of Contents

Table of Figures

Chapter 1: Introduction and Existing Scholarship

Electrical conductors are an essential component of the modern built infrastructure. They enable the generation, transmission and storage of electrical energy. They are greening personal mobility through electrification of vehicles. They function as the backbone of the internet enabling global telecommunications. New technologies and more efficient electrical conductors will help improve efficiency of these systems and help reduce our dependence on fossil fuels.

1.1 Copper Availability and Nanotechnology for Sustainable Energy

2012 marked the United Nation's (UN) "International Year of Sustainable Energy for All". Its charge is to push the development of, access to, and increase the percent share or renewable energy in the world energy mix by 2030. A critical component to meeting the UN's Millennium Goals, is the installation of new clean energy infrastructure (including power generation, storage, and transmission technologies). New energy grids are required to supply sustainable energy from large energy farms in remote locations to villages and cities. Even in smaller distributed sustainable energy systems, where the power is generated and consumed in the same location, it will likely require a small distribution networks to regulate, store, and smooth power.

Initiatives like the UN's "International Year of Sustainable Energy for All" will help accelerate the percentage of renewables in the world energy mix portfolio. Developing technologies such as photovoltaics, wind turbine, geothermal, hydroelectric, and fuel cells will all require electrical conductors for current collectors, turbine motor windings, electrodes, and power distribution cables. Secondary systems which use the generated electricity such as electric vehicles, mobile devices, and portable medical instrumentation will require advancements in energy storage technologies. The development of new conductors that are lighter, more flexible, corrosion

resistant, and more conductive could enable these sustainable energy systems, increase their efficacy, and eventually reduce their cost.

As developing countries continue to build their infrastructure and electrify rural communities, these new installments will add stress to the availability of copper resources. The world is already beginning to experience some of the effects of this copper shortage based on in use stocks alone.[1] Research and development of next generation sustainable materials for conductive wiring is vital. Nanotechnology – specifically, carbon nanotubes (CNTs) have the opportunity to impact many of the millennium goals for a sustainable energy future. CNTs are already showing promise for enabling the sustainable energy systems of the future, and alleviating the pressure on copper consumption.[2-6]

Gordon and Graedel have published extensively on material flows and cycling of many anthropogenic resources. In their analysis of copper, they claim that the discovery rate of new reserves is significantly outpaced by the rate of copper extraction.[7] What is worst is that as more nations increase their level of industrialization (including population increase up to $10x10^9$ people worldwide) they estimate that by the year 2050 the world will need 1,700 Tg of copper just to satisfy in use stocks alone. The projected 1,700 Tg of in use copper stocks is more than the total known reserves of 1,600 Tg and it is unlikely that all known reserves will be completely extracted. Additionally, in their calculation they used an estimated consumption of 170 kg copper per capita, which is the North American average. If the projected copper consumption is recalculated using the current per capita consumption of copper by the united states, 2,380 Tg of copper would be required, which is more than twice that of know copper reserves. A full breakdown of the United States in use copper stocks in provided in (see Table 1).[7]

Table 1.Breakdown of Active Copper Consumption in the United States (1999) from Ref[7].

Sector of Subsector	In Use Stock (kg per Capita)
Infrastructure	95
Building Construction	76
Plumbing	32
Wiring	28
Air Conditioning and Refrigeration	16
Industrial and Domestic Equipment	39
Industrial	26
Domestic	13
Transportation	28
Motor Vehicles	16
Railway, Ships, Aircraft	12
Total	238

Because the projections by Gordon and Graedel are based on in use copper stocks, recycling isn't a viable option for alleviating the problem. They list three options for moving forward:

(1) Discover more major copper reserves
(2) Current technologies which rely on copper need to utilize the resource more efficiently through better product design -- achieve the same function with reduced consumption
(3) Develop suitable substitutions to replace copper with more abundant materials.

Of the three options, they note that it is unlikely that a significant increase in newly discovered reserves will be enough to fix the problem. They also note that the 3rd option is often technically feasible but not economically preferred due to the historically low copper prices. As copper prices continue to increase the economic incentive for using some of the alternative technologies will become more attractive to producers.[7] They conclude their paper with a question: "Do we really envision a developed world quality of life for all people on the planet? and If so, are we willing to encourage the transformational technologies that will be required to make that vision a reality?"[7] The development of carbon based conductors dares to be that transformational technology and could play a vital role in reducing future demand on copper.

1.2 Carbon Nanotube Overview

Independent of the future availability of copper resources, a need exists to develop better conductors with higher electrical conductivity and improved performance. Any conductor with increased electrical conductivity will potentially improve energy generation, transmission, and storage technologies through reduced ohmic losses. Historically, few alternatives to metallic conductors have existed. High temperature super conductors are emerging as one alternative technology to compete with. Another material which shows promise is carbon nanotubes (CNTs).

Single wall carbon nanotubes (SWCNTs) have been extensively researched since their discovery in 1991 by Sumio Iijiama.[8] Their unique nanoscale properties make them an ideal candidate for electrical conductors, including energy generation, transmission, and storage technologies. In addition to their strength and flexibility, SWCNTs are excellent electrical conductors. For individual SWCNTs, an order of magnitude increase in conductivity exists for SWCNTs compared to copper when considering an internal resistance of 4.2 kΩ/μm for a 1 nm SWCNT diameter.[9] This would correspond to a SWCNT resistivity (ρ) of 1.3 x 10^{-6} Ω-cm or a conductivity of 7.7 x 10^{5} S/cm. The bulk ρ for copper at room temperature is 1.7 x 10^{-6} Ω-cm or a conductivity of 5.9 x 10^{5} S/cm. This yields a specific conductivity for Cu (density is 8.92 g/cm^{3}) of 6.6 x 10^{4} (S cm^{2}/g). Using a density of 0.8 g/cm^{3} for SWNTs,[10] yields a specific conductivity for the SWCNTs of 9.6 x 10^{5} (S cm^{2}/g). Thus, there exists a nearly 15X improvement of the specific conductivity when comparing SWCNT wires to copper.

Due to quantum confinement in SWCNTs, changes in diameter and chirality have an impact on the mechanical and electrical properties. It must be noted that SWCNT materials produced through different methods (i.e. laser vaporization, chemical vapor deposition, arc discharge,

flame) will exhibit different bulk properties. Specific arrangements of the carbon atoms result in SWCNTs that behave like semiconductors and SWCNTs that behave like metallic conductors. Some synthesis methods (primarily, chemical vapor deposition) will produce CNTs with more than one concentric wall. These multi walled carbon nanotubes (MWCNTs) are generally much larger in diameter and more rigid than SWCNTS and have different bulk properties. Additionally, the electrical conductivity of the CNT-based ribbons and wires is extremely sensitive to their local environment and can change with different processing procedures. Several factors that alter the electrical conductivity through nanoscale modifications (illustrated in Figure 2) include CNT length, defect density, densification, alignment, purity, and chemical doping. Understanding how to exploit these factors to engineer the bulk properties of CNT wires will be critical to achieving the performance of metallic conductors.

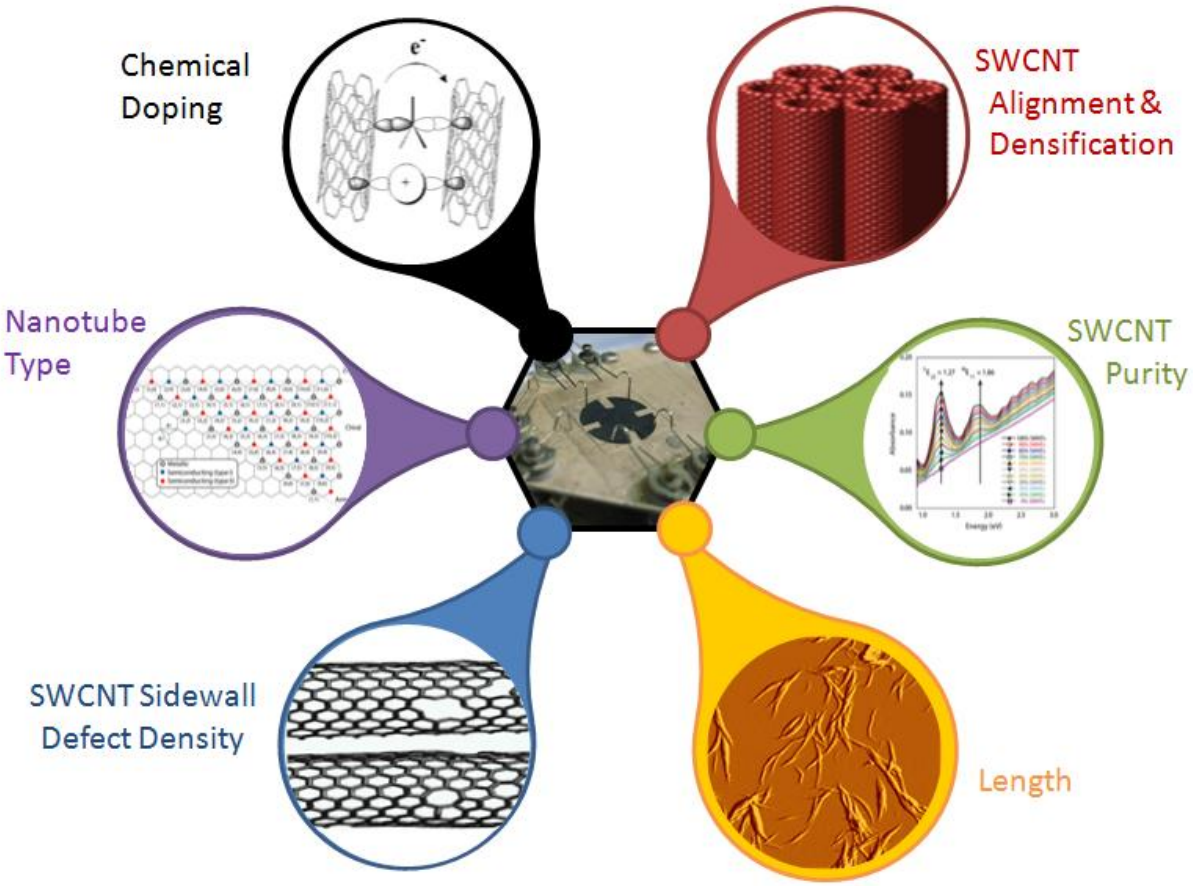

Figure 2. Factors that impact the electrical conductivity (S/m) of individual and bulk single-wall carbon nanotubes (SWCNTs). Original figure created by author.

Several advancements in SWNCT research and development have given rise to the ability to fabricate freestanding, high-purity SWCNT ribbons and wires free of all binders. In recent years, it has been possible to synthesize SWCNTs through laser vaporization with controlled diameter distributions and chiralities by adjusting the synthesis parameters such as reactor temperature, catalysts, and carrier gases.[11] The ability to assess SWCNT purity, via optical absorption spectroscopy from constructed sample sets in conjunction with thermal oxidation profiling,[12] is another major advancement which has resulted in the ability to monitor SWCNT purity (defined as the mass fraction of SWCNTs divided by the total mass of carbonaceous material) at each step

in the purification process. This has lead to increasing both the quality and overall yield of SWCNT material. Additionally, the ability to suspend the high purity SWCNT material in the appropriate solvents via ultrasonication, can be used to fabricate free standing CNT papers absent of all binders. These free standing papers can be used as catalyst supports in fuel cells or batteries.

1.3 Applications of Functional Carbon Nanotube Conductors

CNTs are currently being investigated for a host of different energy-related technologies, consumer products, structural reinforcements, and medical applications. Any material-based technology or industry which uses metals or other forms of carbon, such as graphite, amorphous carbon, or fullerenes could realize potential benefits to the unique quantum confined properties of CNTs. These versatile materials can be modified and developed for a number of different technologies including hydrogen fuel cells electrodes, lithium ion battery current collectors, supercapacitors, and conductive wires.[13-15] SWCNTs are also being investigated as transparent conductive electrodes for touch screen displays and consumer electronics. They are being investigated as thin-film current collectors for both organic and crystalline photovoltaic systems. Specifically, in this dissertation, SWCNTs are being investigated for next-generation of conductive materials to replace conventional metallic wiring for data and power transmission. They show great promise as both DC conductors for power and data transmission and AC conductors as the outer conductors of coaxial wires with improved attenuation while decreasing the mass of the system.[16, 17]

High conductivity lightweight wires systems have the potential to revolutionize mass saving benefits in the aerospace industry, improve fuel efficiency, and reduce costs for airlines and transportation systems. Additionally, carbon-based conductors have the ability to be more

resistant to corrosive and hostile environments. CNT wire conductors have been shown to be stable even in one molar hydrochloric acid bath exposure in excess of 90 days without any measurable degradation in wire performance.[3] Analogous copper wires rapidly decrease in performance under the same acidic conditions and completely dissolve after just a few days of exposure. This resistance to corrosion allows for new application of conductive sensors and wires in hostile and marine environments where metallic conductors require special insulation and coatings to maintain their properties.

1.4 Development of Functional Carbon Nanotube Conductors

The development of functional carbon based conductors will not only depend on the physical and electrical properties but also on understanding how the nanomaterial changes at each point in its life cycle. Figure 3 illustrates the sequential development of CNT conductors in the context of this dissertation: starting from (1) the synthesis of CNTs to (2) the purification and modification of the materials, (3) methods of manufacturing bulk conductors, (4) the CNT conductors use phase where they will eventually (5) reach their end-of-life. This dissertation will focus on each of these key areas of CNT conductor development for sustainable energy systems. SWCNTs will be synthesized in house, where their nanoscale properties will be modified through chemical dopants, mechanical densification, and high weight loading dispersions in superacids. New methods of contacting bulk CNTs to metallic interconnects are developed. Finally recycling options for end-of-life were developed for the first time.

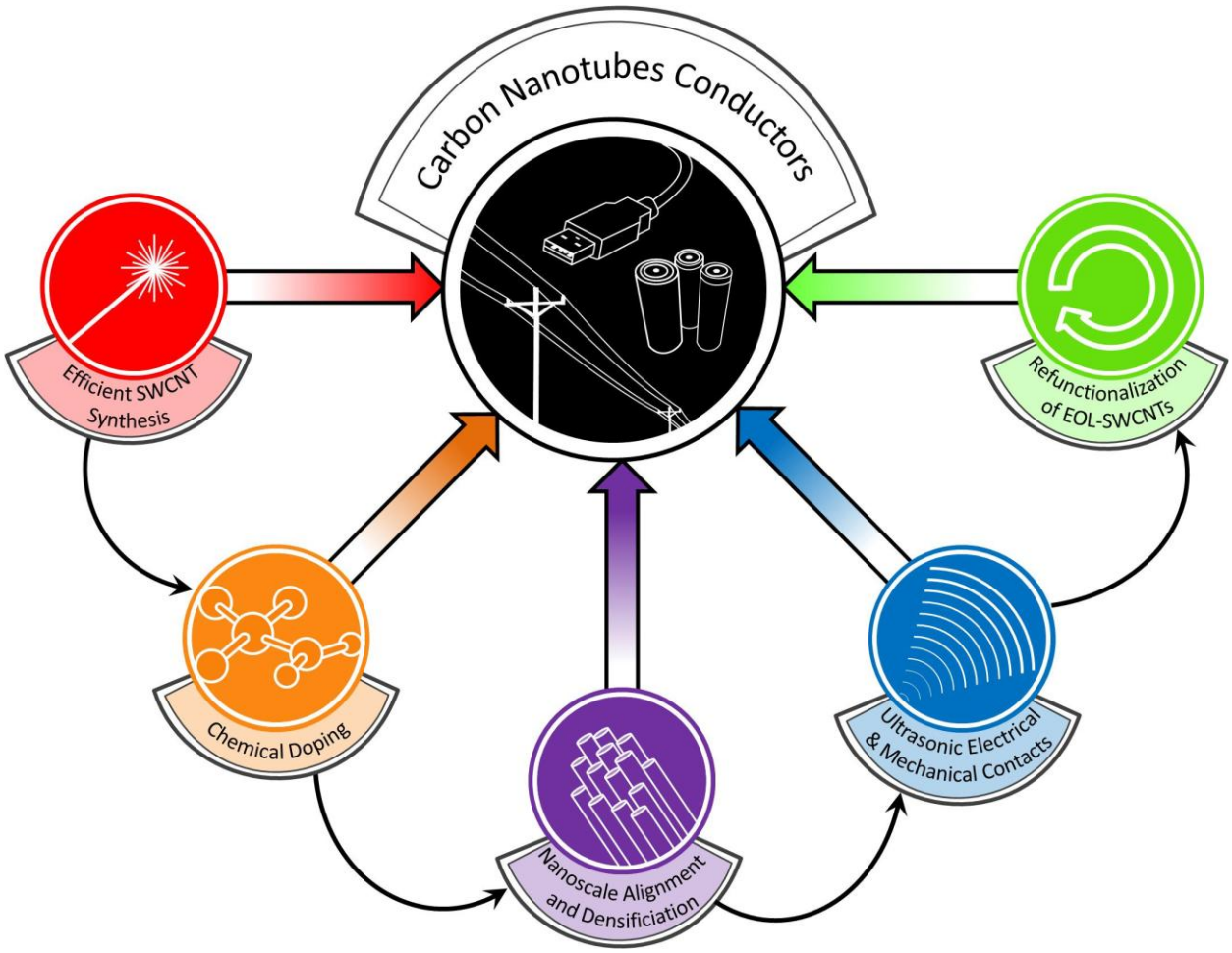

Figure 3. Life cycle flow diagram of carbon nanotube based electrical conductors including end-of-life options. Original figure created by author.

Chapter 2: Life Cycle of CNT Conductors: Laser Vaporization Synthesis of Single-Wall Carbon Nanotubes

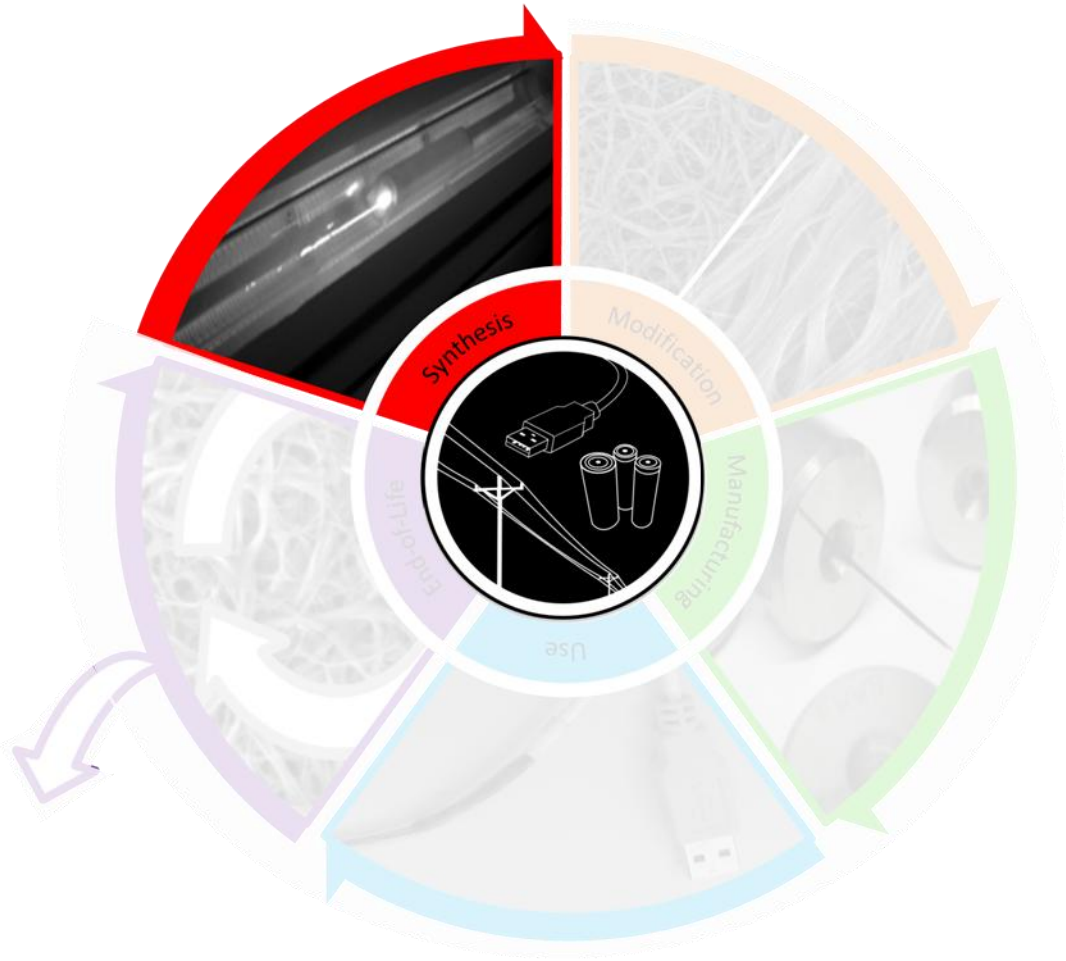

Figure 4. Chapter 2 of the dissertation will focus on the synthesis of carbon nanotube materials through modifications to the laser vaporization reactor and the use of nanometal nickel and cobalt catalysts in the graphite targets. Original figure created by author.

Chapter 2 of the dissertation will examine the synthesis stage of the CNT conductor life cycle. This chapter will focus on modifications to the laser vaporization synthesis procedure used to manufacture SWCNTs. Specifically, a second generation laser vaporization synthesis reactor was

designed with enhanced safety controls developed using a "risk assessment" and "nanoethics" methodology. The dual laser reactor system includes a number of engineering controls to isolate the researcher from the as-synthesized SWCNT material including a glove box enclosure. Utilizing the new laser reactor system, the use of nanometer sized catalyst particles will be investigated to enhance the yield and rate of SWCNT growth. Increasing the production of SWCNTs through the use of more efficient catalyst can potentially lower the direct electricity consumption, per mass, of SWCNTs. Additionally; changes in the ability to purify SWCNTs manufactured using nanometer sized catalyst will be measured.

2.1 Development of a Next Generation Laser Vaporization Synthesis Reactor – Towards Nanoethics, Worker Safety, and Safe Handling Engineering Controls

There has been recent effort to better understand the exact human health and environmental impacts incurred from exposure to SWCNTs.[18-23] Since the exact health risks are still an area of study, there is little regulation governing safe handling practices. Therefore, researchers and manufacturing workers who may come into contact with SWCNT materials on a regular basis need to proactively consider the risks. It is well established that soots, dusts, and aerosols can have potential worker exposure concerns as these materials come into contact with skin, the respiratory tract, and digestive systems. Even in trace amounts per exposure event, the cumulative effect over time could lead to some potential health risks.[21, 22] Thus it is essential to develop engineering solutions to minimize exposure and release of SWCNTs during the synthesis and manufacturing phase of the CNT conductor life cycle as this can significantly impact aspects of social sustainability.

During the course of this dissertation research, a next generation laser vaporization synthesis reactor was developed to potentially eliminate worker exposure. A dual laser vaporization

synthesis reactor was designed to isolate the worker from nanomaterials produced during the synthesis process. The synthesis laboratory has three interlock systems integrated into the design including door interlocks, laser curtain interlocks, and pressure sensitive floor mats. The dual laser reactors are enclosed in a sealed glove box with antistatic paneling, coaxial quartz synthesis tubes, HEPA air filters, and iris port sample exchange chambers (all highlighted in Figure 5). SWCNTs can be synthesized, harvested, and processed without opening the enclosure to the laboratory. Flowing proper procedures, this system of engineering controls prevents accidental contact between the operators and the SWCNTs being manufactured. Although these engineering controls isolate the worker from exposure during normal operation, special care must be taken during cleaning and maintenance of the reactor systems. During these special cases, additional personal protective equipment (PPE) is available and should be worn. The additional PPE includes full length disposable clothing protecting and respirators.

Environmental health and safety regulations don't require this level of engineering and containment controls (currently only gloves, safety glasses, and a lab coat are required), nor is there even consensus in the scientific community if SWCNTs pose a *significant* human health risk. Being proactive in this instance will not only isolate students and researchers from exposure routes, but if future regulations were to mandate exposure controls the reactor systems should meet and requirements. The ethical decision to invest in the engineering controls cost a significant amount of time and money, but the social impact cost if exposure caused human harm is much greater. Ultimately, the system can be used as a model for other research groups or companies synthesizing SWCNTs.

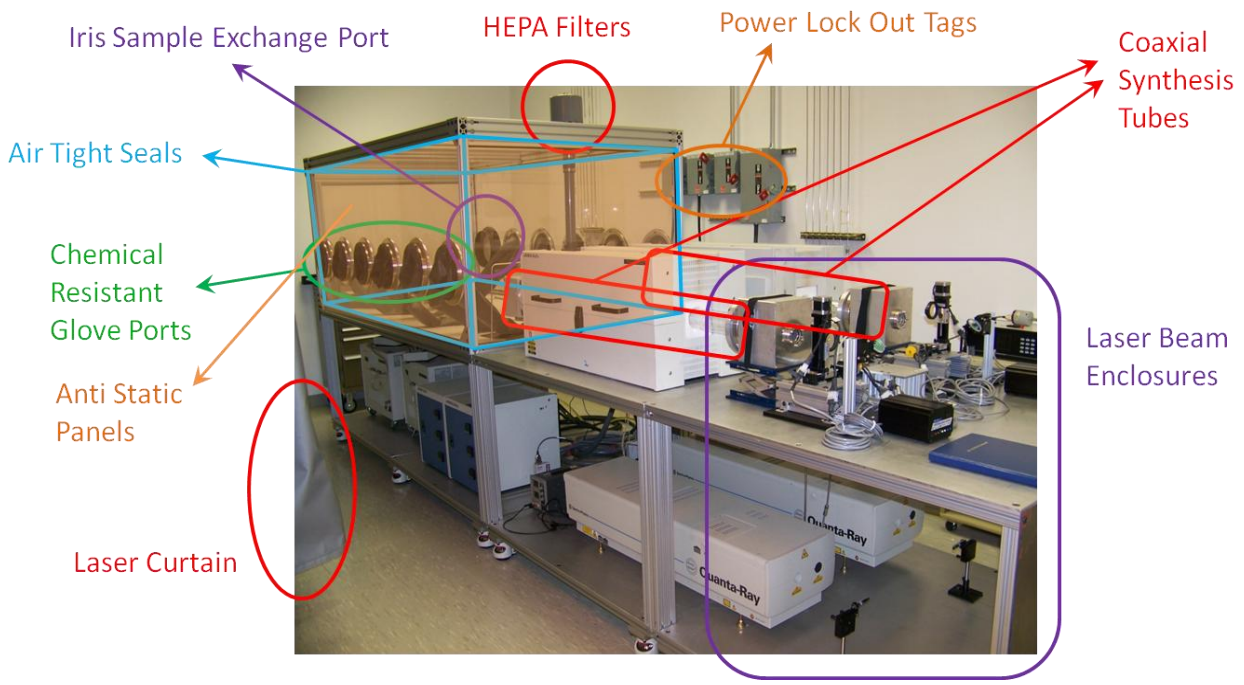

Figure 5. Photograph of two Nd:YAG lasers installed in a new parallel reactor system in the RIT SMFL class 1000 clean room. The new synthesis reactor is complete with several engineering controls including a heap-filtered enclosed harvesting chamber to prevent worker exposure to manufactured nanomaterials. Photograph and original figure created by author.

When the dual laser vaporization reactor was first designed in the Fall of 2010, engineering controls were developed and implemented into the design to minimize or eliminate worker exposure. Two years later, in May of 2012, the National Institute for Occupational Safety and Health (NIOSH) published a report; General Safe Practices for Working with Engineered Nanomaterials in Research Laboratories. In the report they summarize a list of the best practices for the safe handling of nanomaterials in a research laboratory facility. The NIOSH report focuses on a "prevention through design" approach to minimizing exposure. This methodology follows closely with the previous ethical decision made two years ago to spend the extra time, effort, and money to develop a reactor system that isolates the operator from the nanomaterials

they produce. Specifically detailed in the report are the recommendations listed in the table below:

Table 2. List of NIOSH recommended nanomaterial safe handling practices.

Recommended Exposure Prevention Method	Implemented	Not Implemented
Elimination or substitution		✘
Administrative controls	☑	
Isolation and engineering controls	☑	
Containment and ventilation	☑	
Chemical fume hoods	☑	
Personal Protective Equipment	☑	
Protective eyewear	☑	
Protective clothing, including reusable clothing designated use with nanomaterial	☑	
Nitrile or chemically impervious gloves	☑	
Respirators*	---	---
Glove box enclosures	☑	

*The use of respirators is not required for handling single-wall carbon nanotube material as the glove box prevents release into the laboratory. Respirators are available during cleaning and maintenance of the laser reactors.

Of all the controls and safe handling practices outlined in the NIOSH safe practices report, the use of glove box enclosures for handling dry CNT powders should provide the highest level of exposure risk mitigation. When using glove boxes for SWCNT handling, the highest chance for worker exposure occurs when transferring samples to and from the enclosure and therefore proper ventilation and surface cleaning should be utilized to minimize particle release into the laboratory. The report does caution that the use of a glove box enclosure can often come at the expense of dexterity and caution that extra care should be used when conducting experiments. The proactive approach taken in NPRL to conduct research responsibly within a nanoethical

framework has been shared with other research groups and can serve as a model system for future installations.

Impact of Nanometal Catalyst on the Laser Vaporization Synthesis of SWCNTs

The new laser vaporization synthesis reactors were used to manufacture SWCNTs utilizing nanometal catalyst. The hypothesis was that nanometer diameter particles could be more evenly distributed in the graphite targets, more easily vaporized, and would be more uniformly distributed in the vaporization plume. This would lead to a higher percentage of SWCNT growth compared to the formation of amorphous carbon.

2.2Nanometal Catalyst Introduction

Single wall carbon nanotubes (SWCNTs) are being investigated for many power generation and storage technologies which rely on amorphous carbon/graphite for conductive electrodes including Li^+ batteries [14, 24], proton exchange membrane fuel cells [25], and super capacitors [15]. Of the prevalent approaches used to produce SWCNTs for these applications, laser vaporization synthesis presents certain advantages, including tunable SWCNT chirality distributions [26] and well established purification processes [13]. The intent to increase SWCNT yield during the laser synthesis process has resulted in various studies on the experimental parameters' including reactor temperature, pressure, and catalyst composition [27-31]. However, until recently, the lack of a calibrated purity assessment method precluded these early reports from validating the degree of change that these parameters had on the purity (defined as the total mass fraction of SWCNTs, w_{SWCNTs}) of SWCNTs contained in a sample. Although empirical analysis has suggested that a bimetallic composition of Ni and Co in the graphite target leads to the highest purity SWCNTs, it is now possible to quantify the impact of metal catalyst properties (e.g. particle size, stoichiometry, etc.) on the resulting SWCNTs. In the present study, the effects of catalyst particle

size on the properties of SWCNTs produced during the laser vaporization synthesis are investigated.

2.3 Experimental:

SWCNT material was produced via laser vaporization synthesis using previously published synthesis conditions [12-14, 26, 32] described briefly as follows: 760 Torr, 200 sccm flowing Ar, alexandrite laser power density of 100 watts/cm^2, and 1150 °C. SWCNT material produced from targets fabricated with 3% w/w nanonickel (13 nm, Quantum Sphere Inc.) and 3% w/w nanocobalt (13 nm, Quantum Sphere Inc.) was compared with the material produced using conventional 3% w/w micronnickel (2.2-3.0 µm Alfa Aesar) and 3% w/w micronmetal cobalt (2 µm Sigma-Aldrich) [13, 26]. The two catalyst types were used in combination with 94% w/w graphite flake (7-10 µm Alfa Aesar), mechanically mixed for 48 hours, and pressed into targets at 2,500 psi. The as-produced material condensed in multiple zones on the inside of the quartz tube, with the majority of the material condensing in a thick carpet at the exit of the furnace. This carpet material was removed from the reactor and used for all characterization and post synthesis processing. Smaller quantities of material which condensed on the quartz tube at the front of the furnace as well as at the rear of the reactor were not included as part of the characterization. The use of both target types exhibited similar production rates exceeding 100 mg of as-produced material per hour. The as-produced SWCNTs from each set of targets using micronmetal and nanometal catalysts will be referred to as µ-SWCNT and n-SWCNT, respectively.

The synthesized µ-SWCNT and n-SWCNT materials were characterized by scanning electron microscopy (SEM), transmission electron microscopy (TEM), optical absorption spectroscopy, Raman spectroscopy, and thermogravimetric analysis (TGA). SEM was performed using a field emission Hitachi S-900 at 2 kV. Quantitative assessment of the SWCNT purity was performed

by optical absorption spectroscopy on stable SWCNT-N,N-dimethylacetamide (DMA) dispersions using a Perkin-Elmer Lambda 900 spectrometer from 300 nm (4.13 eV) to 1600 nm (0.77 eV)[12]. Raman spectroscopy was performed using a 1.96 eV He-Ne laser on a JY-Horiba Labram spectrophotometer over the range of 100 cm^{-1} to 2800 cm^{-1}. Thermogravimetric analysis (TGA) was performed using a TA Instruments 2950 TGA on multiple samples obtained from each as-produced n-SWCNT and µ-SWCNT carpet materials [13]. TEM analysis of the n-SWCNT and µ-SWCNT non-combustible TGA residues was performed using a Joel CX II 100 at an accelerating voltage of 100 KeV. TEM samples were prepared by suspending the TGA residue in acetone using an ultrasonic bath. A TEM grid was subsequently dipped in the solution and allowed to dry in air. SWCNT material was also produced with a 1064 nm Nd:YAG Lab-150 laser from Spectra Physics, in parallel with the alexandrite laser, following the same synthesis and characterization procedures.

2.4 Results and Discussion

SEM analysis provides visual confirmation of carbon nanotubes in both the n-SWCNT and µ-SWCNT materials (Figure 6). In general, the quality of the raw soot is similar between samples and consistent with previous SEM analysis [12-14, 26, 32]. The surface morphology for each as-produced material shows bundled carbon nanotubes, metal catalyst clusters, and amorphous carbon impurities, typical of laser-produced SWCNTs.

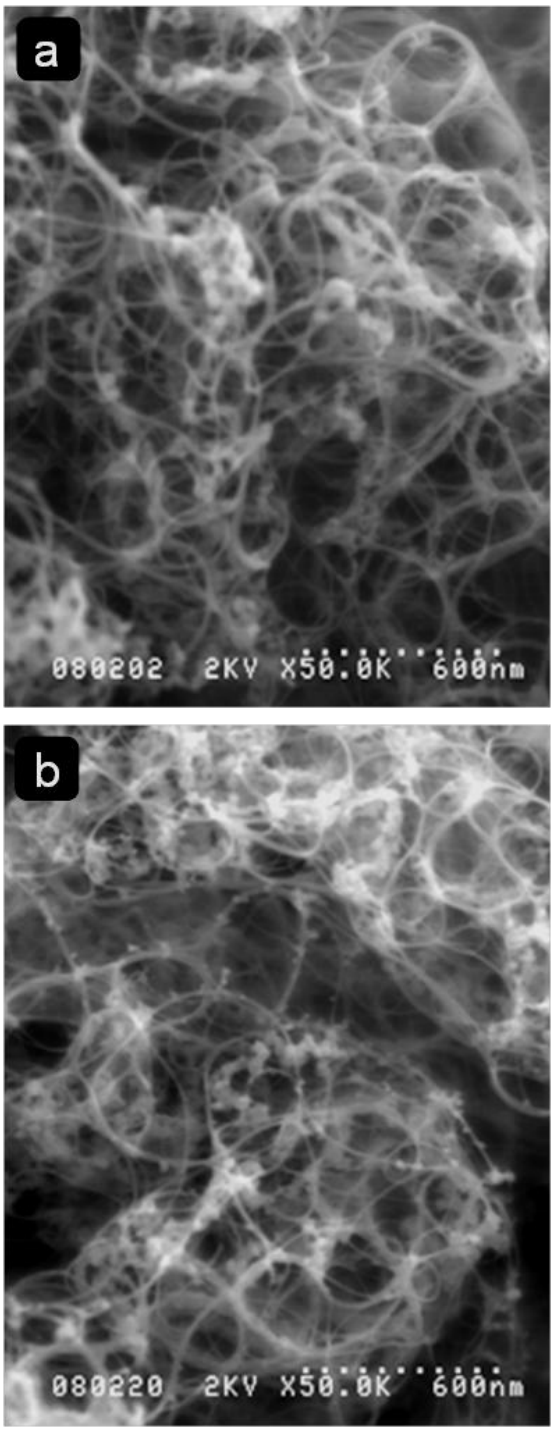

Figure 6. Scanning electron microscopy micrographs of as-produced laser generated a) n-SWCNT and b) µ-SWCNT. Original figure created by author and reproduced with permissions from Schauerman, C.M. et al "Impact of nanometal catalysts on the laser vaporization synthesis of single wall carbon nanotubes." *Carbon* 2009, *47*, 2431-2435 for use in dissertations.

Quantitative assessment of the SWCNT carbonaceous purity values ($^{C}w_{SWCNTs}$ is defined as the mass fraction of SWCNTs in the carbonaceous portion of a sample) were obtained from the peak ratios of the absorption maxima at 650 nm (1.9 eV) and 950 nm (1.3 eV) for both µ-SWCNT and n-SWCNT samples using the previously reported method [12, 13]. It was determined that the SWCNT purity of the µ-SWCNT was 25% ± 2% and the n-SWCNT had a purity of 35% ± 2%. To help illustrate the difference in purity, peak maxima tie lines have been drawn in Figure 7 to serve as a guide to the eye. As per the previous report, a more positive tie line slope corresponds to higher SWCNT purity in the sample [12].

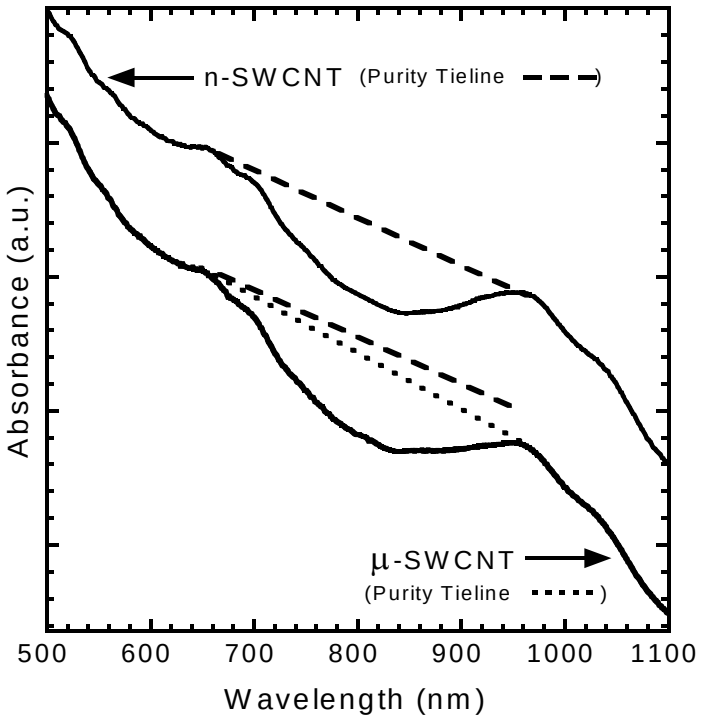

Figure 7. Optical absorbance spectra for n-SWCNT and µ-SWCNT as-produced SWCNT material. Absorbance values are the average of 3 separate samples for each catalyst SWCNT material. Original figure created by author and reproduced with permissions from Schauerman, C.M. et al "Impact of nanometal catalysts on the laser vaporization synthesis of single wall carbon nanotubes." *Carbon* 2009, *47*, 2431-2435 for use in dissertations.

The Raman spectra confirmed that there was no measurable change in the average D/G ratio observed between the n-SWCNT and µ-SWCNT samples (Figure 8). Comparisons of the radial breathing modes (RBM) between samples at 100 – 300 cm^{-1} show a similar range of diameters in resonance. However, there is a relative distribution variation between samples with the n-SWCNTs showing a propensity toward smaller diameter chiralities as compared to the more uniform distribution of diameters in the µ-SWCNTs. Overall, the SWCNT diameter range shows only a small dependence on initial catalyst particle size as compared to the much larger change in SWCNT diameter distributions dependent on catalyst type (i.e. Ni and Co) [28, 31].

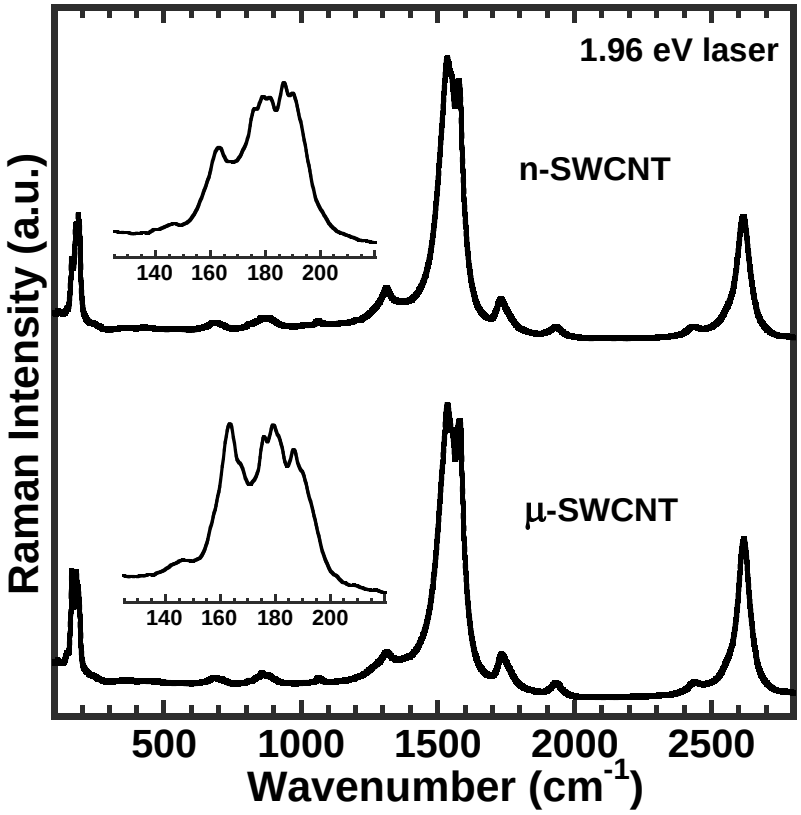

Figure 8. Raman spectra for n-SWCNT and µ-SWCNT. Insets are magnified radial breathing modes of n-SWCNT and µ-SWCNT. Raman spectra are the average of 3 separate samples for each catalyst SWCNT material. Original figure created by author and reproduced with permissions from Schauerman, C.M. et al "Impact of nanometal catalysts on the laser vaporization synthesis of single wall carbon nanotubes." *Carbon* 2009, *47*, 2431-2435 for use in dissertations.

TGA data in Figure 9 shows representative thermograms illustrating the change in weight percent and first order derivative weight change for each sample. The µ-SWCNT samples showed an average residue of 10% w/w after ramping to 800°C with the 1st derivative profile exhibiting a peak decomposition rate at 490°C. The n-SWCNT showed an increase in the 1st derivative peak temperature to 585°C, while also significantly decreasing the average residue to 5.5% w/w. The higher carbonaceous purity and decreased residue content for the n-SWCNT sample results in an overall purity ($^{C}w_{SWCNTs}$) improvement of *50%* over that of the sample made with conventional micron catalysts.

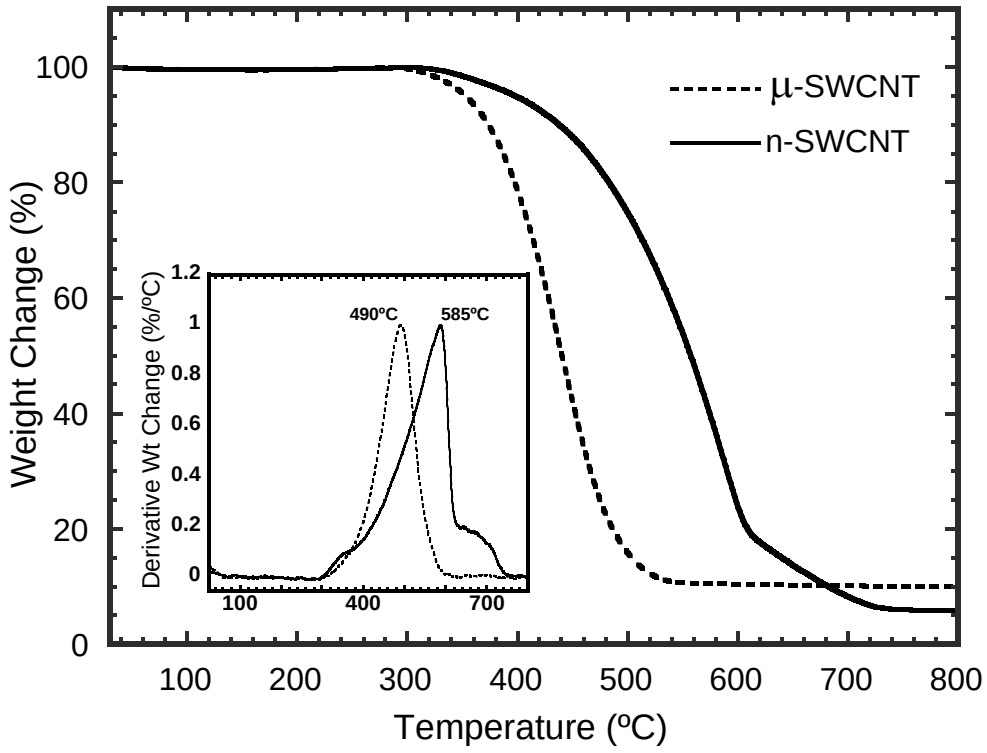

Figure 9. Thermograms for n-SWCNT and µ-SWCNT material ramped at 10°C/min. Insets shows the derivative weight change for the same materials. Thermograms are the average of 3 separate samples for each catalyst SWCNT material. Original figure created by author and reproduced with permissions from Schauerman, C.M. et al "Impact of nanometal catalysts on the laser vaporization synthesis of single wall carbon nanotubes." *Carbon* 2009, *47,* 2431-2435 for use in dissertations.

The shift to a higher combustion temperature in the case of the n-SWCNTs could result from a variety of factors including: sample morphology, SWCNT crystallinity, or oxidation state of metal catalyst impurities. The reduction in metal catalyst impurities for the n-SWCNT sample, based upon TGA residue, is expected to decrease the amount of exothermic energy released during thermal oxidation of metals which in turn would suppress the precombustion of SWCNTs [13]. The observed reduction in TGA residue for the n-SWCNT material could have resulted from differences in the distribution of condensed material inside the reactor, specifically, the relative concentration of metal catalyst impurities in the different condensation zones inside the quartz tube. Although the laser vaporization reactor conditions were constant between samples, the surface of the nanometal and micronmetal graphite targets showed visible differences in morphology post-synthesis. Such variability may influence the quantity of metal vaporized in the as-produced material. Finally, it is also expected that differences in the oxidation state of the post-synthesis catalyst particles based upon size could also contribute to the discrepancy in the TGA reside between the two materials.

The n-SWCNT and µ-SWCNTs TGA residues were analyzed using TEM to investigate the differences in the vaporization of each catalyst type. TEM images were acquired for both TGA residues and representative images are provided in Figure 10. Statistical analysis of multiple TEM images yielded mean catalyst particle diameters of 18 ± 6 nm and 3 ± 1 nm for the µ-SWCNT and n-SWCNT material, respectively. This analysis shows, under equivalent synthesis conditions, starting with two different catalyst particle sizes will produce observed differences in

the post-synthesis catalyst particle diameters. Smaller more homogenous catalyst particles, post-vaporization, would increase the available surface area for seed growth of the SWCNTs and possibly give rise to the increased SWCNT concentration in the as-produced n-SWCNT material. The surface area to volume ratio for an 18 nm µ-SWCNT is 0.033 and for a 3 nm n-SWCNT is 0.20. This means for a given volume of catalyst, there could be up to six times more surface area available for the growth of SWCNTs when using nanometal catalysts.

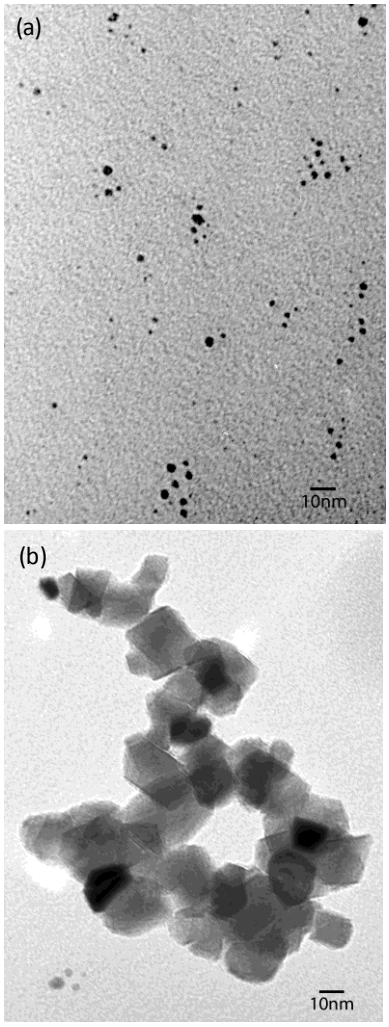

Figure 10. Transmission electron micrographs of non-combustible thermogravimetric residue from as-produced laser generated (a) n-SWCNT and (b) µ-SWCNT. Original figure created by author and reproduced with permissions from

Schauerman, C.M. et al "Impact of nanometal catalysts on the laser vaporization synthesis of single wall carbon nanotubes." *Carbon* 2009, *47*, 2431-2435 for use in dissertations.

The effects of metal catalyst precombustion can be inferred from a systematic analysis of the thermal oxidation profiles (TOP) for each sample [13]. The TOP is performed by monitoring SWCNT properties after thermal oxidation, in air, to incrementally increasing temperature intervals (ramping at 10°C/min). Optical absorption spectroscopy was subsequently performed on representative samples of both materials at each temperature interval in the TOP to calculate the carbonaceous purity. Shown in Figure 11 is the TOP analysis comparing carbonaceous purity as a function of oxidation temperature for the n-SWCNT and µ-SWCNT materials. There is a clear divergence in the observed trend at ~500°C where the µ-SWCNT material shows the expected [13] decrease in SWCNT purity with increasing oxidation temperature. In contrast, the n-SWCNT material shows a successive increase in SWCNT carbonaceous purity at higher oxidation temperatures; achieving > 90% at 615°C. The ability to use "soft-bake" techniques to purify as-produced pulsed laser vaporization SWCNTs has been recently reported [33], however the reported soft-bake process involves multiple thermal oxidations and acid treatments resulting in a total purification time of one week. The purification of the n-SWCNT material, demonstrated herein, requires a single thermal oxidation to remove carbonaceous impurities. In addition, the exposed metal catalyst particles can then be easily removed with a single acid treatment. The entire n-SWCNT purification process requires less than a day to achieve >90% SWCNT carbonaceous purity. The use of nanometal catalysts for the laser vaporization synthesis of SWCNTs demonstrates promise towards fast, simple, and potential large-scale purification of SWCNTs produced via laser vaporization.

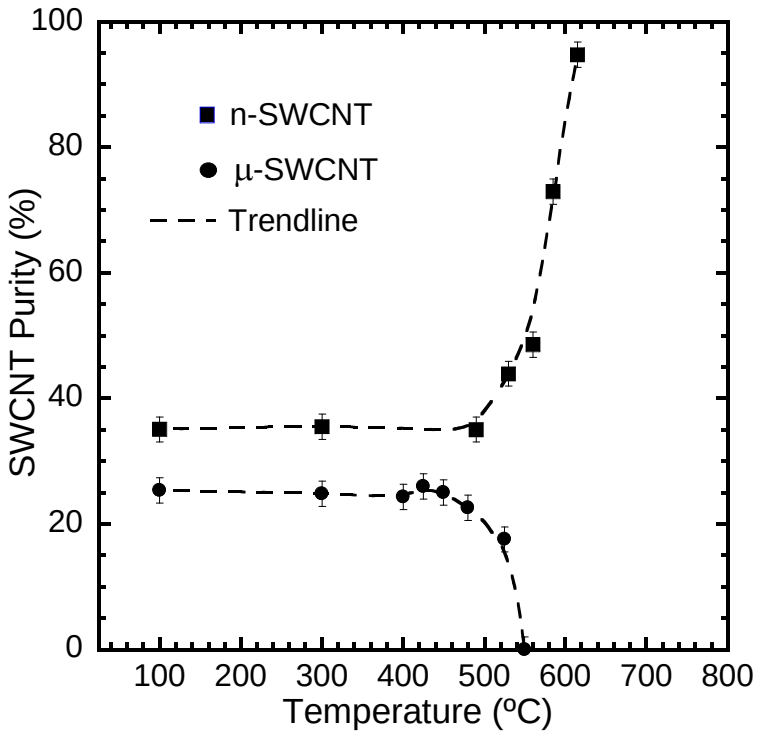

Figure 11. SWCNT purity as a function of maximum thermal oxidation temperature for both n-SWCNT and µ-SWCNT materials. Error is provided for each data point. Original figure created by author and reproduced with permissions from Schauerman, C.M. et al "Impact of nanometal catalysts on the laser vaporization synthesis of single wall carbon nanotubes." *Carbon* 2009, *47*, 2431-2435 for use in dissertations.

2.5 Conclusion

In conclusion, the particle size of metal catalysts for the laser vaporization synthesis of SWCNTs shows little effect on sample morphology and comparable chirality distributions. However, there is an overall 50% improvement in SWCNT purity through the use of nanometal (13 nm) nickel and cobalt catalysts compared to conventional micron-sized particles. In addition, TOP analysis has shown a dramatic difference in the combustion properties between the as-produced samples; the n-SWCNT exhibit a suppression of the SWCNT precombustion due to the exothermic oxidation of the metal catalyst particles. Thus, the use of nanometal catalysts in the laser vaporization process significantly increases synthesis yield and offers simplified thermal

oxidation procedures to improve purification efficiency. TEM analysis showed clear differences in the catalyst residue size in the as-produced SWCNTs suggesting improved material properties are a direct result of unique vaporization and condensation mechanisms for each starting catalyst size. Equivalent results have been achieved for SWCNT material produced using nanometal catalysts in conjunction with a Nd:YAG laser vaporization reactor (1064 nm), and therefore, represents a general trend for pulsed laser vaporization synthesis.

There are several limitations to the work presented in this section. The use of nanometals to improve CNT yield was only investigated for laser vaporization synthesis and could be expanded to other CNT synthesis methods (e.g. chemical vapor deposition and arc discharge). Additionally a full LCA should be conducted to quantify the impacts of CNT synthesis with a focus on how scaling up to industrial levels of CNT production will change the LCA impacts.

Chapter 3: Life Cycle of CNT Conductors: Modification of Nanoscale Properties

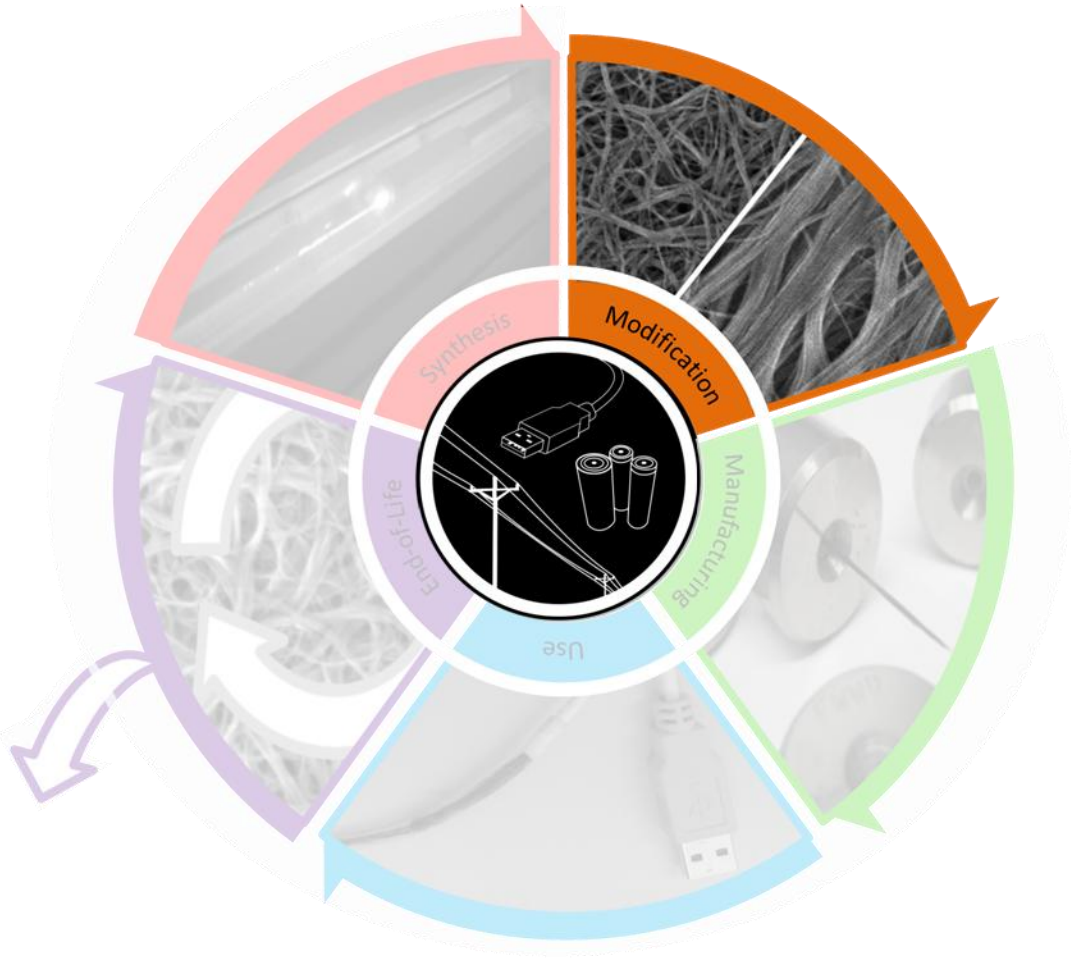

Figure 12. Chapter 3 of the dissertation will focus on the modification of carbon nanotube materials through chemical and mechanical methods.

3.1 Introduction

Chapter 3 of the dissertation investigates the modification stage of the CNT conductor life cycle. Specifically, chemical treatment methods to increase the electrical conductivity in bulk networks of SWCNTs synthesized in chapter 2. Increasing the electrical properties of bulk SWCNT networks is a critical component of making functional devices out of the nanomaterials.

Understanding how to properly control and modify the chemical environment around CNTs to increase the electrical conductivity will aid in the ability to assemble macro systems of highly conductive SWCNTs networks.

Engineering the electronic properties of CNT networks is a critical step towards developing functional materials for applications ranging from nanoscale transistors to bulk conducting wires. In addition to physical modifications to the nanoscale network (e.g. densification or nanoscale alignment), chemical doping species can be introduced to enhance the electronic properties. Three primary doping strategies exist for chemical doping of SWCNTs: endohedral doping, in-plane doping, and exohedral doping.[34] Endohedral doping relies on the intercalation of chemical species inside the CNTs. In-plane doping involves the substitution of carbon atoms along the lattice by other atoms (e.g. boron or nitrogen), resulting in p-type or n-type semiconductors. In the case of exohedral doping, organic and inorganic molecules can be chemically adsorbed or physically absorbed onto the CNT surface and junction locations between neighboring CNTs.[34] Exohedral doping represents a rapid and reproducible method for doping bulk CNT networks and is the focus of this work.

The doping susceptibility (whereby the term "susceptibility" is used to refer to a material response to chemical dopants and is *not related* to the concept of magnetic susceptibility from physics) of CNT networks was divided into two main sections. The first section focuses on published literature values for SWCNT electrical conductivity, and the susceptibility of SWCNT networks to $KAuCl_4$ and $KAuBr_4$ family of salts. The second section investigates the impact of CNT species (e.g. SWCNT and MWCNTs) on the doping susceptibility of the mixed CNT network to chemical dopants.

3.1.a Electrical Conductivity of Single-Wall Carbon Nanotubes

Individual CNTs

The highest measured current carrying capacity for an individual SWCNT is 10^7 A/cm^2 and predicted current carrying capacities have been as high as 10^{13} A/cm^2.[35] The highest measured resistance of 1 nm diameter SWCNT is 4.2 kΩ/μm.[9] This corresponds to an individual SWCNT conductivity of 3 x 10^8 S/m which is almost an order of magnitude higher than that of copper (5.96 x 10^7 S/m). Theoretical calculations have predicted that ballistic conductance would occur along a defect-free metallic CNT; meaning that in the absence of any electron scattering, the resistance would not vary along the length of the CNT.[36] The ballistic resistance in metallic SWCNTs has been estimated to be 6.45 kΩ,[37] while the resistance of MWCNTs is slightly higher at 12.9 kΩ.[38] The strong covalent carbon-carbon bonding in CNTs also provides them with high resistance to electromigration, a current-assisted diffusion process. For very small diameter metal wires, this effect can cause failure at relatively low currents, resulting in a current-carrying capacity of ~10 nA/nm^2.[39] In defect-free carbon nanotubes, the current-carrying capacity can exceed 10 μA/nm^2, also due in part to the absence of electron scattering and resistive heating.

Bundled and Bulk Single-Wall Carbon Nanotube Networks

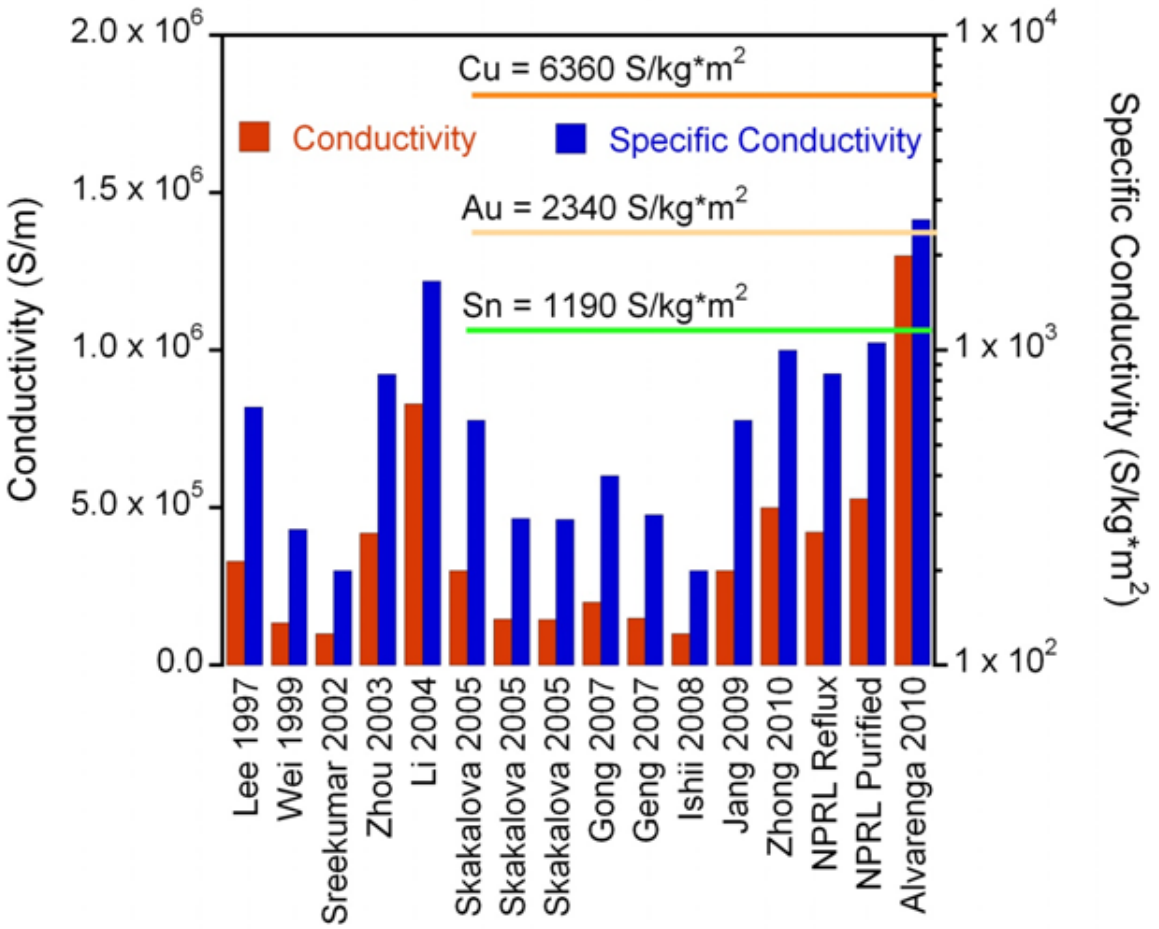

Figure 13. Electrical conductivity (S/m) and specific conductivity (S/kg*m^2) of bulk single-wall carbon nanotube materials referenced in published literature.[40-56] Original figure created by Paul Jarosz and reproduced with permissions from Jarosz, P.; Schauerman, C.M. et al "Carbon Nanotube Wires and Cables: Near-Term Applications and Future Perspectives." *Nanoscale*, 2011, *3* (11), 4542 – 4553 for use in dissertations.

The reported electrical conductivities of bulk SWCNT papers span a wide range of values from $2x10^3$ S/m to $3x10^5$ S/m.[43],[56] Sources of variability between the publications include purity of the SWCNT material, density of the bulk papers, processing procedure, and different doping chemicals. These differences make it important to understand how the conductivity of these materials changes with processing and testing conditions. In comparison to measured conductivity values for metals (e.g. copper, aluminum, gold, silver) which have a known

electrical conductivity, the published literature values for the electrical conductivity of SWCNT is widely varying across more than two orders of magnitude (Figure 13). Reasons for the large range include differences in the material properties from the synthesis, to the processing, and assembly of macroscopic bulk networks. The ability to control synthesis conditions, purification parameters, alignment and density will have a large impact on the resulting electrical properties and a CNT networks susceptibility (the term susceptibility is used to refer to a material response to chemical dopants and is *not related* to the concept magnetic susceptibility from physics) to doping. A diagram illustrating the 6 major contributors to variations in electrical conductivity is provided in Figure 2.

3.2 Experimental

A critical component of this dissertation is the accurate measurement of the electrical properties of CNT and conductive materials. Two specific methods of measuring the electrical conductivity are 4-point probe measurements and the Van der Pauw method.

3.2.a Four Point Probe Method

The 4-point probe method is an essential part of accurately measuring the electrical conductivity of conductive wiring. Electrical measurements using only 2-probes not only measure the electrical resistance of the sample but the measurement also includes the resistances of the measuring wires and contact resistance with the sample. The 4-point probe method uses two outer probes to source (and drain) a current in a wire, and two inner probes to measure a voltage drop across the known spacing of the voltage probes. In this configuration, a very large (~10 MΩ) resistor prevents current from flowing down the voltage probes. Because current does not

flow through the voltage probes, this method removes the contact resistance and resistance of the electrical probe leads from the measurement. The resistance of the wire can then be calculated using Ohm law (V=I*R) with known values for the voltage drop and applied current.

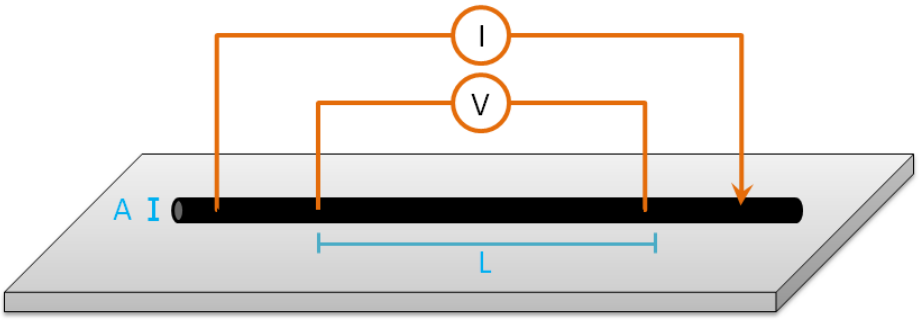

Figure 14. Schematic of the 4-point probe configuration for measuring the electrical conductivity (S/m) of wire. Current is sourced on the outer probes and the voltage drop is measured across the two inner probes. Using the spacing between the inner probes (L) and the cross-sectional area of the wire (A) it is possible to calculate the electrical conductivity (S/m) of the sample. Original figure created by author.

3.2.b Van der Pauw Method

The Van der Pauw method of measuring the electrical conductivity of a sample was originally developed in 1958 as a means to remove the contact resistance (Ω) between the measurement probes and a sample of arbitrary size and shape.[57] Although the method can measure the conductivity (S/m) of a sample of any arbitrary shape (as long as the probes are placed at the edge of the sample), the clover leaf geometry is the preferred shape because the deep channels force current to flow around the cuts which simulates "infinite" size contacts located at the exact corners of the inner square (Figure 15).[57]

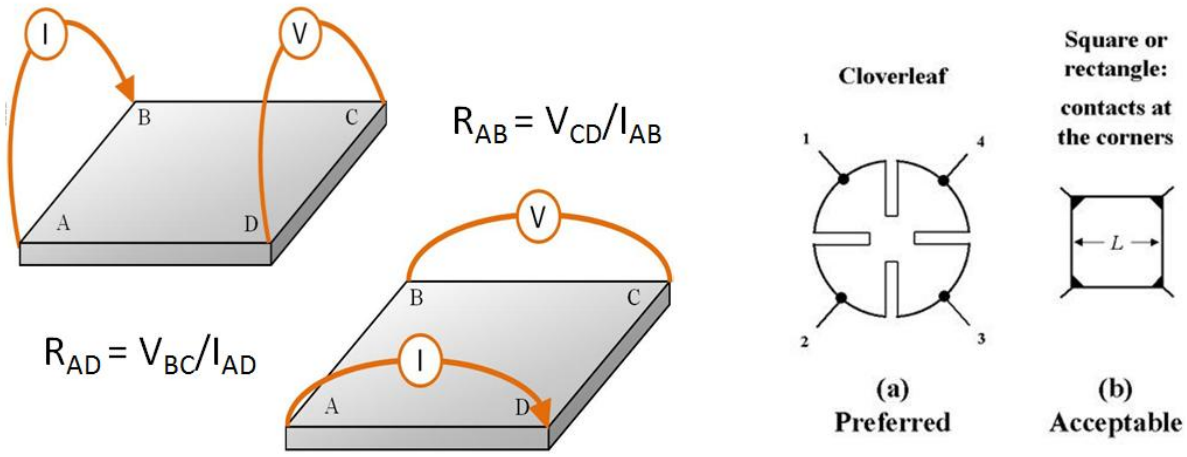

Figure 15. Diagram of the Van der Pauw geometry for measuring the electrical conductivity of a material. The cloverleaf geometry is preferred over the square pads in that it simulates infinite contacts placed at the exact corners of the square design.[57] Original figure created by author.

To apply the Van der Pauw method for measuring the electrical conductivity of CNT samples, a source measure unit from National Instruments (NI PXIe-1062Q) was used in conjunction with a National Instruments (NITB-2606) matrix terminal block for rapid switching between all four probe configurations in the Van der Pauw method. By measuring the resistance (Ω) in all 8 directions (R_{AB}, R_{BA}, R_{BC}, R_{CB}, R_{CD}, R_{DC}, R_{DA} R_{AD}) an average resistance along the length and width of the sample can be obtained and used to calculate the electrical conductivity (S/m) by solving the Van der Pauw equation (1).

$$e^{\frac{-\pi * R_{length} * d}{\rho}} + e^{\frac{-\pi * R_{width} * d}{\rho}} = 1 \quad (1)$$

R_{length} and R_{width} are the averaged measured resistance (Ω) values perpendicular to each other on the Van der Pauw SWCNT square, d is the thickness of the SWCNT paper and ρ is the resistivity (Ωm) of the SWCNT paper which numerically satisfies the equation.

3.2.c Purification of Single-Wall Carbon Nanotubes

Purification of the as-produced SWCNT material occurs through a series of acid and thermal treatments developed in the NPRL. The reflux process removes metal catalyst as well as some amorphous carbons impurities, and is depicted graphically in Figure 16. In general, 100 mg of as-produced SWCNT material is brought to reflux at 125 °C in 3M nitric acid for 16 hours. The SWCNTs material is then vacuum-filtered onto 1 µm PTFE membrane filter papers with copious amounts of water to remove residual acid. The filter paper was rinsed consecutively with acetone, and H_2O until filtrate became colorless after each step. The vacuum filtration process produces a reflux-SWCNT paper which is easily separated from the PTFE membrane filter. The SWCNT paper is then dried at 200°C in a muffle furnace for 1 hour to remove any residual solvents.

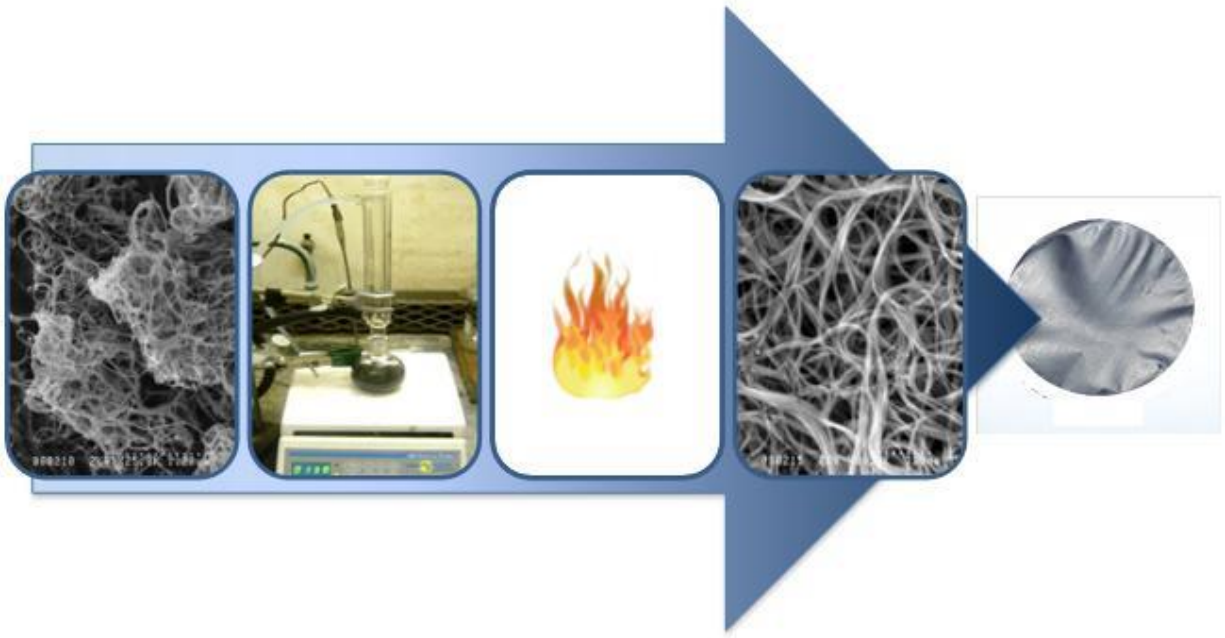

Figure 16. Purification process consisting of nitric acid reflux and thermal oxidation used to purifiy as-produced single-wall carbon nanotubes (SWCNTs) into high purity free standing SWCNT papers. Original figure created by author.

Following the reflux procedure, a thermal oxidation is performed in air at 525°C using a temperature ramp rate of 10 °C/minute in a Lindberg BlueM 1200 furnace. The thermal oxidation exposes any remaining metal particles not removed in the reflux procedure (Figure 16). Therefore, a 6M Hydrochloric acid wash is performed on the SWCNT paper for 60 minutes using magnetic stirring. The purified SWCNT material was then removed from the acid solution using similar filtration steps as above. A final thermal oxidation is performed at 525°C for 20 minutes to remove any intercalated acids and thus completes the purification procedure. SEM, optical absorption, and Raman analyses are conducted during the purification process to assure that the quality of the purification achieved at least 95% w/w pure SWCNTs.

3.2.d Chemical Doping

A number of ionic species (e.g. $AuCl_3$, $HAuCl_4$, $AuBr_3$, $HAuBr_4$, $KAuCl_4$, $KAuBr_4$) have been demonstrated to be good electrical dopants in CNT networks.[2, 58, 59] $KAuCl_4$ doping solution was prepared at a concentration of 0.001 M by mixing potassium tetracloroaurate hydrate (Sigma Aldrich) in deionized water. CNT hybrid materials were exposed to the doping solution for 30 minutes before being dried in a vacuum over at 100 °C for 2 hours. Solvent specific chemical doping was performed by preparing 0.001 M solution of $KAuCl_4$ in each of the solvents investigated and measuring the electrical conductivity as a function of time. The impact of co-metals on the ability to dope SWCNT networks was performed by introducing co-metals during the doping process by exposing the SWCNT materials to the $KAuCl_4$ doing solution and the metals at the same time.

3.3 Results and Discussions

There has been considerable research on the chemical doping of CNTs, and the exact doping mechanisms are still being investigated. Recently, a new strategy has been proposed for controlling the doping types by selecting possible dopants based upon their reduction potential, relative to that of CNTs.[60] Doping of CNTs using salt solutions such as $AuCl_3$, $AuBr_3$, $KAuCl_4$ and $KAuBr_4$ can have different reaction mechanisms compared to direct adsorption of organic molecules.[61] The doping method which has been proposed is a redox reaction which occurs due to the higher reduction potentials of the cations in solution. The charge transfer reduces positive ions such as Au^{3+} to metal particles and results in p-type doped CNTs.[62] Since CNTs possess a reduction potential of about +0.5 V vs. SHE (standard hydrogen electrode), the reduction of Au^{3+} ($AuCl_4^-$/Au, +1.002 V vs. SHE) into metal nanoparticles can occur without the aid of a reducing agent.[62]

Based on studies involving CNT thin films, a significant reduction in sheet resistance was measured using Au^{3+} ions.[60] This suggests that the gold nanoparticles (Au^0) that spontaneously form on the surfaces of CNTs do not aid in electron transport. Experiments conducted with various Au^{3+} ionic salts during this work also support these findings. In the present work, when CNT papers were submerged into aqueous solutions of $KAuCl_4$ and $KAuBr_4$, roughly the same electrical conductivity was measured for all the samples, yet significant gold plating only occurred with the $KAuCl_4$ samples. In addition, increasing exposure to both the $KAuCl_4$ and $KAuBr_4$ increased the amount of Au^0 plating, but did not result in a further increase in the electrical conductivity above that measured at 30 min exposure to 0.05 M concentration (Figure 17). Thus, it was determined that the gold plating was not essential for high electrical conductivity. Since many cases prefer a low mass CNT conductor, the performance of $KAuBr_4$-doped CNTs which plates less was the more desirable dopant species.

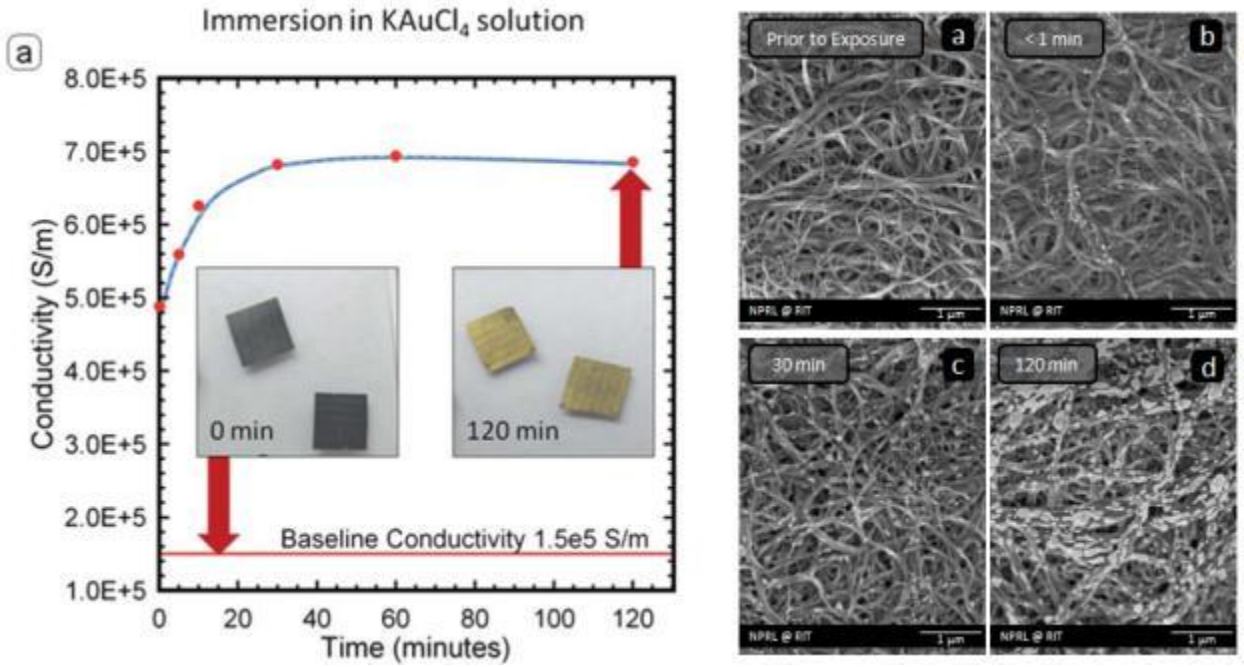

Figure 17. (a) Conductivity of CNT squares as a function of time in contact with aqueous KAuCl4 solution. Inset: photographs of squares of purified SWCNTs before and after immersion. (b–e) SEM images of CNT material after

various times in contact with KAuCl4 solution. Measurement error is within the data points. Original figure created by author and reproduced with permissions from Jarosz, P.; Schauerman, C.M. et al "Carbon Nanotube Wires and Cables: Near-Term Applications and Future Perspectives." *Nanoscale,* 2011, *3* (11), 4542 – 4553 for use in dissertations.

In addition to the extent of Au plating on the SWCNT surface, the network's susceptibility (the term susceptibility is used to refer to a material response to chemical dopants and is *not related* to the concept of magnetic susceptibility from physics) to $KAuCl_4$ chemical dopant is impacted by the choice of carrier solvent used for delivery. As a control, the electrical conductivity of SWCNT Van der Pauw electrode squares was monitored as a function of exposure time to each solvent (Figure 18a). The conductivity of each sample remained low over the course of the measurement except for deionized water and acetone which showed a modest increase in the electrical conductivity approaching $8x10^4$ S/m. When $KAuCl_4$ was dissolved into the same solvents and the conductivity was measured as a function of time both the rate of chemical doping and the maximum achieved conductivity changed (Figure 18b). Solvents which have a high affinity for the SWCNTs such as DMA and CHP did not result in an increase in the measured conductivity. Carrier solvents which have minimal interaction with the SWCNTs such as deionized water, isopropanol, and methanol resulted in the highest increase in electrical conductivity up to $6.5x10^5$ S/m. The results suggest that the carrier solvent can compete with dopants like $KAuCl_4$ for active dopant sites and reduce or prevent an increase in the electrical conductivity of the SWCNTs.

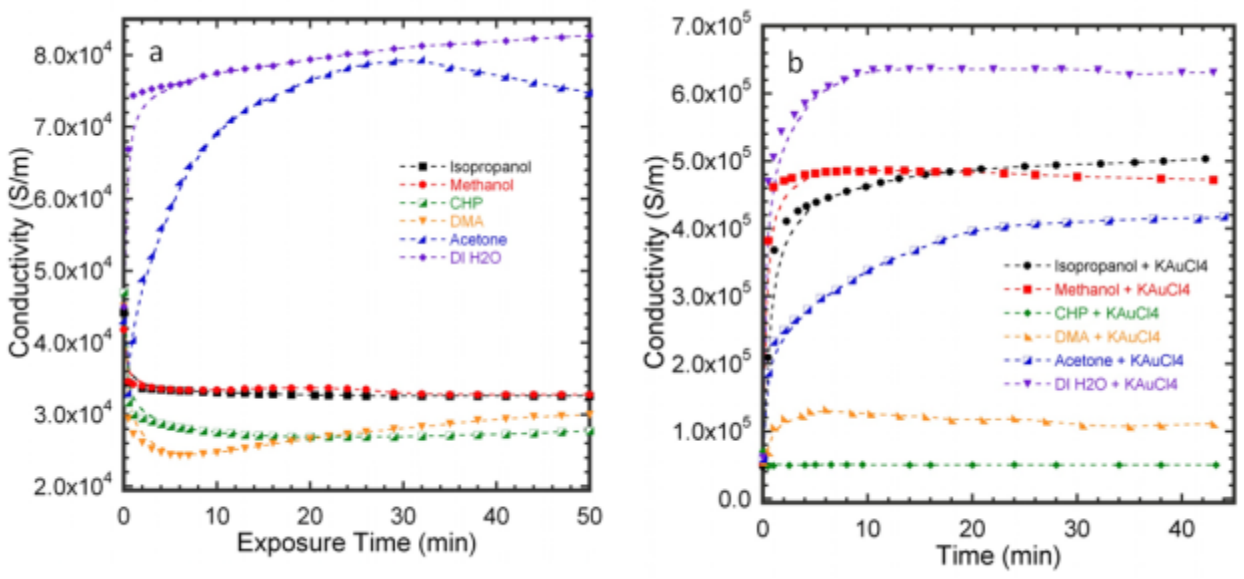

Figure 18. Electrical conductivity (S/m) of single-wall carbon nanotubes of as a function of exposure time to (a) carrier solvent and (b) carrier solvent and $KAuBr_4$. Measurement error is within the data points. Original figure created by author.

Metallic and semiconducting type separated SWCNTs, purchased from NanoIntegris, were also used for chemical doping with a $KAuCl_4$ solution. Electrical conductivity of the SWCNT sample was measured, in situ, as a function of doping time. The metallic SWCNT enriched sample shows an increase in electrical conductivity with increasing exposure time to the doping solution. The semiconducting enriched SWCNT sample, however, maintains the same baseline conductivity with increased exposure time (Figure 19). This difference in the doping ability between semiconducting metallic samples would suggest that the salt solution plays a role in depleting the valence band electrons from the metallic material and improves transport between individual SWCNTs.

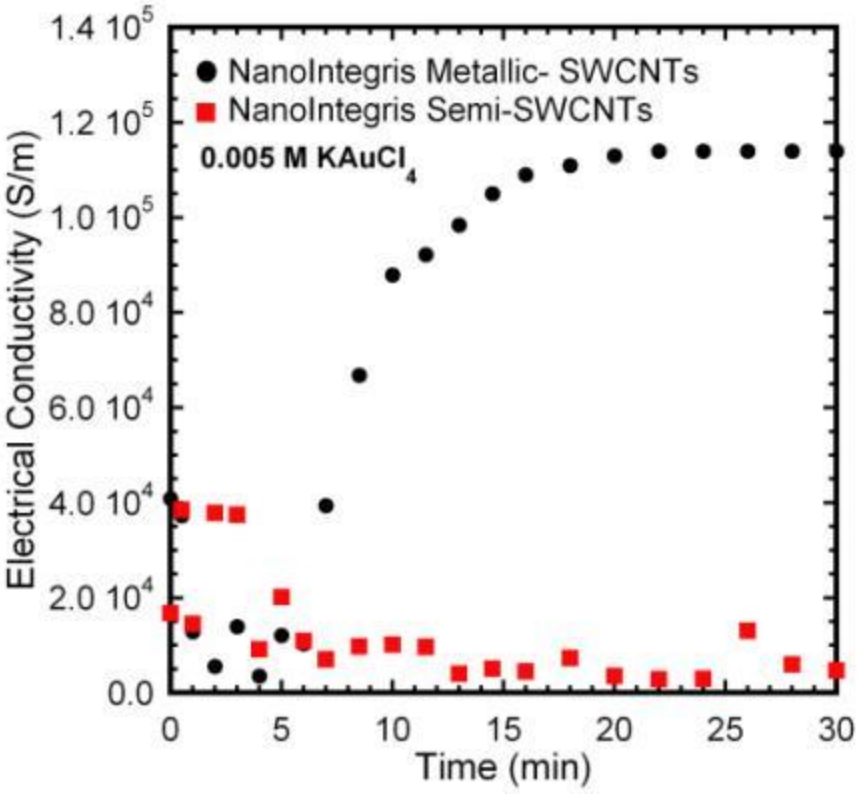

Figure 19. Electrical conductivity of electronic type separated SWCNTs purchased from NanoIntegris and doped with 0.005M $KAuCl_4$. Measurement error is within the data points. Original figure created by author.

The extent of doping SWCNT materials by $KAuCl_4$ can be influenced by the existence of co-metals present as impurities in the SWCNT matrix. These metals can be present in the SWCNT matrix as residual catalyst particles left over from the synthesis process (e.g. laser vaporization, chemical vapor deposition). If these metals are not entirely removed during the purification process, they can influence the electroless decomposition of the gold salt on the surface of the SWCNTs and affect the extent of chemical doping and plating. Therefore, a series of metal catalysts (Figure 20) were investigated to determine the impact they have on the electroless plating and subsequent doping of CNT materials. Of particular interest are nickel, cobalt, and iron. These metals are common metallic catalysts used in synthesis processes and will likely be present as impurities in SWCNT materials. Of these three metals, iron has the most visual

reaction with the gold salt (Figure 24) followed by cobalt (Figure 23). Nickel, shows minimal visible interaction with the gold salt solution and resulted in the smallest degree of plating (Figure 22).

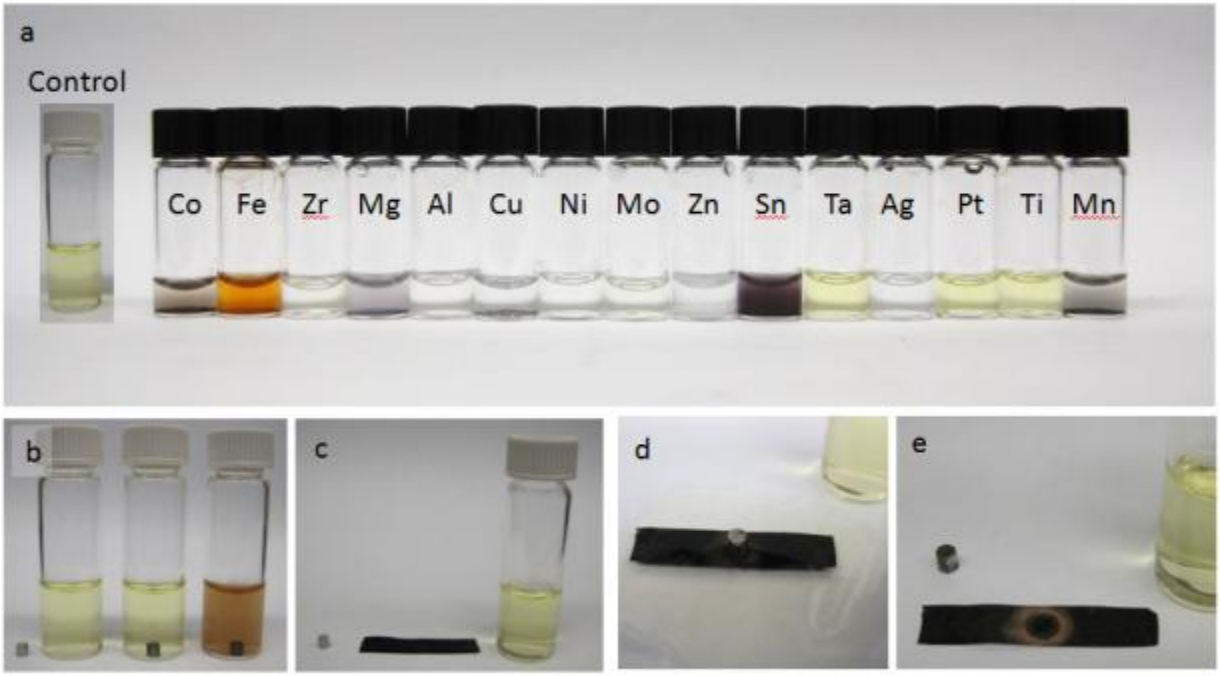

Figure 20. Reactions of (a) various co-metals with $KAuCl_4$ salt in deionized water, (b) specific interaction of iron and $KAuCl_4$ salt and (c-e) the electroless plating of gold-iron nanoparticles onto the surface of single-wall carbon nanotube ribbons following 10 seconds of exposure to the iron pellet and doping solution. Original figure created by author.

The co-metals used in the gold salt doping process affect the SWCNT doping mechanism enough to alter the maximum achievable electrical conductivity (S/m). Elements such as Mn, Fe, Cu, and Al tend to react enough with the $KAuCl_4$ salt to change the charge transfer between the SWCNT resulting in almost no change between the baseline conductivity and doped conductivity values (Figure 21). More stable elements such as Ni, Co, Cr, Pt don't seem to affect the chemical doping process allowing the electrical conductivity to increase to the average values without any

co-metals present in solution (green bar in Figure 21). This suggests that metal catalyst impurities, such as Ni and Co, present in the SWCNT network are not as critical to remove than other metal catalysts such as Fe. It is important to note that this is the residual most often found in CNT samples from chemical vapor deposition synthesis methods.

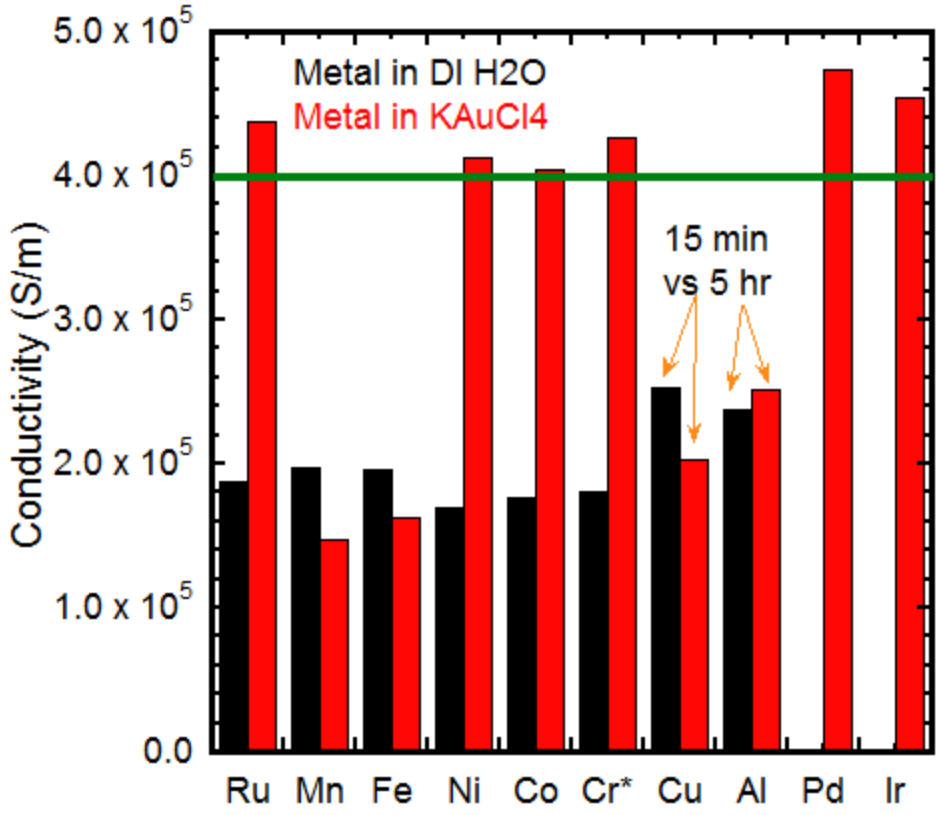

Figure 21. Electrical conductivity of single-wall carbon nanotubes (SWCNTs) doped with $KAuCl_4$ using co-metals to facilitate electroless decomposition onto the surface of the SWCNTs. Measurements were conducted on several samples and the best case values are plotted. Original figure created by author.

Scanning electron microscopy was used to image the electrolessly plated particles on the surface of SWCNTs for Fe, Ni, and Co catalyst particle impurities. A test SWCNT ribbon strip was immersed into 0.05 M $KAuCl_4$ gold salt doping solutions and a Ni pellet was pressed into the

surface of the SWCNTs and held in place for 10 seconds after which the pellet was removed and the SWCNT ribbon strip was rinsed and dried. The surface of the SWCNT ribbon shows minimal plating at the interface with the Ni pellet (Figure 22). Three different locations were chosen for SEM analysis: (1) directly underneath the Ni Pellet (highlighted in red in Figure 22), (2) at the edge of the Ni Pellet (highlighted in green in Figure 22), and (3) outside of the contact area (highlighted in blue in Figure 22). Directly underneath the Ni pellet there was the highest density of nucleation points which grew into small colonies sometimes coalescing into sheets with their nearest neighbor. At the edge of the Ni Pellet there was a lower density of nucleation points completely isolated from each other. Outside the contact region no nucleation was observed in the sample.

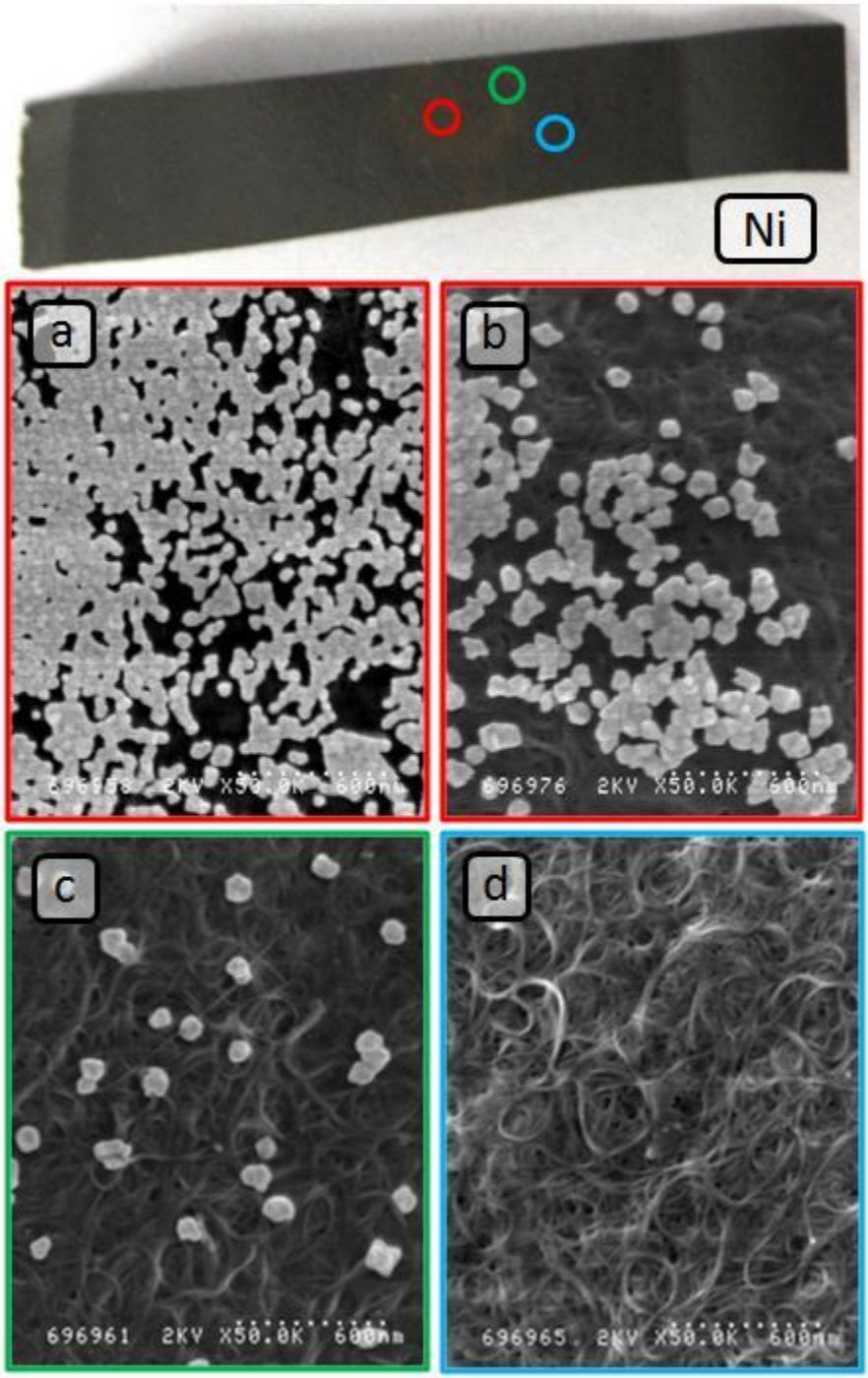

Figure 22. Scanning electron microscope images showing changes in particle size, density, and structure of electroless plating of Au-Ni nanoparticles from $KAuCl_4$ (a-b) underneath of (b) at the edge and (c-d) outside of the contract area between Ni pellet and single-wall carbon nanotubes (10 seconds exposure). Original figure created by author.

Scanning electron microscopy was used to image the electrolessly plated particles on the surface of SWCNTs when Co was used as the co-metal. A test SWCNT ribbon strip was immersed into 0.05 M $KAuCl_4$ gold salt doping solutions and a Co pellet was pressed into the surface of the SWCNTs and held in place for 10 seconds after which the pellet was removed and the SWCNT ribbon strip was rinsed with deionized water and dried. The surface of the SWCNT ribbon shows minimal plating at the interface with the Co pellet (Figure 23). Three different locations were chosen for SEM analysis: (1) directly underneath the Co Pellet (highlighted in green Figure 23), (2) at the edge of the Co Pellet (highlighted in red in Figure 23), and (3) outside of the contact area (highlighted in blue in Figure 23. Figure 23Directly underneath the Co pellet a medium density of nucleation points were observed in comparison to the edge of the Co pellet where there was a higher density of triangularly shaped nucleation points which coalesced into a jagged sheet of particles. Outside the contact region, fewer nucleation points were observed with the particles growing into rose-shaped crystals.

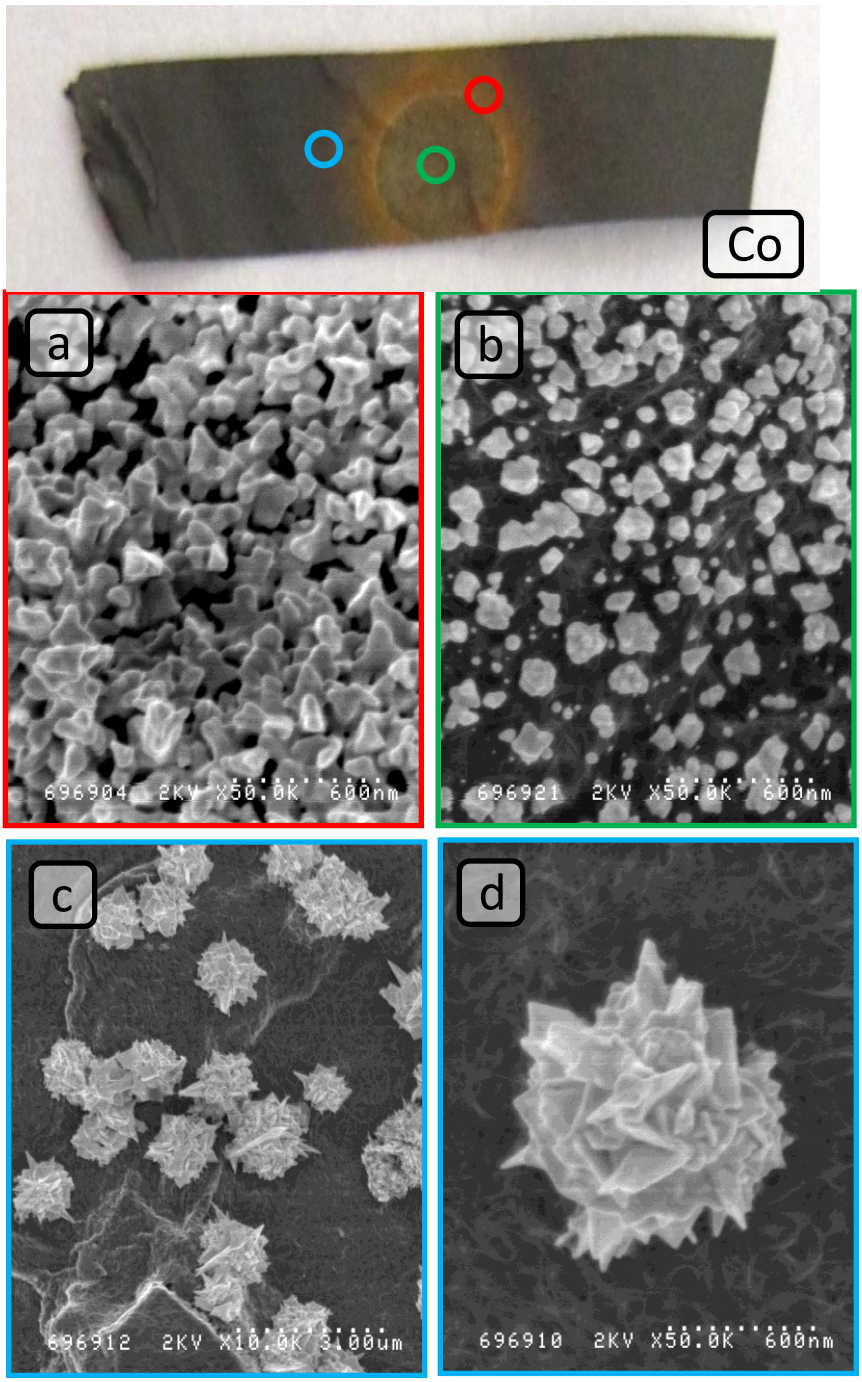

Figure 23. Scanning electron microscope images showing changes in particle size, density, and structure of electroless plating of Au-Co nanoparticles from $KAuCl_4$ (a) at the edge of (b) underneath and (c-d) outside of the contract area between Co pellet and single-wall carbon nanotubes (10 seconds exposure). Original figure created by author.

Scanning electron microscopy was used to image the electrolessly plated particles on the surface of SWCNTs when Fe was used as the co-metal impurity. A test SWCNT ribbon strip was immersed into 0.05 M $KAuCl_4$ gold salt doping solutions and a Fe pellet was pressed into the surface of the SWCNTs and held in place for 10 seconds after which the pellet was removed and the SWCNT ribbon strip was rinsed and dried. The surface of the SWCNT ribbon shows minimal plating at the interface with the Fe pellet (Figure 24). Three different locations were chosen for SEM analysis: (1) directly underneath the Fe Pellet (highlighted in green in Figure 24), (2) at the edge of the Fe pellet (highlighted in red in Figure 24), and (3) outside of the contact area (highlighted in blue in Figure 24). Directly underneath the Fe pellet a medium density of nucleation points were observed in comparison to the contact edge of the Fe pellet where there was a higher density of plated particles. Outside the contact region, fewer nucleation points were observed with the particles growing into larger spherical or star-shaped crystals.

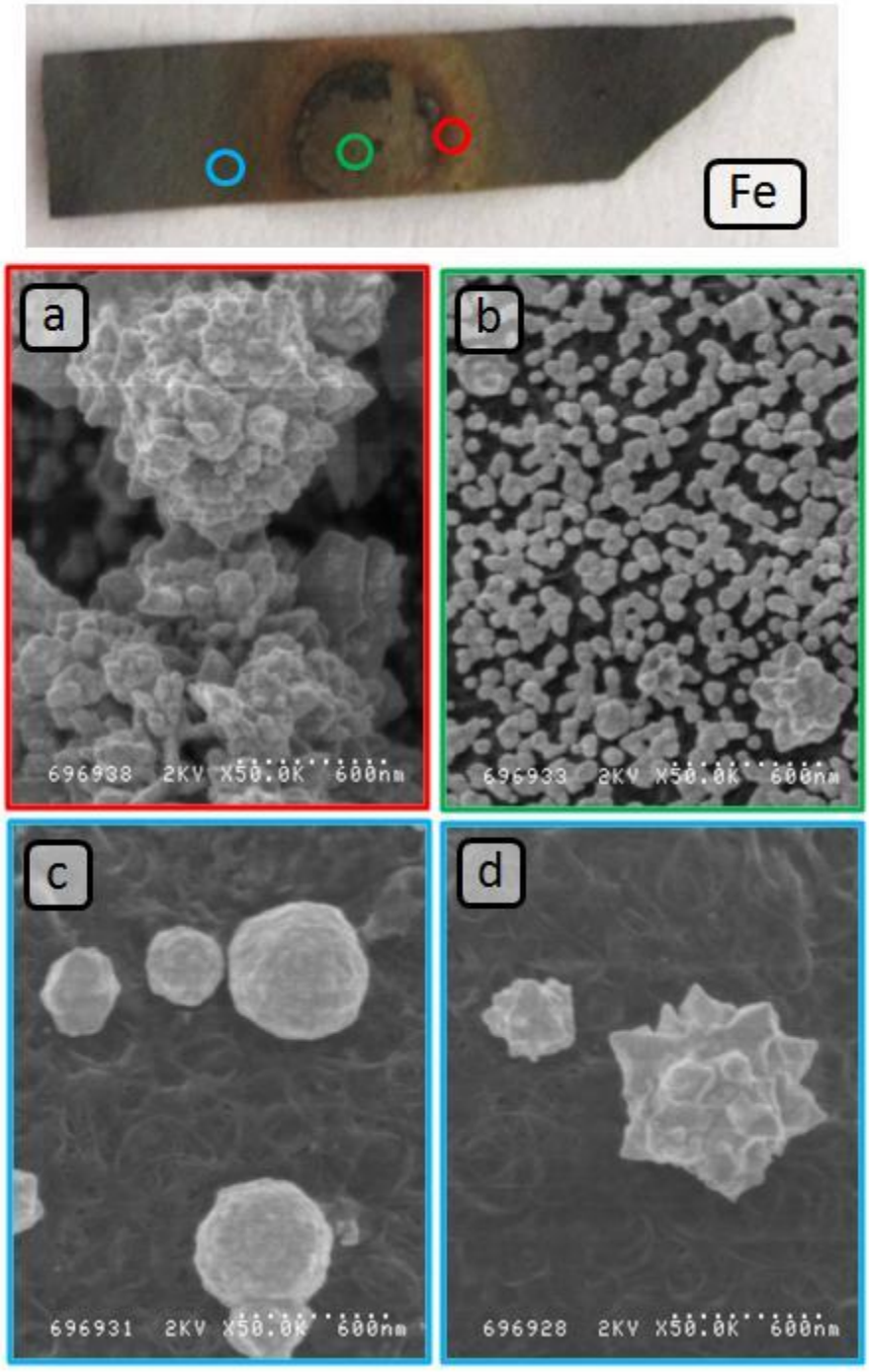

Figure 24. Scanning electron microscope images showing changes in particle size, density, and structure of electroless plating of Au-Fe nanoparticles from $KAuCl_4$ (a) at the edge of (b) underneath and (c-d) outside of the contract area between Fe pellet and single-wall carbon nanotubes (10 seconds exposure). Original figure created by author.

3.4 Conclusions

The ability to increase the electrical conductivity of SWCNT materials using $KAuCl_4$ depends on a number of different factors, including solution concentration and dopant exposure time; which are shown to be closely linked. Sufficient time is required for the chemical dopant to fully penetrate the SWCNT network before the conductivity asymptotes to a maximum value, but too much time results in increased electroless plating without an increase in conductivity. The magnitude of this maximum value is influenced by the choice of carrier solvent and how well that solvent interacts with the SWCNTs. The higher the affinity of the solvent for the SWCNTs the lower the corresponding increase in conductivity. Additionally, impurities such as residual catalyst particles (Ni, Co, Fe, etc.) can react with the $KAuCl_4$ salt causing a decomposition that results in heavy particle plating while suppressing an increase in electrical conductivity.

Chapter 3.5: Electrical Conductivity and Doping Between SWCNTs and MWCNTs through Hybrid Sample Sets

The second half of Chapter 3 deals with mixed systems of SWCNTs and MWCNTs. Because commercial sources of CNTs vary in synthesis method (e.g. HiPCO, CoMoCAT, CVD, arc, flame) they also vary in composition. Amorphous carbon impurities and residual catalyst impurities will impact the quality and usability of the resulting CNT materials. Synthesis methods like CVD will also produce SWCNTs, DWCNTs, and MWCNTs in varying quantities. Understanding how these mixed CNT samples pack, bundle, and chemically dope will influence the ultimate properties of bulk materials.

3.6 Introduction

Before widespread adoption of CNT based conductors, they need to meet the performance of metallic counterparts as well as the production scalability required to produce miles of power transmission lines or data cables. [2, 3] Current materials and manufacturing techniques are struggling at satisfying both aspects. To achieve the higher production rates, control and uniformity in the manufacturing process are often sacrificed. At the higher production volumes, CNTs are produced with increased defect density, increased impurities, and increased distribution of CNT species (e.g. single wall, double wall and multi wall carbon nanotubes).

Understanding how individual CNTs interact with each other in a network depends on a number of different factors including the quantum confined nature of the 1-dimensional materials. The nanoscale properties of individual CNTs are be determined by specific arrangement of carbon atoms (chirality) in the carbon allotrope including the number of concentric shells. Although SWCNTs and MWCNTs are both being investigated to enhance the next generation of power devices only a few reports investigate specific interactions of each CNT type.[63-67] Differences in the conduction mechanism between SWCNTs and MWCNTs could be problematic when

manufacturing methods produce mixtures of each CNT type. Additionally, impurities present in the CNT network such as amorphous carbons, graphitic carbons, and residual catalyst particles (e.g. Fe, Co, Ni, Mo) will also impact how the CNTs interact and respond to chemical dopant species.[3, 16, 17]

To date, only a few reports examine the specific interaction between mixed samples of SWCNTs and MWCNTs on the resulting electrical conductivity of the mixed CNT network.[65-68] In those reports, the authors claim that the maximum current carrying capacity of CNT based materials is a function of the material's electrical and thermal conductivity.[68] The current carrying capacity of a CNT material has been shown to scale linearly with the electrical conductivity and although SWCNTs are more conductive than MWCNTs, MWCNTs have higher thermal stability. Therefore a mixed system of SWCNTs and MWCNTs, although less conductive (S/m), can ultimately withstand higher current densities before it burns itself out.[68] These previous studies were performed on non-chemically doped low conductivity bulk materials. This motivates the need to look at mixed systems of high conductivity (> $1x10^5$ S/m) SWCNTs and MWCNTs and how they respond to chemical dopants.

In the present study, a constructed sample set of SWCNT and MWCNTs free-standing papers are used to measure differences in each material's susceptibility to known CNT dopants (e.g $KAuBr_4$, $I_{2\ (gas)}$, and Tetracyano-p-quinodimethane (TCNQ)). Scanning electron microscopy (SEM) is used to qualitatively assess the nanoscale morphology. Four point probe is used to measure the electrical conductivity (S/m) as a function of SWCNT:-MWCNT loading ratios before and after chemical doping. Raman spectroscopy is used to measure changes in the phonon modes before and after doping.

3.7 Methods and Experimental

3.7.a SWCNT Synthesis

The SWCNTs in this study were synthesized via pulsed laser vaporization using a 1064 nm Nd:YAG laser under previously published conditions.[13, 69, 70] Briefly, SWCNT material was synthesized from a Ni (3 % w/w) and Co (3 % w/w) doped graphite flake (1-2 μm) target (pressed to 25,000 psi) in a 1150°C three-zone tube furnace, and 200 SCCM flowing argon at 760 ± 10 torr. Purification of the as-produced SWCNT material occurs through a series of acid and thermal treatments developed following established procedures.[12, 13, 69, 70] For example, 150 mg of as-produced SWCNT material is brought to reflux at 125 ºC in 3M nitric acid for 16 hours and then is vacuum-filtered onto 1 μm PTFE membrane filter papers with copious amounts of water to remove residual acid. The SWCNT paper from acid reflux was thermally oxidized in air at 525°C at a ramp rate of 10 °C/minute in a Lindberg BlueM 1200 furnace. SEM, TGA, optical absorption, and Raman spectroscopy analyses were conducted during the purification process to assure that the quality of the purification was > 95 % w/w SWCNTs. The abbreviation "pure-SWCNTs" will be used when referencing high purity SWCNT material (purified via the above method) prior to electrochemical cycling in a Li^+ battery coin cell for the remainder of the discussion.

3.7.b MWCNT Synthesis

The MWCNTs used in this work were synthesized using an injection chemical vapor deposition (CVD) reactor with a coaxial injection design following previously published conditions.[71] The injection tip was fabricated using quartz capillary tubing (i.d. 1 mm, o.d. 3 mm) encased in a stainless steel jacket. Synthesis of the MWCNT material was performed in a Lindberg BlueM 3-zone tube furnace at 850 °C. Cyclopentadienyl iron(III) dicarbonyl dimer was used as a

precursor at a concentration of 0.08 M in xylene, a gas flow rate of 0.75 l/min, and a precursor delivery rate of 3.5 ml/h. Raman spectroscopy was used to assess the purity of the as-produced MWCNTs based on a calibration curve developed from a constructed sample set of relative 100 % MWCNTs and 0 % MWCNTs-carbonaceous impurities. The average nanotube diameter is 60 nm, with minimal metal catalyst residue and amorphous carbon.

3.7.c Hybrid Sample Set Fabrication

The constructed sample set of freestanding hybrid SWCNT – MWCNT samples were prepared by dispersion in N,N-dimethylacetamide (DMA) using an ultrasonic bath. The total mass of each CNT hybrid dispersion was kept constant at total carbonaceous mass of 10 mg in 20 mL DMA. Weight loadings of MWCNTs and SWCNTs at were prepared at 20% w/w step increases from 0% - 100% SWCNT in MWCNTs. After homogenizing each dispersion for one hour, the samples were filtered onto a 1 µm PTFE filter paper, rinsed with acetone and dried for two hours in a 100° C vacuum oven. Van der Pauw squares were cut from each sample and used for all doping and conductivity measurements. For clarity, The SWCNT-MWCNT hybrid materials will be referenced by the % w/w SWCNT content (e.g. the 80 % SWCNT – 20 % MWCNT will be referred to as 80 % SWCNT and similarly, the 0 % SWCNT – 100 % MWCNT sample will be referred to as 0 % SWCNT) for the remainder of the chapter.

3.7.d Chemical Doping

Three published chemical dopants used to enhance the electrical conductivity of CNT networks were investigated for the context of this work: potassium tetrabromoaurate, iodine gas, and Tetracyano-p-quinodimethane.

3.7.d.i Potassium tetrabromoaurate ($KAuBr_4$)

Au salts (e.g. $AuCl_3$, $HAuCl_4$, $AuBr_3$, $HAuBr_4$, $KAuCl_4$, $KAuBr_4$) have be demonstrated to be good electrical dopants in CNT networks.[2, 58, 59] $KAuBr_4$ doping solution was prepared at a concentration of 0.001 M by mixing Potassium tetrabromoaurate hydrate (Sigma Aldrich) in deionized water. CNT hybrid materials were exposed to the doping solution for 30 minutes before being dried in a vacuum over at 100 °C for 2 hours.

3.7.d.ii Iodine Gas (I2 gas)

$I_{2\ gas}$ has been shown to be an efficient dopant of CNT networks.[72-74] Recently, the use of I_2 gas as a dopant for DWCNT networks was successful at increasing the electrical conductivity of micron-sized bundles of DWCNTs to $6x10^6$ S/m.[72] $I_{2\ gas}$ doping of the CNT materials was performed by sublimating solid iodine on the CNT hybrid materials using a hotplate at 90 °C. The CNT hybrid materials were exposed to the I_2 gas vapor for approximately 1 hour.

3.7.d.iii Tetracyano-p-quinodimethane (TCNQ)

TCNQ is a known electron-acceptor molecule, which has been successfully used for the preparation of electrically conducting salts and charge-transfer complexes to induce p-type doping by encapsulating CNTs.[75] For this work, TCNQ doping solution of 7,7,8,8-Tetracyanoquinodimethane was prepared in acetonitrile at a concentration of 4 mg/mL. CNT hybrid electrodes were exposed to the TCNQ doping solution for 30 minutes before drying in a vacuum oven at 100 °C for 2 hours.

3.7.e Electrical Conductivity Measurements

The Van der Pauw method was used to measure the electrical conductivity of the SWCNT-MWCNT hybrid materials.[57] The method was followed as described in chapter 3. For quick reference the Van der Pauw equation (1) is provided again below:

$$e^{\frac{-\pi * R_{length} * d}{\rho}} + e^{\frac{-\pi * R_{width} * d}{\rho}} = 1 \quad (1)$$

R_{length} and R_{width} are the averaged measured resistance (Ω) values perpendicular to each other along the edges of the Van der Pauw SWCNT square, d is the thickness of the SWCNT paper and ρ is the resistivity (Ωm) of the SWCNT paper which numerically satisfies the Van der Pauw equation.

3.7.f Characterization

The SWCNT material was characterized via scanning electron microscopy (SEM), optical spectroscopy, thermogravimetric analysis (TGA), and Raman spectroscopy. SEM analysis was performed using a Hitachi S-900 field emission electron microscope with an accelerating voltage of 2 kV. Optical absorption spectroscopy was performed in N,N-dimethylacetamide (DMA) 99+ % spectro-photometric grade (Sigma Aldrich) with a Perkin-Elmer Lambda 900 spectrophotometer from 300 nm – 1600 nm. SWCNT carbonaceous purity (w/w %) was obtained from the peak ratios of the absorption maxima at 650 nm (1.9 eV) and 950 nm (1.3 eV) using the previously reported method.[69] Raman spectroscopy was performed using a 1.96 eV He-Ne laser with a JY-Horiba Labram spectrophotometer over the range 100 cm^{-1} to 2800 cm^{-1}. TGA was

performed up to 1000°C at 10 ^{o}C/min using a TGA Q5000IR from TA instruments on representative portions of the as-produced SWCNT material.

3.8 Results and Discussion

Optical micrographs were taken on cross-sections of each of the six SWCNT-MWCNT hybrid free-standing papers, and the thicknesses were measured. As the % SWCNT loading increases, the measured thickness of the CNT paper decreased (Figure 25 top). The 100 % SWCNTs paper has an average thickness of 32 µm ± 2 µm and the 0 % SWCNT paper has an average thickness of 96 µm ± 5 µm. As a result, the 0 % SWCNT material has a physical character consistent with a felt in comparison to the 100% SWCNT material that behaves more like a paper textile. SEM images of the hybrid CNT paper surface shows SWCNTs arranging into dense entangled bundles of individual SWCNTs whereas the MWCNTs in the hybrid materials tend to remain rigid and do not form bundled networks. Mixtures of SWCNTs and MWCNTs show SWCNTs wrapping around the MWCNTs and filling the larger mesopores between MWCNTs. The flexibility and bundling properties of the SWCNTs allow for greater filling of the nanoscale network with carbonaceous material and thus result in a reduction of the measured cross-sectional thickness.

The density (g/cc) of each of the hybrid papers was measured and plotted versus SWCNT loading (Figure 25d). As the SWCNT content increases the measured density of the CNT papers increased. Image J software was used to adjust the exposure of the images and calculate an estimated nanoscale void space from each of the SEM micrographs (at 50,000x magnification).Representative images are provided in (Figure 25) for the 100 % SWCNTs and 0 % SWCNTs materials.

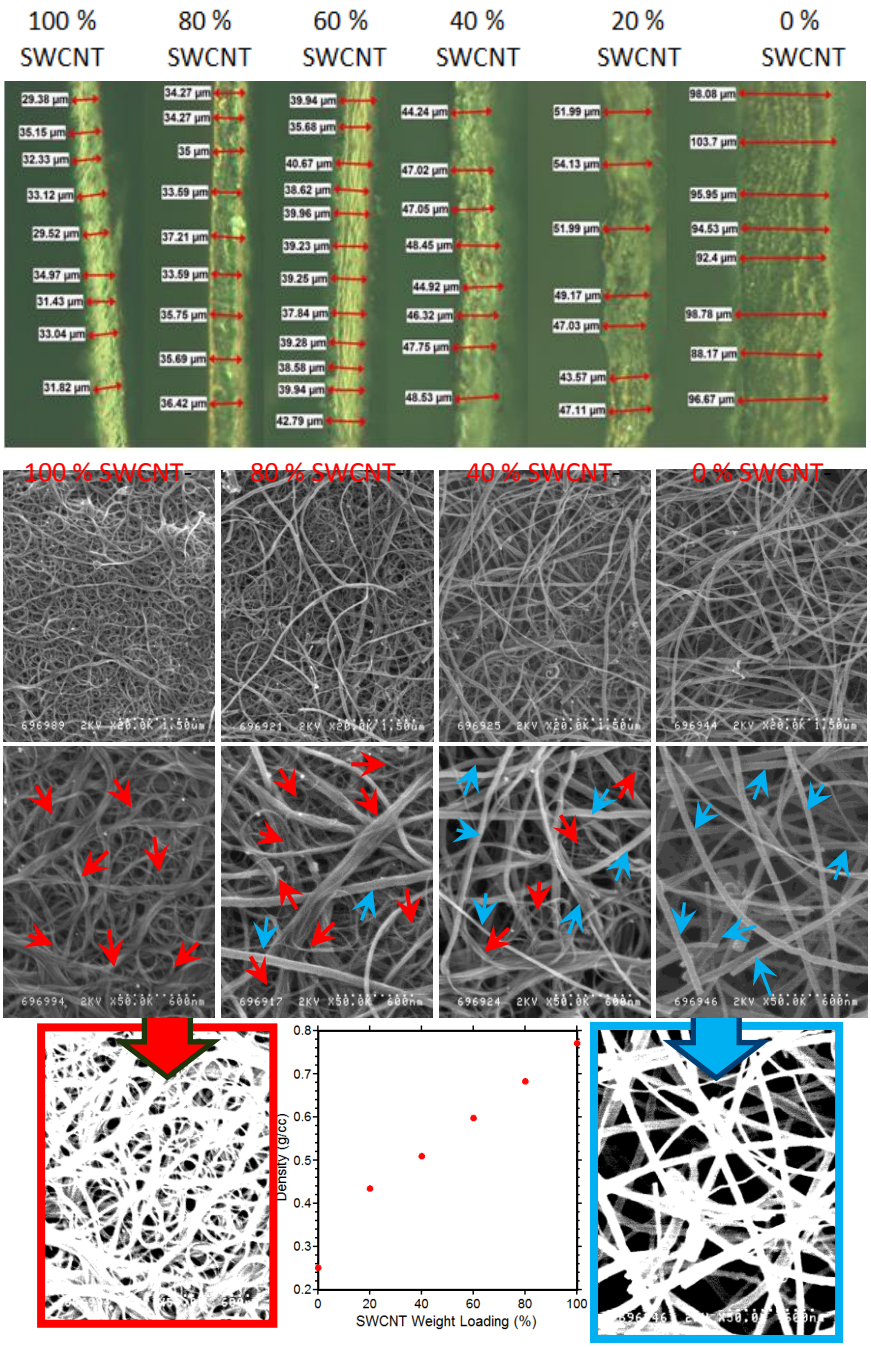

Figure 25. Constructed sample set and cross-sectional optical micrographs (top) of increasing single-wall carbon nanotubes (SWCNTs) in multi walled walled carbon nanotubes (MWCNTs). Scanning electron microscope images at 20K and 50K magnification are provided for representative hybrid materials. SWCNTs are indicated by the red arrows and MWCNTs are indicated by blue arrows. Image J processed micrographs are provided (bottom) to illustrate the differences in the nanoscale void space between SWCNTs and MWCNTs samples with the corresponding measured density for each of the hybrid CNT materials. Original figure created by author.

The Raman spectrum was acquired for each of the hybrid SWCNT-MWCNT free standing papers before and after exposure to $KAuBr_4$, TCNQ and I_2 gas. Baseline measurements prior to chemical doping show increasing RMB, G and G'-peaks Raman intensity (counts) with increasing SWCNT content (Figure 26a). The 0 % SWCNT sample contains the characteristic MWCNT peaks although at really low intensity when taken at equivalent acquisition parameters. Additionally, radial breathing mode (RBM) peaks (between ~100 and 300 cm^{-1}) were not visible in the 0 % SWCNT material. RBM peaks are clearly visible in the 20 % SWCNT sample and continue to increase in relative intensity up to the 100 % SWCNT material. Similarly, the D-band (between ~1250 and 1380 cm^{-1}) has a high intensity in the 0% SWCNT sample and decreases significantly with the addition of SWCNTs. G-band (between ~1400 and 1650 cm^{-1}) splits from a single peak in the 0 % SWCNT material to a multi-peak G^+ and G^- with increasing SWCNT content. This splitting of the G-band is consistent with previous measurements on SWCNT materials.

Both the peak intensity and peak location of the G'-band are sensitive to chemical dopants in the CNTs network. Other factors such as carbonaceous impurities, sidewall defects, and doping species will also shift and alter the peak intensity. Following exposure to the chemical dopants the 0 % SWCNT material showed little response to the doping species (Figure 26b2). The degree of peak shift and suppression increased with increasing SWCNT content. It is expected that larger shifts in both the G' peak location and intensity will correspond to a larger change in the macroscale properties due to greater penetration of the chemical doping species. Based on changes in the G' band it would be expected that the largest change in the electrical conductivity would be measured for the 100 % SWCNT material following exposure to both the $KAuBr_4$ and I_2 gas species (Figure 26d2).

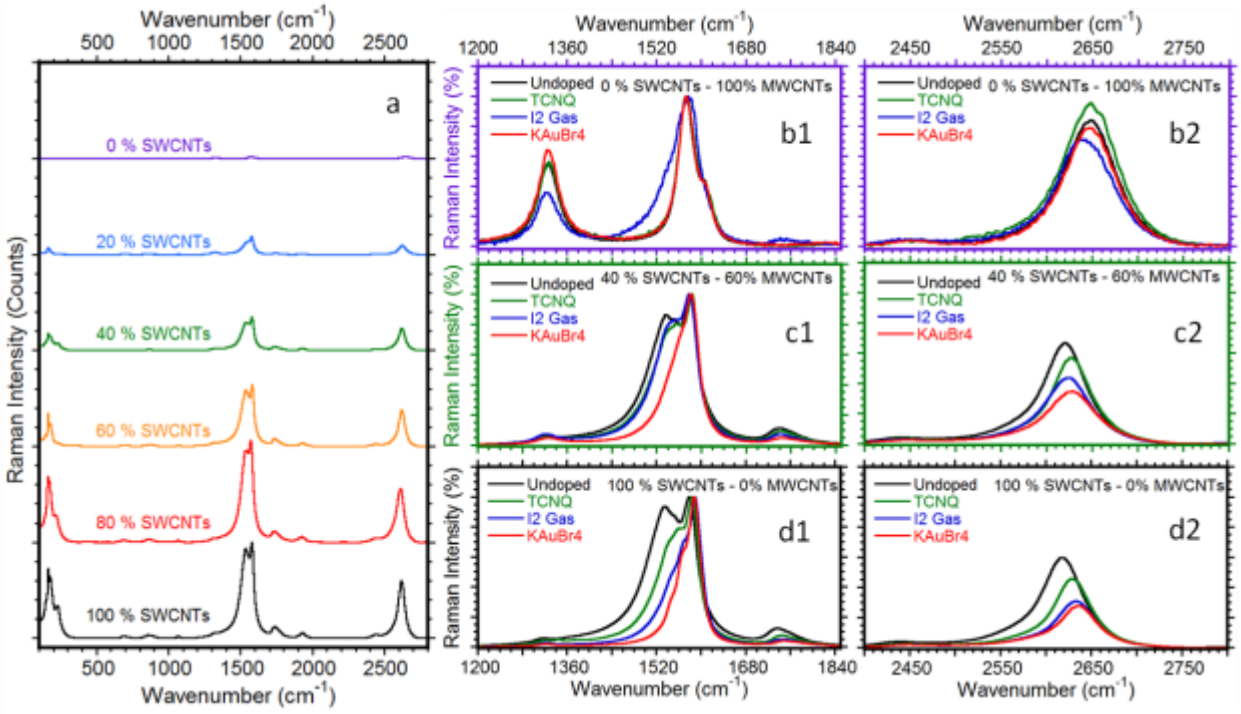

Figure 26. Offset Raman spectra of the free standing hybrid SWCNT-MWCNT papers plotted using the measured signal intensity (a). The Raman spectra flowing exposure to TCNQ, $KAuBr_4$, and I_2 gas are plotted as overlaid curves normalized to the each spectra's G band intensity for the 0 % SWCNTs (b), 40 % SWCNT (c) and 100 % SWCNT (d) representative hybrid materials. (1) and (2) refer to zoomed in regions of the D (~1325 cm^{-1}) and G-Bands (~1500-1650 cm^{-1}) and the G' band (~2600 cm^{-1}) respectively. The plotted Raman data is a combination of three different measurement points taken on each sample, averaged, and baseline corrected. Original figure created by author.

The electrical conductivity of the SWCNT-MWCNT free standing hybrid materials was measured before and after exposure to chemical doping (Figure 27a). In the baseline measurements of the hybrid papers a small reduction in the absolute resistance was measures as the samples moved towards increasing % SWCNT content. The decrease in resistance of the undoped measurements is attributed to a more dense nanoscale network with better electrical percolation networks achieved in the highly entangled bundled SWCNTs. When the reduced

thickness of the Van der Pauw squares is taken into account there is a further increase in the calculated electrical conductivity as the % SWCNTs increases.

Following exposure to the three chemical dopants, an increase in the electrical conductivity was measured for all of the hybrid CNT materials containing SWCNTs. No increase in the electrical conductivity over the baseline value was measured for the 0 % SWCNTs material. The measured increase in electrical conductivity followings a linear relationship for each of the chemical dopants that are proportional to the % SWCNT content (Figure 27b). The highest increase in the electrical conductivity was measured for the 100 % SWCNT materials doped with $KAuBr_4$ followed closely by I_2 gas. $KAuBr_4$ and I_2 gas also showed the largest peak shift (cm^{-1}) and suppression of the G' peak in the Raman spectra (Figure 26d2).

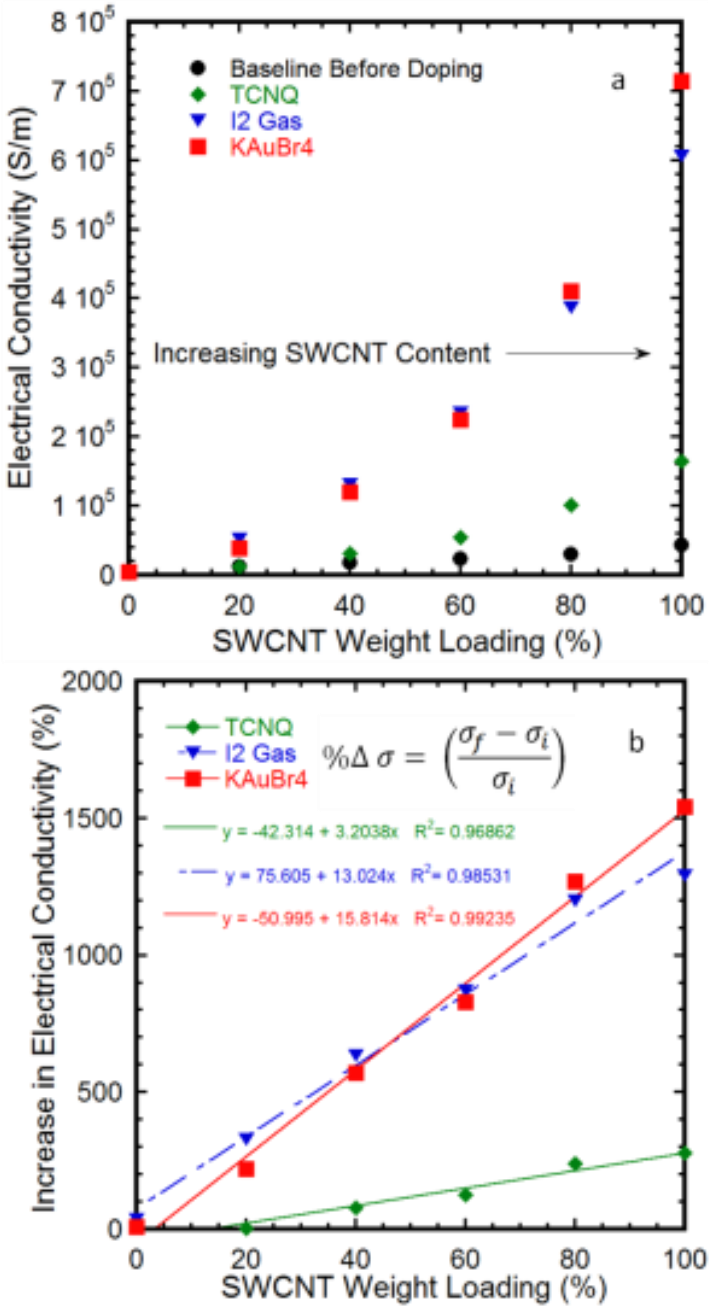

Figure 27. Electrical conductivity (S/m) of single-wall carbon nanotubes (increasing concentration towards the right y-axis) in and multi walled carbon nanotubes (decreasing concentration towards the right y-axis) hybrid papers before and after chemical doping with TCNQ, $KAuBr_4$, and I_2 gas. Measurement error is within the data points. Original figure created by author.

The susceptibility of the hybrid SWCNT-MWCNT materials to the chemical dopants is attributed to the nanoscale morphology differences between the SWCNT and MWCNT materials. Previous studies show a reduction in the tunneling barrier between neighboring SWCNT materials from the addition of chemical dopants.[2] It should be noted that the CNT intersection points have a substantially higher contact resistance than the internal resistance of an individual CNT.[3] This would imply that the bundled and highly entangled morphology of the SWCNTs allows for the greatest extent of interaction between the doping species and the SWCNTs to reduce the tunneling barrier between SWCNTs. The more rigid MWCNTs have fewer points of intersection and thus have a reduced number of opportunities for the $KAuBr_4$, I_2 gas and TCNQ to lower the tunneling barrier and increase the network's electrical conductivity. The bundled and entangled network formed by SWCNTs allow for the greatest penetration of the species examined in this study. Therefore to maximize the electrical conductivity of CNT conductors with ionic dopants moving to sources of CNTs that are predominantly SWCNT, DWCNT will allow for the greatest increase in the electrical conductivity over the baseline undoped network.

3.9 Conclusions

In this study, SWCNT-MWCNT hybrid electrodes were fabricated by combining increasing mass loadings of SWCNTs with MWCNTs at 20 % w/w increments. The hybrid electrodes were exposed to three dopants: $KAuBr_4$, I_2 gas, and TCNQ. The electrical conductivity of the treated CNT hybrid papers was measured via four point probe and compared to baseline conductivity values. An increase in the electrical conductivity was measured for all SWCNT-containing hybrid materials and the largest increase in electrical conductivity was measured for the 100 %

SWCNT material for all three dopants investigated. Changes in the G and G' bands of the Raman spectra were measured for SWCNT containing hybrid materials and correlate with changes in the electrical properties. The results suggest that to achieve bulk CNT conductors with the electrical conductivity approaching metals, it's important to balance the inter and intra CNT conduction networks. Therefore, the use of smaller diameter CNTs, such as SWCNTs, will allow for the largest increase in electrical conductivity from chemical doping species.

There are several limitations to the work presented in this section. The research focused on a narrow subset of chemical dopants and could be expanded to include a larger scope of chemicals. Additionally, more CNT species could be included in the analysis such as double wall carbon nanotubes (DWCNTs).

Chapter 4: Life Cycle of CNT Conductors: Manufacturing of CNT Conductors

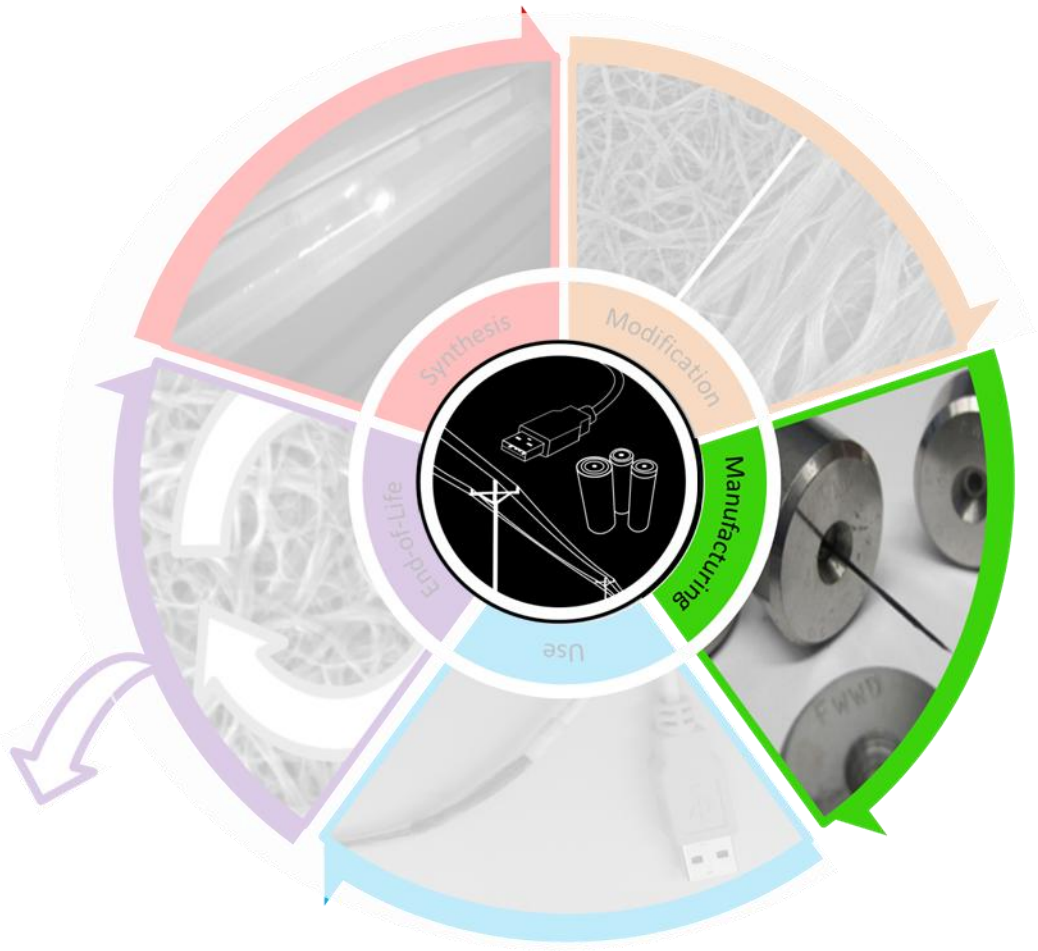

Figure 28. This chapter of the dissertaion looks at methods of manufacturing CNT based wires and cables. Original figure created by author.

Chapter 4 of the dissertation builds off of the findings of chapter 3 and investigates the manufacturing stage of CNT conductor life cycle. Specifically in this section, superacids are used to dissolve CNTs at high weight loadings and reassemble them into highly dense aligned bundles. Semi-continuous wires can be extruded from the high weight loading dispersions. Modified SWCNT electrodes can also be produced by controlling the nanoscale morphology

(e.g. bundling, alignment) though applied current and thermal energy (heat). Progress towards these modifications will be discussed.

4.1 Introduction

Since the first publication on the use of superacids to disperse CNTs in 2004, a lot of progress has been made to modify the nanoscale structure and morphology of CNT networks. Superacid has been used to make high weight loading dispersions of CNTs (2 orders of magnitude higher than organic solvents and an order of magnitude higher than surfactants). Superacids are extremely effective dispersing agents for CNTs because of their ability to directly protonate the sidewalls. The buildup of positive charges on the surface of the CNTs is enough to overcome the attractive Van der Wals forces that keep nanotubes in closely packed bundles. If a sufficient concentration (> 11% w/w) of CNTs are dispersed, the positive charges on the CNT surface begin to assemble themselves in a minimum energy (hexagonally close packed) state. The assembly of individual nanotubes in to larger macro structures of aligned tubes is referred to as liquid crystals.

Rice University developed a mechanical extrusion method for fabrication continuous CNT wires from superacid dispersions. Although a number of different superacids have the capability to disperse CNTs in high enough weight loading to extrude wires, they identified chlorosulfonic acid (CSA) as having the highest dispersion limit and thus use CSA for the majority of their extrusion tests. Of particular importance to achieving highly uniform dispersions and extrusion of conductive wires are CNT purity, CNT diameter, and CNT length.[76-79] Of particular importance to achieving highly uniform dispersions and extrusion of conductive wires extrusion tip diameter, choice of solvent bath, and the weight loading of CNTs in dispersion are more important factors.[5, 6]

4.2 Experimental

Following the Rice University extrusion procedure, SWCNTs were dispersed in chlorosulfonic acid (CSA) using a combination of mixing techniques. Although SWCNTs will spontaneously disperse in the highly protonating superacids, mechanical mixing methods are required to achieve higher weight loadings sufficient to form liquid crystal dispersions (>11 % w/w CNTs in CSA).[76] A rotor stator mixer (Figure 29) was used in combination with a dual centrifugal mixer and a stir bar/stir plate to slowly increase SWCNT concentration. As the SWCNT weight fraction in CSA increases so does the viscosity of the dispersion. At very high weight loadings >20 mg/mL the viscosity requires extended dual centrifugal mixing to keep the material mixing. At very high weight loadings >30 mg/mL the dispersion becomes too viscous and no longer freely flows with the rotor stator or stir plate mixing methods, and mixing must be achieved solely by the centrifugal technique.

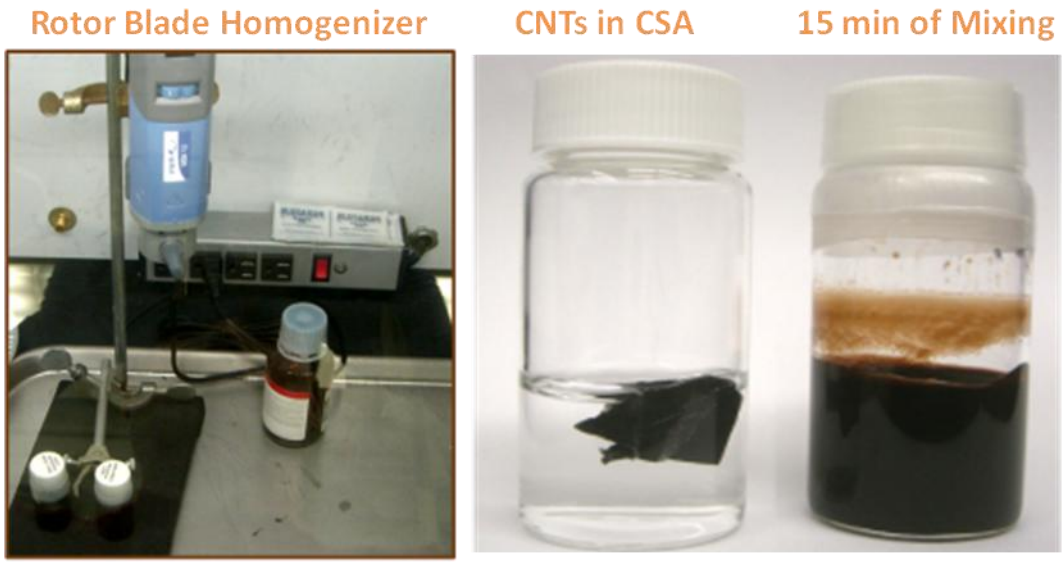

Figure 29. Mixing apparatus for dispersing single-wall carbon nanotubes in chlorosulfonic acid. Original figure created by author.

From these high weight loading dispersions (20-40 mg SWCNTs in 1 mL CSA), semi-continuous SWCNT wires can be extruded into a solvent bath. Extrusions SWCNT wires were performed using a glass syringe, with 20, 22, or 24 gauge stainless steel needle tips. The dispersion was extruded using a syringe pump at a rate between 0.05 - 0.1 mL/min into a solvent bath. Choice of solvent impacts both the quality and uniformity of the extruded wire. Solvents such as deionized water tend to remove the CSA too quickly from the wire and results in rapid gas evolution and damage to the wire sidewall. Similarly, solvents such as chloroform remove the CSA too slowly and lead to breaks and in the extruded wires. Acetone was determined to provide rapid removal of CSA without the formation of hydrochloric acid gas. Extruded wires were then coiled onto spools for drying using a variable speed torque motor matched to the extrusion rate of the wires. Extruded wires were dried in a vacuum oven at 100 °C for 1 hour. A schematic representation of the extrusion process is provided in Figure 30.

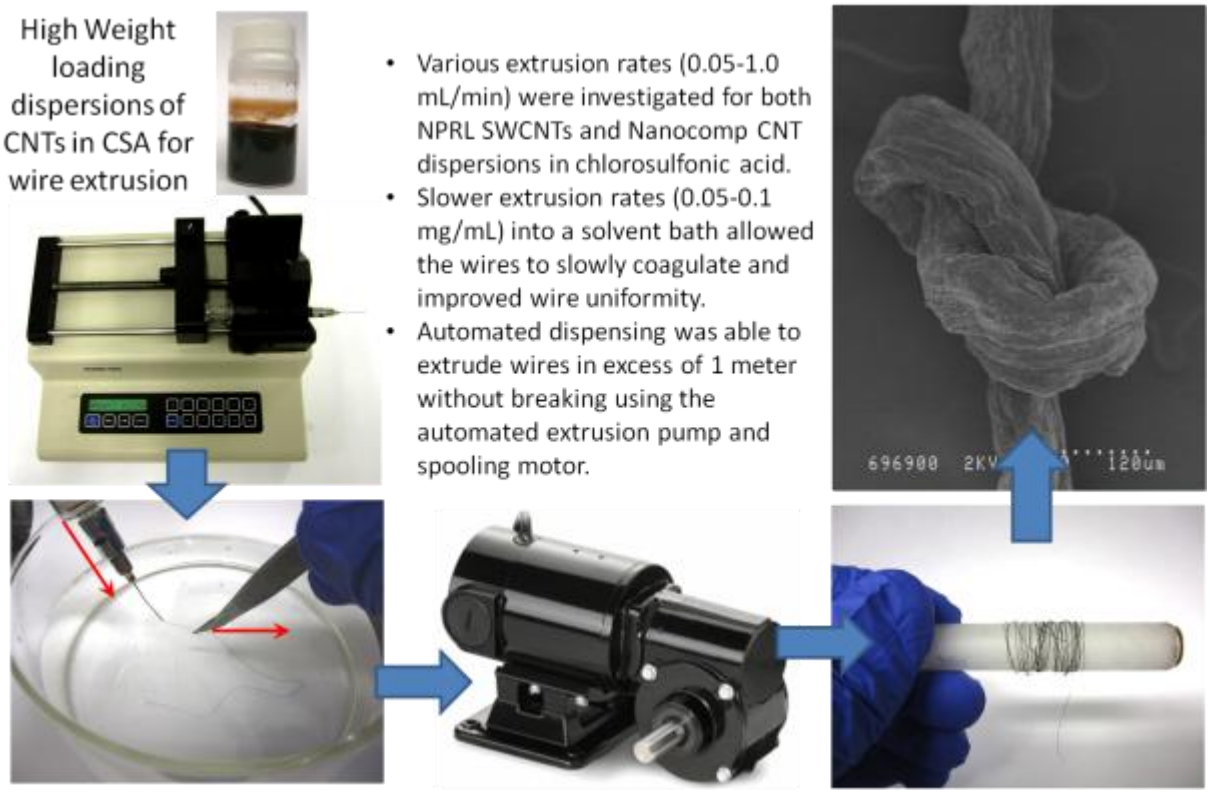

Figure 30. Schematic representation of the CNT wire extrusion process from dispersions of carbon nanotubes in chlorosulfonic acid. Original figure created by author.

4.3 Results and Discussion

The extruded SWCNT wires can have non-uniform cross-sectional geometries based on the extrusion parameters used. Because the electrical conductivity of a wire is the product of the unit resistance per length and the geometrical cross-sectional area accurately quantifying the cross sectional area is important. Using a 4-point probe station and measuring the distance between voltage probes results in a resistance per length measurement with relatively small error bars. Measuring a material's cross-sectional area accurately can pose significantly more problems especially when the conductor is irregularly shaped. Smaller diameter conductors will be more

affected by error in the cross-sectional area whereas larger diameter conductors will be affected proportionately less.

Cross-sectional area dependent measurements (e.g. conductivity and maximum breaking stress) of extruded CNT wires, are especially subject to error in their area measurement due to large non-uniformities along their length. A lot of conditions determine the geometrical shape of extruded CNT wires such as type of solvent bath used, extrusion tip diameter, and weight loadings of CNTs in CSA. Figure 31 illustrates three different geometrical cross-sections that can be obtained from extrusions using CSA. Most common is a solid core wire, which is composed of highly aligned and dense CNT networks. However, if the solid core wires solidify while touching a surface, they can easily be formed into thin, flat ribbon like structures. Similarly, ribbon-like structures can wrap onto themselves, forming a hollow core cylindrical wire. Because of these different geometries assumptions on the cross-sectional composition of CNT conductors can result in large error propagation in the calculated electrical conductivity and maximum breaking strength.

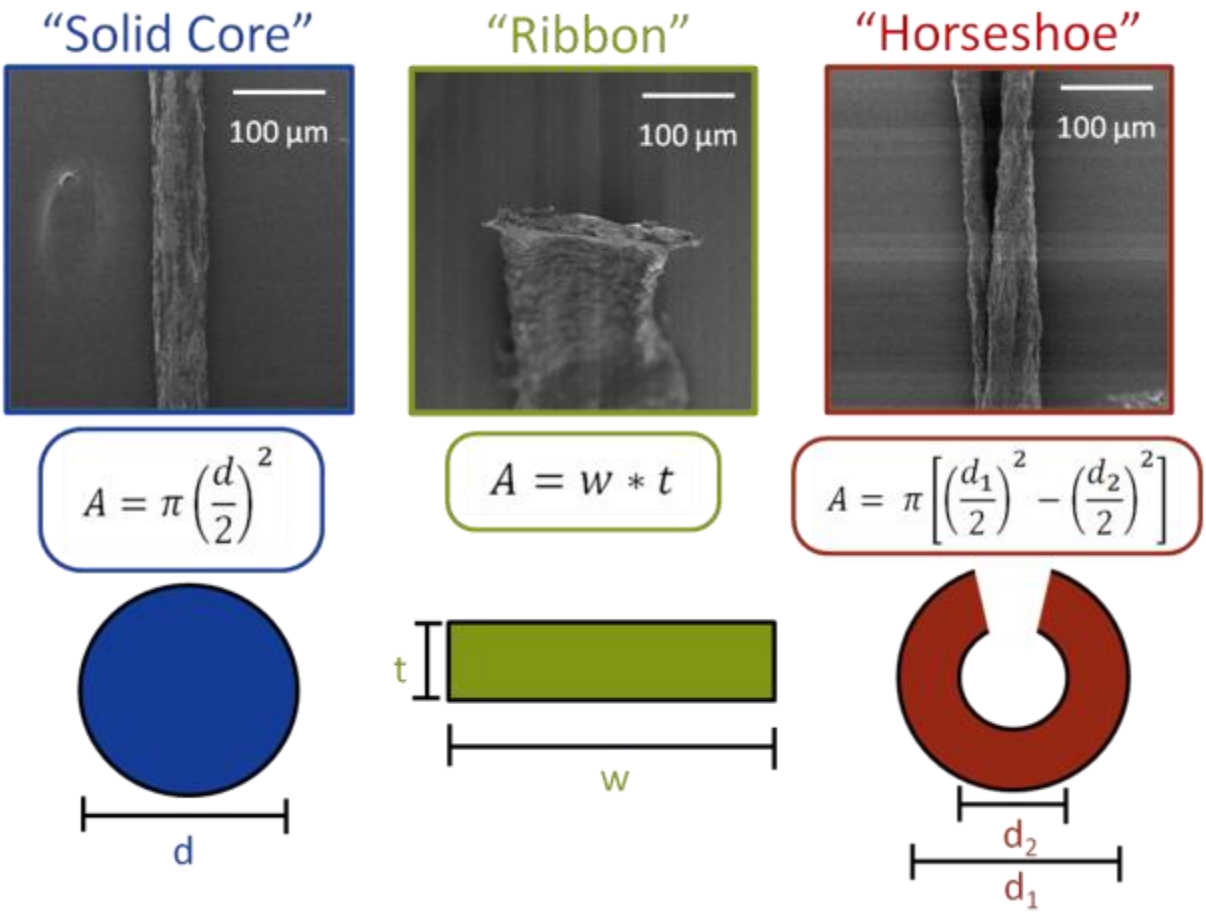

Figure 31. Scanning electron micrographs and their corresponding cross-sectional area equations for single-wall carbon nanotube extruded wires. Original figure created by author.

A series of extruded CNT wires were used to illustrate the effect of measurement error on the cross-sectional area dependent properties of the wires. Figure 32 shows how the calculated properties of a single wire would change if only one diameter measurement was used to calculate the electrical conductivity and maximum breaking stress of the material. The SWCNT wire was extruded from a CSA dispersion at 30 mg/mL weight loading into an acetone bath. Based on SEM images, the actual shape of the wire is a "horseshoe" geometry. Using only the SEM outer diameter measurement, a modified cross sectional area was calculated for an assumed

rectangular and solid core wire. From the modified cross-sectional a reduction in both the calculated conductivity and breaking stress resulted. Solid core geometry overestimated the cross-sectional area because it assumed the void space and the horseshoe geometry were occupied by conductive material. Similarly, the rectangular form factor also overestimated the cross-sectional area by filling in the structure with length and width square measurements.

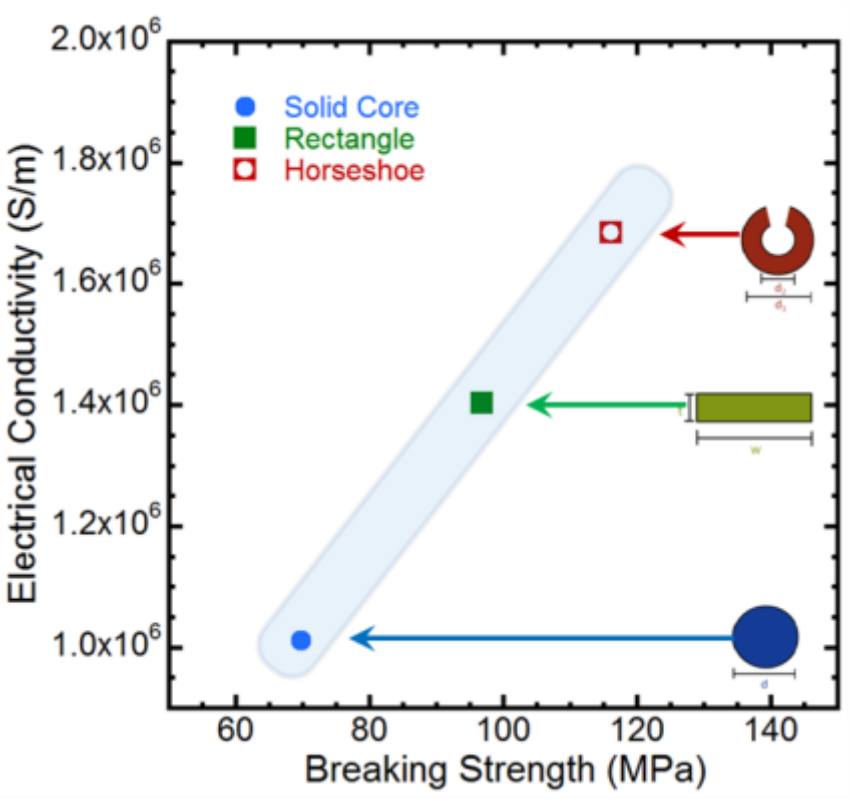

Figure 32. The electrical conductivity (S/m) and breaking strength (MPa) of a "horseshoe" shaped extruded single-wall carbon nanotube were recalculated if a rectangular and solid core wire geometries were assumed to highlight the decrease in materials properties induced by error in the cross-sectional area measurement. Original figure created by author.

The above plot shows the conductivity and breaking pressure of the best 30 mg/mL extruded wire. Using the correct “horseshoe” geometry from the SEM images the highest measured breaking force was 120 MPa with a corresponding electrical conductivity of $1.7x10^6$ S/m.

SWCNT alignment is an important factor for maximizing the electrical conductivity of bulk SWCNT conductors. To achieve alignment in extruded SWCNT wires, a higher weight loading of SWCNTs in CSA dispersions leads to the formation of liquid crystals in solution. The liquid crystals contribute to long range order in bundled SWCNT networks. Extrusion of these liquid crystals through a syringe needle tip forces liquid crystal grain boundaries to align parallel to the direction of the extrusion. Upon injection into the solvent bath, the CSA is removed from the CNT network causing the liquid crystals to collapse onto themselves, forming highly dense bundled networks of aligned SWCNTs. When the CSA is completely removed from the extruded wires individual and bundled CNTs are fixed in a direction parallel to conduction along the length of the wire. Figure 33 shows SEM images of extruded wire surface with highly aligned bundled networks of CNTs down the length of the wire. A section of the wire's surface was fractured and internal network was exposed. The internal part of the extruded CNT wire reveals highly aligned networks not only on the surface but on the interior of the wires with little void space present.

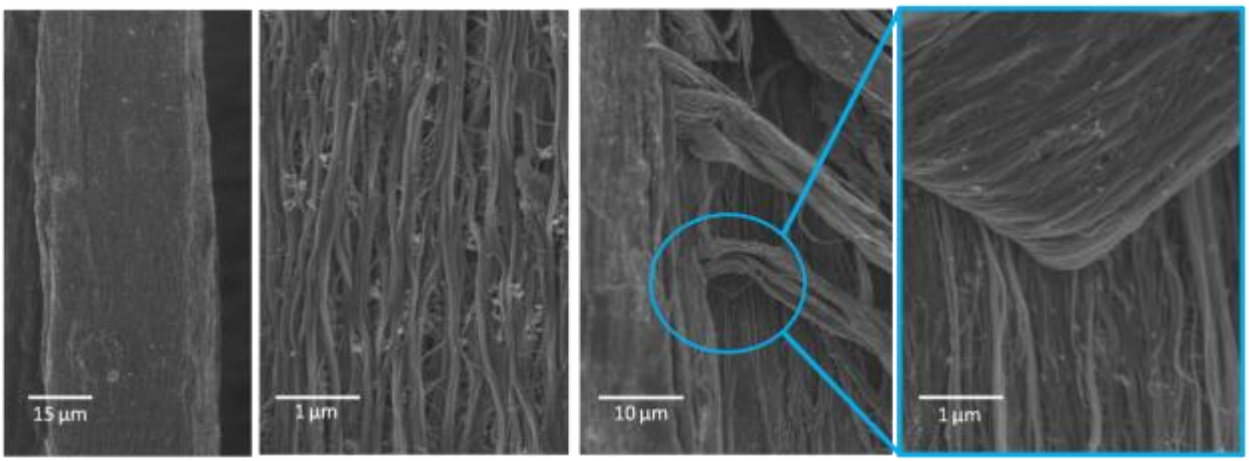

Figure 33. Scanning electron micrographs of an extruded single-wall carbon nanotube (SWCNT) extruded wire. The surface morphology is comprised of highly bundled, dense SWCNT networks. Magnifying the blue section of a cut location along the wire shows the alignment of SWCNTs continues below the surface and into the core of the wire. Original figure created by author.

Instead of the extrusion of wires, the same liquid crystal dispersions can be used to form SWCNT electrodes with different bundling states. The dispersion of CNTs in CSA is capable of producing highly individualized CNTs as well as highly bundled entangled networks through selective coagulation of the material. Changes in the bundling state can reveal important factors on how CNT networks conduct electricity and respond to chemical dopants. To control the bundling state of CNTs, low weight loading dispersions (less than 1 mg/mL) of CNTs in CSA were used to individualize SWCNTs. If these low weight loading dispersions are vacuum filtered, as is, into freestanding SWCNT papers, the individualized SWCNTs will remain relatively unbundled. However, if water is slowly introduced into the CSA dispersions, it will lower the dispersion limit of the CSA until CNTs begin to precipitate from dispersion. As the CNTs precipitate, they bundle, forming entangled networks of hexagonally close packed arrays. The extent and degree of bundling is determined by how much water is used to decompose the CSA. When the desired level of coagulation is achieved (more coagulation results in larger

SWCNT bundles), vacuum filtration can be used to remove remaining CSA. Once the filter paper is dried freestanding SWCNT electrodes can be removed which retail the highly bundled coagulated SWCNTs. Differences in the network morphology are clearly visible using scanning electron microscopy (Figure 34) between the non-coagulated and coagulated samples.

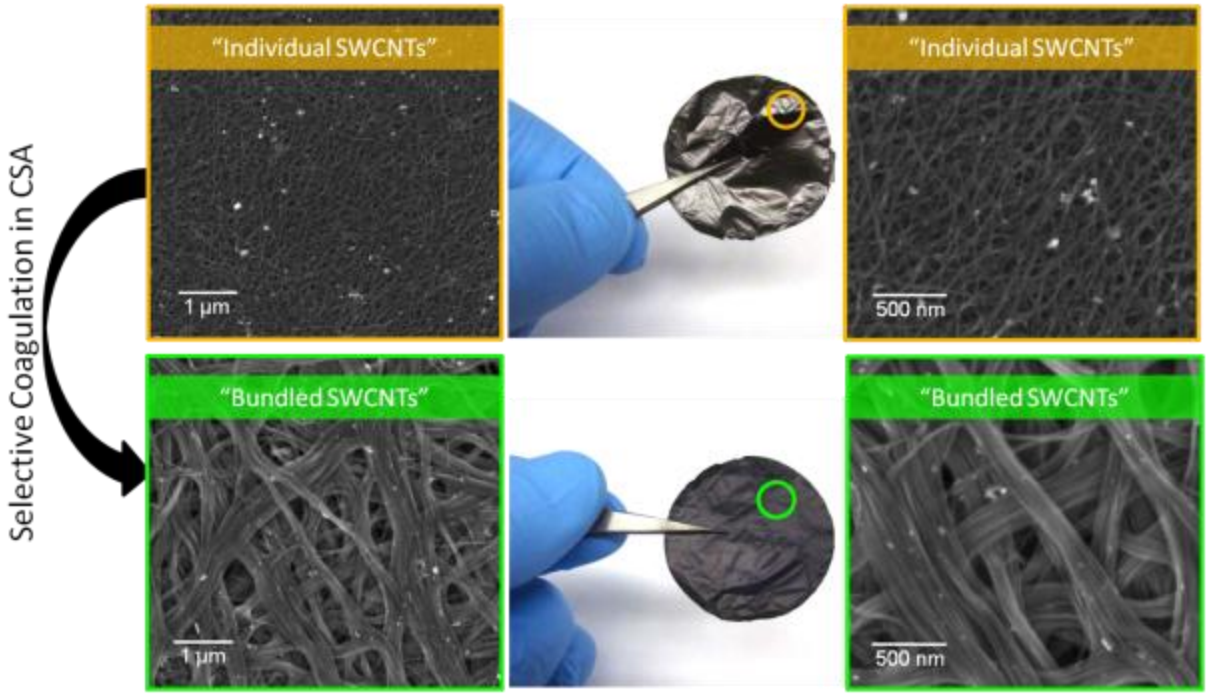

Figure 34. Scanning electron micrographs of individualized and bundled single-wall carbon nanotube free standing papers prepared though selective coagulation by addition of water to chlorosulfonic acid dispersions (~1 mg/mL). Original figure created by author.

In addition to the use of water to cause coagulation and bundling of SWCNTs in dispersion, the use of an applied current and thermal energy (100 °C hot plate) can also be used to influence coagulation. Figure 35 shows the change in morphology of SWCNT papers prepared from dispersions in CSA. Coagulation occurs in the SWCNT dispersions as the thermal energy (heat) decomposes the unstable CSA molecule. As CSA is heated it breaks down into sulfuric acid and hydrochloric acid gas, the dispersion limit of CSA is reduced. As the SWCNTs begin to

precipitate, they begin to bundle together and eventually form solid free standing SWCNT papers (Figure 35). Because evaporation of the CSA is occurring radially inwards, the surface tension while drying causes the liquid crystals of SWCNTs to orientate themselves radially inwards (illustrated graphically in Figure 36). Similarly, when an electric current is applied to the dispersion prior to thermal heating SWCNTs begin aligning themselves parallel to the direction of the applied current. As the CSA is removed, the already aligned SWCNTs begin to coagulate together and form bundles that precipitate and solidify, forming a free standing paper.

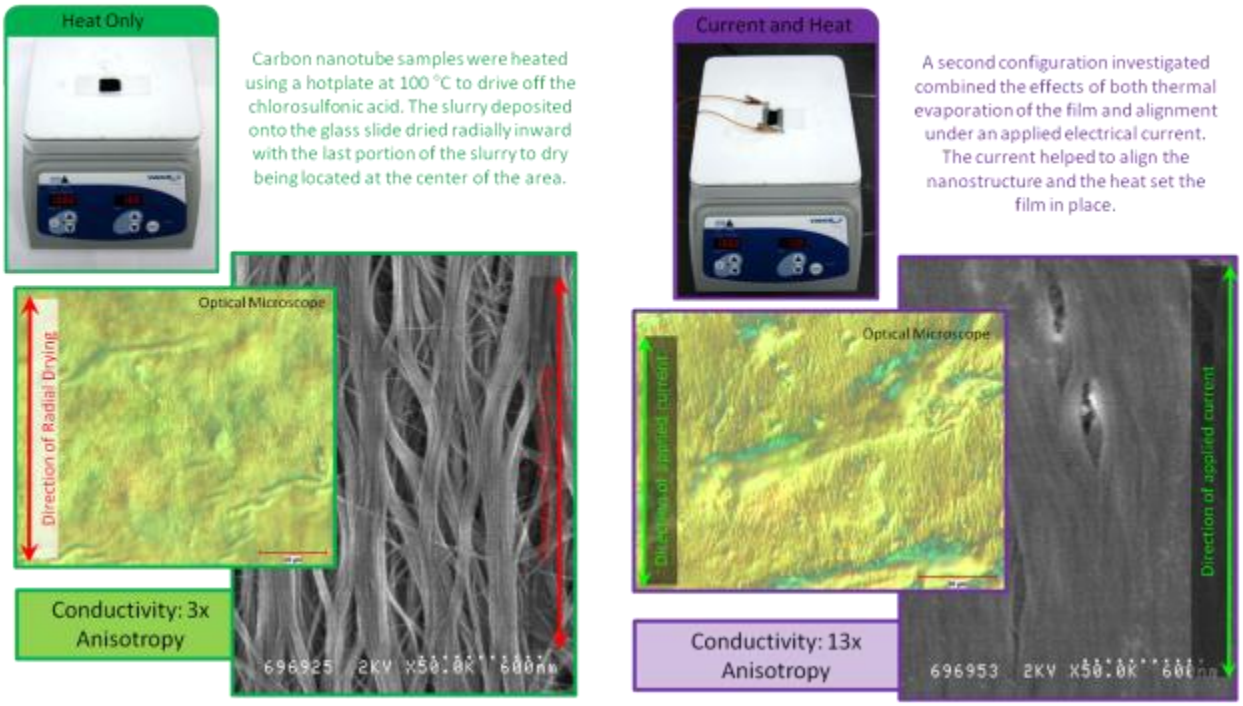

Figure 35. Scanning electron micrographs of SWCNTs aligned from dispersions in CSA with applied current and heat. Original figure created by author.

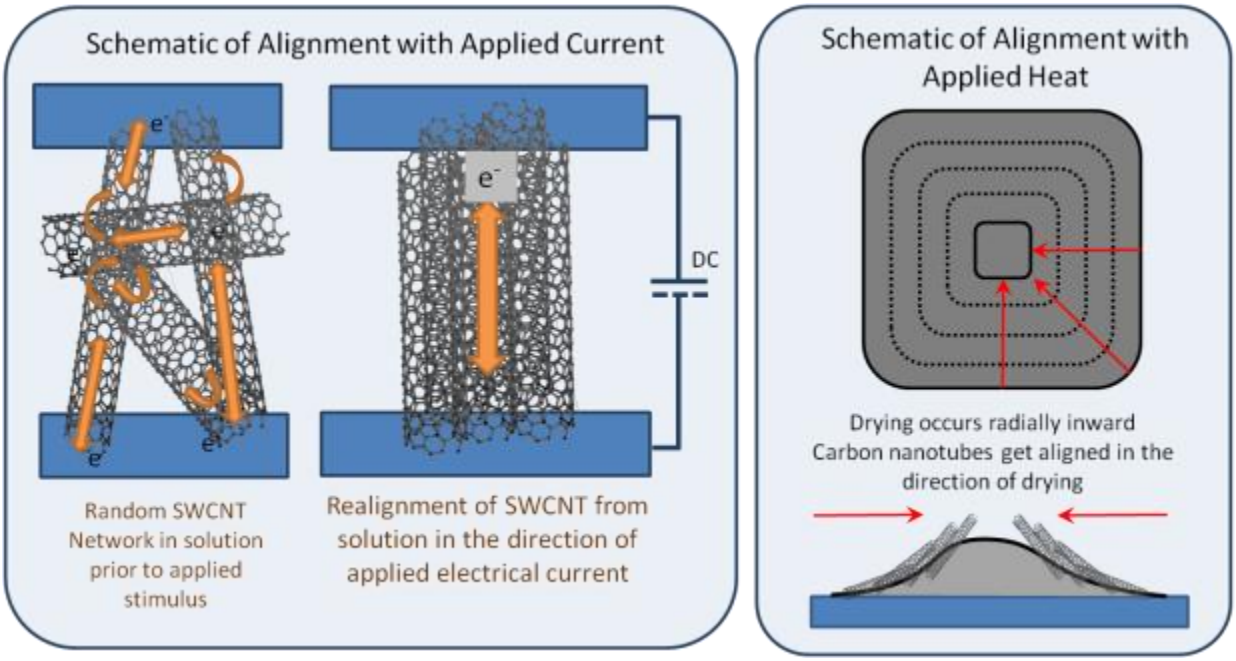

Figure 36. Schematic representation of the proposed alignment method during the coagulations of SWCNTs in to aligned networks. Original figure created by author.

CSA also can act as an acid dopant in the extruded SWCNT wires and free standing papers. Successively higher burn temperatures were used to determine the thermal stability of CSA doped extruded wires. It can be shown in Figure 37, that temperatures at or below 200°C, result in little change in measured electrical conductivity. At thermal oxidation temperatures of 300°C, a decomposition of the CSA resulted in evolution of white gas and corresponded with a measured decrease in electrical conductivity. A second decomposition and evolution of white gas occurred at a thermal oxidation temperature of 400°C. Following this thermal oxidation temperature the lowest electrical conductivity value measured for the wires (red data points in Figure 37). At 400°C thermal oxidation temperature the chemical doping effect of CSA was removed to a point where a minimum conductivity was measured for the extruded wires.

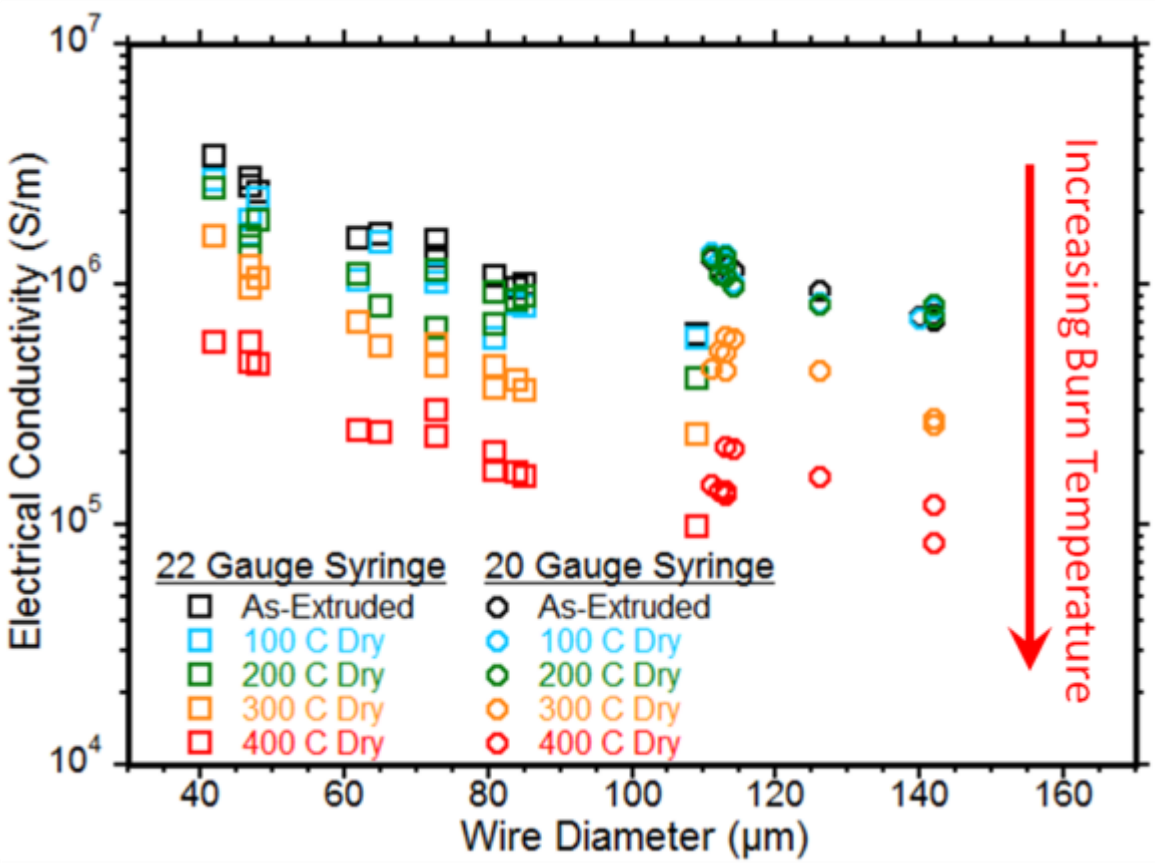

Figure 37. A 35 mg/mL dispersion of single-wall carbon nanotube in chlorosulfonic acid (CSA) was extruded using 22 and 20 gauge syringe tips. The extruded wires were then dried at increasing temperatures in 100 °C increments up to 400 °C. The electrical conductivity (S/m) was measured as a function of temperature to determine the thermal stability of the CSA. Absolute conductivity values varied across several wires, the raw data is plotted with individual sample measurement error within the data points. Original figure created by author.

Raman analysis (Figure 38) confirms the removal of CSA from the extruded SWCNT wires following the 400 °C burn. CSA suppresses both the radial breathing modes and the G' band relative to the intensity of the G band. Additionally, doping from CSA changes the line shape of the G-band from multiple peaks to the right G^- peak. Following removal of the CSA at 400 °C,

the RBM intensity, G band line shape, and the G ' band intensity return to values consistent with high purity undoped SWCNTs.

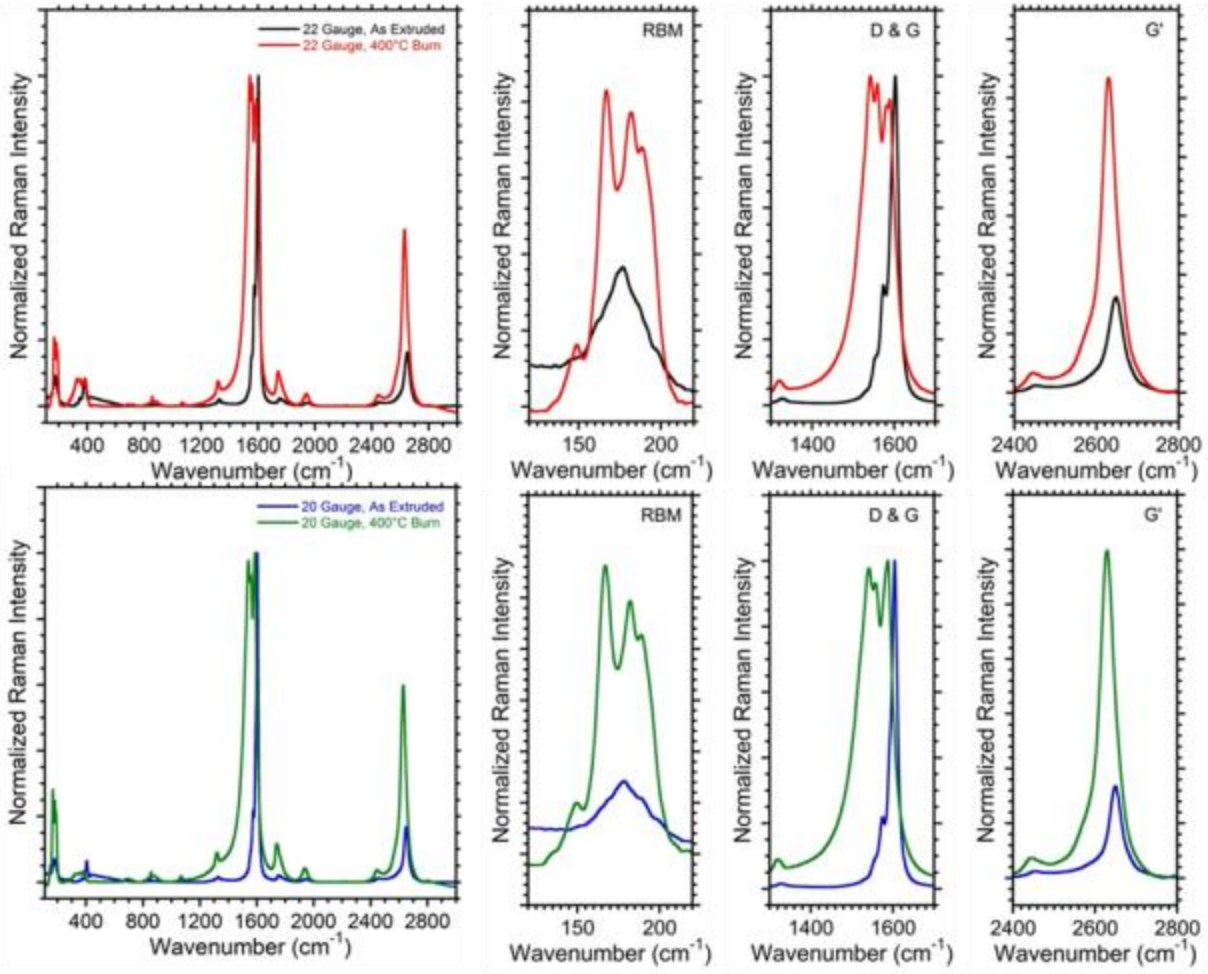

Figure 38. Raman spectroscopy of chlorosulfonic acid doped single-wall carbon nanotube extruded wires before and after 400 °C burn for both 22 and 20 gauge syringe needle extrusion tips. The plotted Raman data is a combination of three different measurement points taken on each sample, averaged, and baseline corrected. Original figure created by author.

4.4 Conclusions

Across all of the CNT wire extrusion trials a wide range of wire diameters and conductivities were measured. Conductivities ranged from low ($1x10^4$ S/m) to the highest conductivity wires at

$4.4x10^6$ S/m. The highest values from this dissertation are compared to the highest values measured by Rice University and Nanocomp Technologies Inc. in Figure 39. The ability to modify, control, and extrude CNT wires represents a significant step forward in the processing and development of functional carbon based conductors to replace metallic wires.

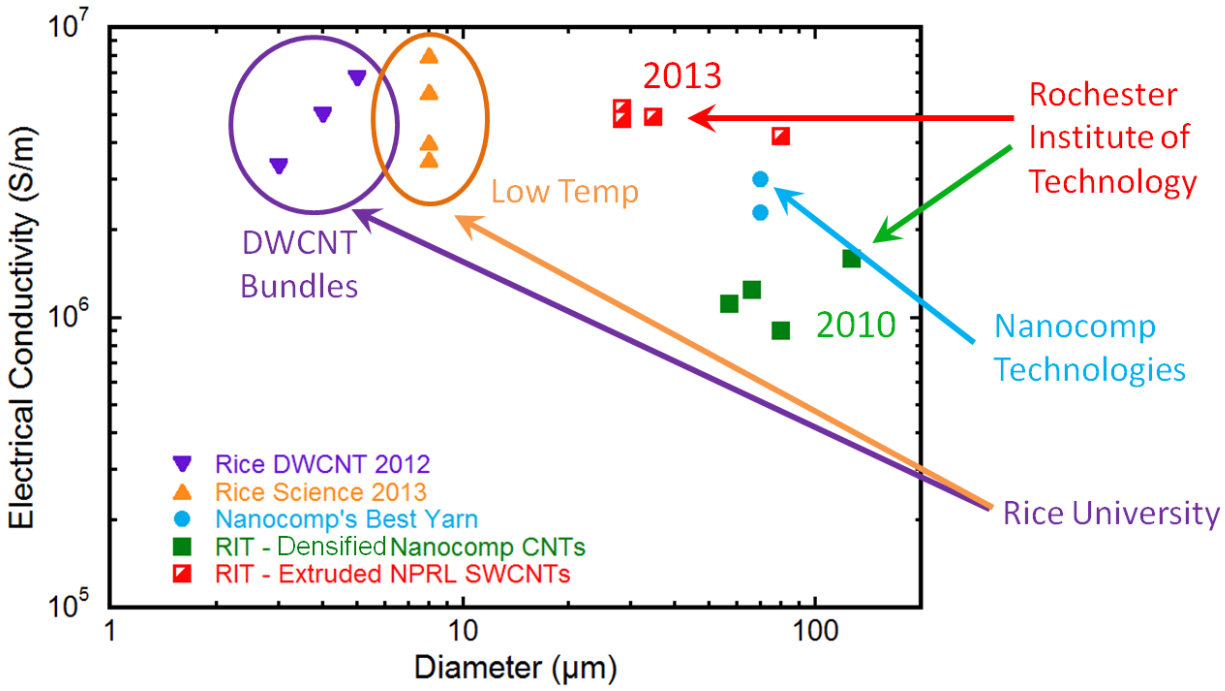

Figure 39. Summary conductivity plot of electrical conductivities of carbon nanotube electrical conductors. Measurements were taken across hundreds of wire segments under different processing condition and the best measured values are plotted. Original figure created by author. Original figure created by author.

There are several limitations to the work presented in this section. A continuous extrusion system would need to be developed and the material properties as a function of extruded wire segment should be characterized to ensure uniform wire properties. Also increasing the maximum weight loading of SWCNT in CSA above 35 % w/w should be a key focus of future research.

Chapter 5: Life Cycle of CNT Conductors: Use Phase of CNT Wires: Methods of contacting and Functional CNT Device Demonstration

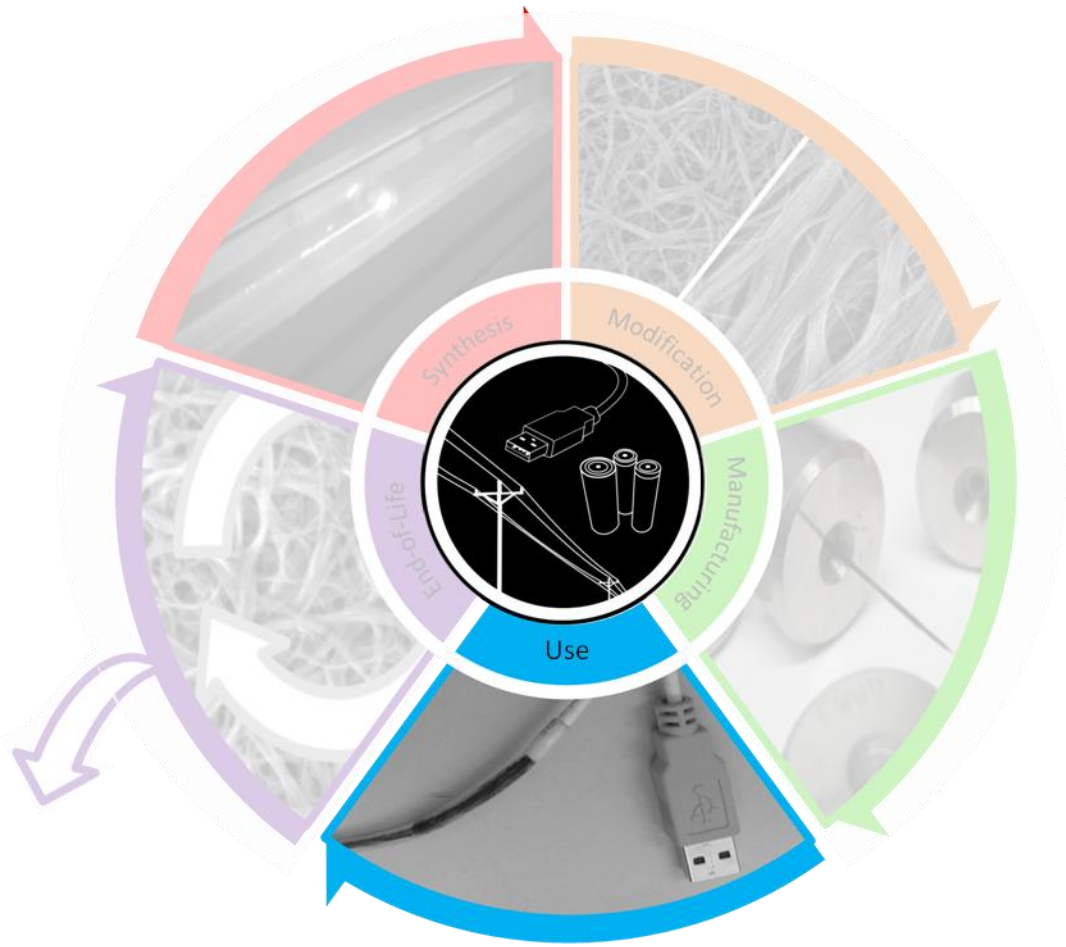

Figure 40. This chapter of the dissertation looks at methods of contacting CNT wires to metallic interconnects and the performance of functional materials for conducting applications. Original figure created by author.

Chapter 5 of the dissertation investigates the use phase of CNT conductor life cycle. Identifying methods to effectively contact the bulk CNT conductors manufactured in the previous chapter to real-world metallic contacts is a key focus. Mechanical crimping and conductive epoxies can be used to make reliable connections to metallic interconnects. In other applications where crimping and epoxy cannot be used such as lithium ion battery electrodes, another method contacting was investigated: ultrasonic welding. In this method ultrasonic energy is used to mechanically and

electrically contact bulk CNT materials to metallic conductors. The mechanical strength and specific contact resistances of these welds are measured.

5.1 Introduction

The measured properties of carbon nanotube (CNT) based materials make them a competitive option to replace copper as a next generation conductive material. Recent advances in chemical doping and CNT wire fabrication techniques have led to bulk CNT conductors approaching the electrical conductivity of copper at a fraction of the weight.[2, 17] CNT based conductors can already provide significant advantages over metallic wiring in a number of niche applications.[17] Applications which require high flexure tolerance, corrosion resistance, and high performance to weight ratios can especially benefit from the electrical and mechanical properties of CNTs. For example, CNT sheet materials are also performing as well as metallic foils and braided wires when used as the outer conductor in coaxial wires but at a fraction of the weight. [16, 17] Opportunities to use CNT sheets as active material supports for high capacity materials in lithium ion battery electrodes motivates a robust and effective method for contacting to metallic interconnects. Despite their functional and weight saving advantages, making electrical and mechanical contacts to these CNT electrodes, wires, and cables is an area of increased interest and may require special methods of attachment.

A functional connection must be both mechanically and electrically robust. Traditional methods of connecting wires (e.g. soldering, conductive epoxy, mechanical crimping) are not always practical for carbon-based conductors. Of the methods to contact CNT conductors, there are both advantages and disadvantages of each technology Figure 41. Solders do not wet to the CNTs, and therefore pre-metallization of the carbon surface is required in order to make a solder connection. These soldered connections are often mechanically weak and prone to failure. Other

methods contacting, such as conductive silver epoxy can provide good mechanical connections, however, the silver epoxy requires long curing times and can easily create shunt paths in closely space electrodes. Additionally, the polymer and solvents in the epoxy can lead to higher contact resistances and contamination of the CNT network. Methods like mechanical crimping can provide a strong mechanical connection to carbon-based wires. Additionally, the contact resistance of mechanical connections is dependent on the crimping force, and in some instances the crimp connector itself can be large and bulky.[17] In the case of lithium-ion battery electrodes, large bulky crimp connections add inactive mass which reduces energy density and are not consistent with industry methods. Ultrasonic welding of bulk CNT conductors directly to metallic electrodes could be an efficient method to provide both the mechanical and electrical contacts without the shortcomings of the other aforementioned connection methods.

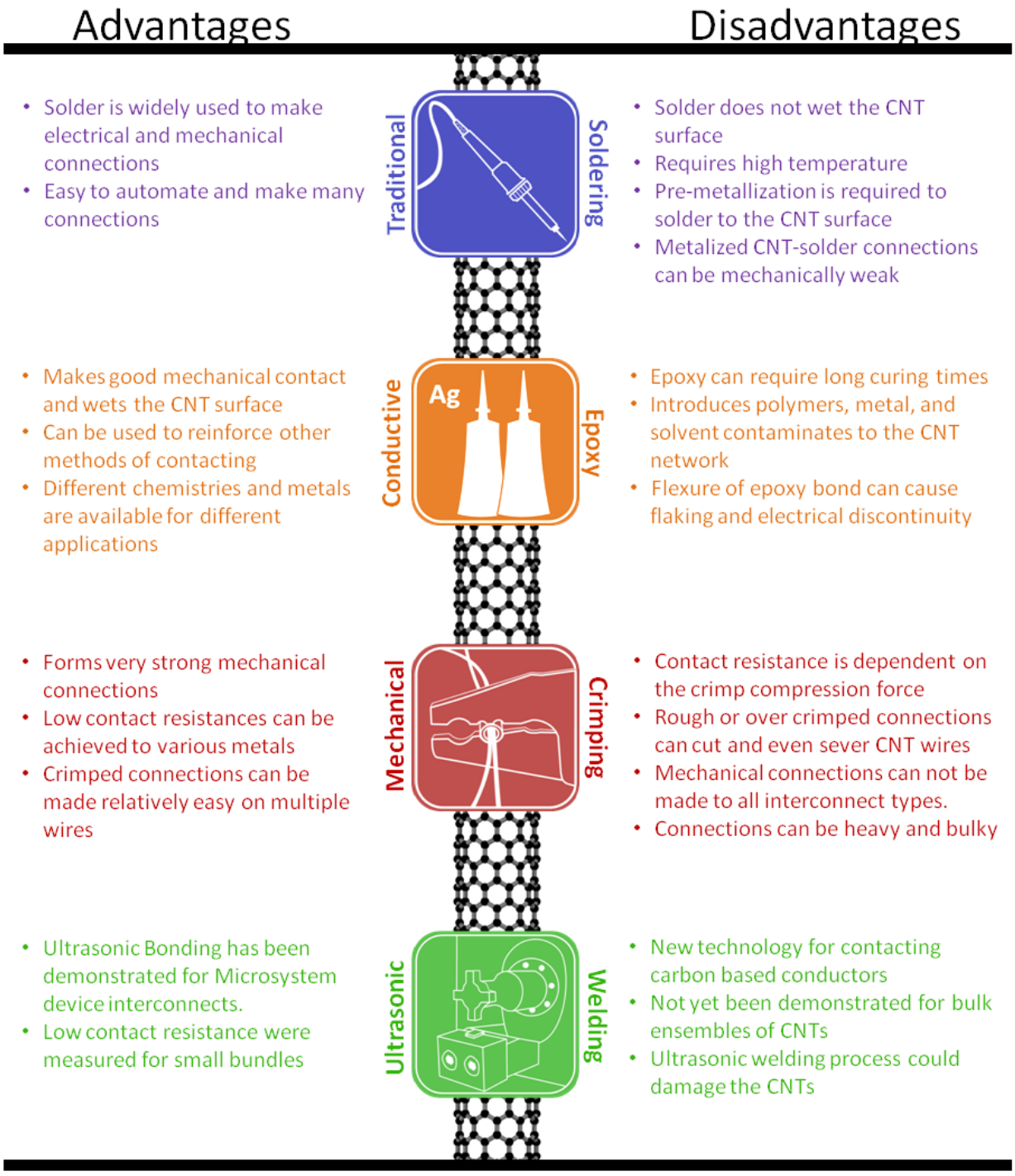

Figure 41. Table illustrating different techniques used for contacting carbon nanotubes to metallic interconnects. Original figure created by author.

5.2 Experimental

5.2.a Ultrasonic Welding

Ultrasonic welding was performed using a 4 kW Branson - AmTech Ultraweld 40 ultrasonic welder operating at 40 kHz with a 0.5 cm x 0.5 cm welding area. The ultrasonic welding system has user adjustable welding parameters:(1) to control the displacement amplitude of the ultrasonic horn (investigated between 12 and 18 μm), (2) total welding energy (investigated between 40 and 160 J), and (3) contacting/welding pressure (investigated between 40 and 60 psi). Interchangeable knurl patterns are available for both the ultrasonic horn and welding anvil. The CNT sheet materials, used in the current ultrasonic welding process, were obtained from Nanocomp Technologies Inc. and were purified prior to ultrasonic welding and using the purification procedure developed as part of this doctoral work and described in detail below.

Characterization of the CNT materials and ultrasonic welds were performed using physical, mechanical, and electrical techniques. Scanning electron microscopy (SEM) was performed at the weld interface using a Hitachi S900 field emission SEM at an accelerating voltage of 2 kV. Raman spectroscopy was performed using a JY Horriba Raman spectrometer with a laser excitation energy of 1.96 eV. Dynamic mechanical analysis (DMA) was performed using a TA instruments Q800 DMA. Stress strain curves were performed at a 0° angle in plane with the ultrasonic welding surface. A force ramp rate of 0.01 N/min was used until material failure. Electrical measurements were performed on ultrasonic welded CNT materials using a four point probe system connected with the National Instruments, NI – 2600 source measure unit. TLM measurements?

5.2.b Purification of Nanocomp Technologies Inc. As-Received CNT Sheet Material

Nanocomp CNT sheet materials were purified using a combination of acid and thermal oxidation treatments. First, as-received Nanocomp CNT sheet material was thermally oxidized up to a maximum temperature of 560°C (10 °C/min ramp rate) under 5 L per minute flowing, dry air to remove amorphous carbon impurities. Following the thermal oxidation procedure, the CNT sheet material was then treated with concentrated HCl acid for 30 minutes to remove residual Fe catalyst particles. During the acid rinsing procedure a noticeable color change is observed for the high-temperature burned CNTs sheet materials where the dissolved iron catalyst particles turn the acid a bright yellow (bottom vial in Figure 42). In comparison, as-received sheet materials treated with concentrated hydrochloric acid do not produce a visible color change (top vial in Figure 42). The difference in the ability of the HCl to dissolve the iron catalyst particles after thermal oxidation is attributed to the carbon coatings on the Fe being removed in the as-received CNT materials which prevent their dissolution into the HCl.

SEM analysis shows dramatic change in surface morphology at each step of the purification procedure. Large chunks of catalysts and other carbonaceous impurities are observed on the as received CNTs sheet material (Figure 42a). The dramatic reduction in the size of these impurities is observed following thermal oxidation with small clusters of catalyst particles dominating the surface features (Figure 42b). Finally, with the acid rinsing procedure, very few impurities remain on the surface of the CNTs sheet materials and the surface morphology is that of typical high purity CNT materials (Figure 42c).

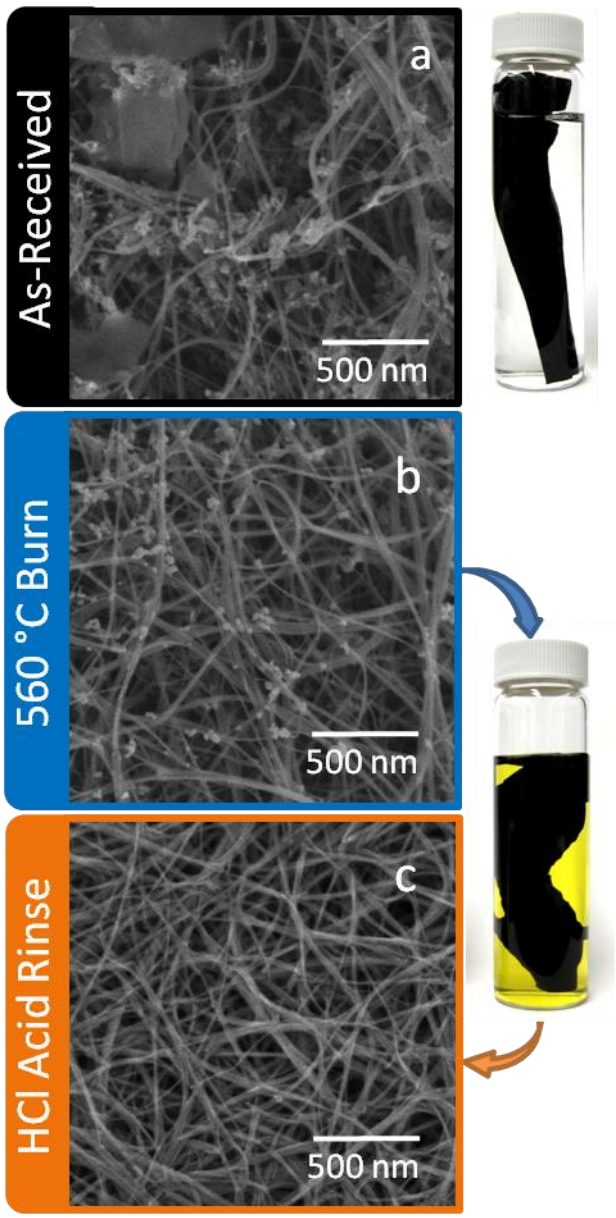

Figure 42. Scanning electron microscopy images of Nanocomp carbon nanotube sheet materials as-received (a), following a 560 C burn in air (b), and following a HCl acid rinse. No color change is visible when as-received sheet materials are treated with concentrated HCl (top vial). Following thermal treatment, carbon coatings are removed from the Fe catalysts particles and the can be dissolved using HCl with a visible color change. Original figure created by author.

Thermal gravimetric analysis was used to monitor the weight change as a function of thermal oxidation temperature. Low temperature thermal oxidation steps resulted in little weight loss due to the combustion of carbonaceous material. Increasing the thermal oxidation temperature resulted in higher weight losses during the burn procedure up to a maximum weight loss of 40% at 580°C (Figure 43). Additional weight was removed following the acid rinsing procedure due to the dissolution of iron catalyst particles. The total amount of Fe removed using the HCl increased with increasing thermal oxidation temperature up to a maximum of 20 % w/w at a temperature of 550 °C. As the thermal oxidation temperature was increased above 550 °C no additional increase in the Fe removal was measured. This suggests that a thermal oxidation temperature of 550 °C is sufficient at removing carbon encapsulation and exposing the Fe catalyst particles to the HCl.

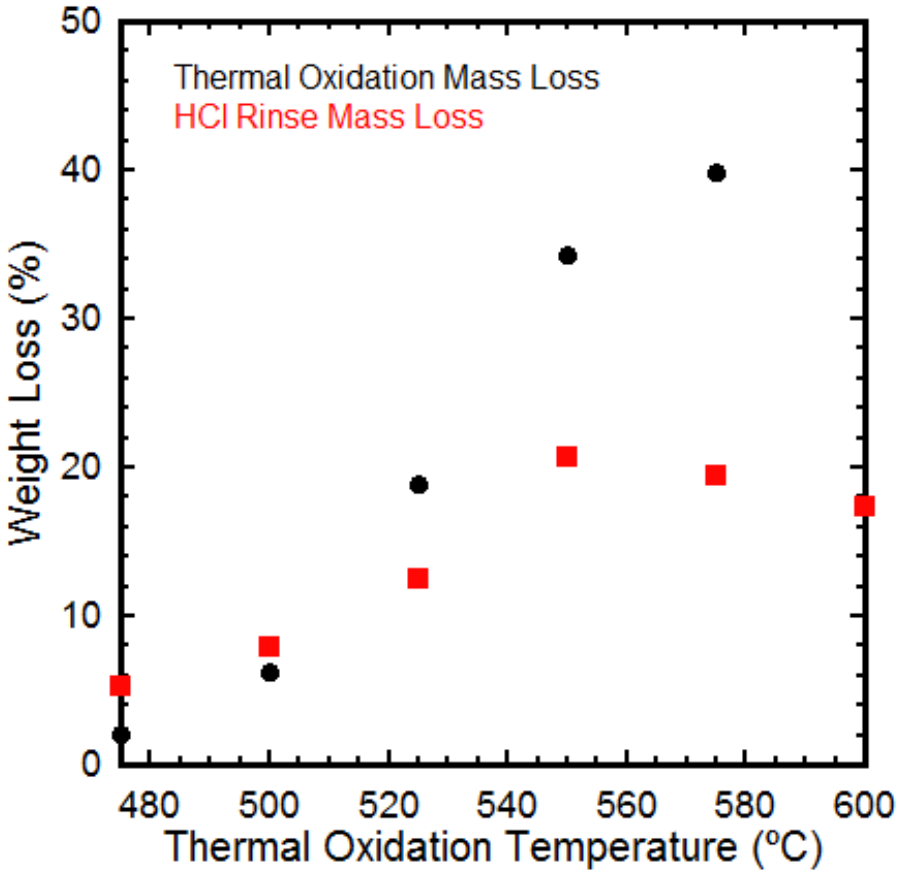

Figure 43. thermal gravimetric analysis of the % weight loss of Nanocomp carbon nanotube sheet materials burned at a 10 °C/min ramp rate under flowing air to different maximum burn temperatures. The red (square) data points show the relative Fe catalyst mass loss following a concentrated HCl rinse. Measurements were conducted on several CNT paper segments and the data plotted represents average weight losses at each temperature. Original figure created by author, data taken by Anthony Sammarco

Raman spectroscopy was also performed as a function of thermal oxidation temperature on each of the CNTs sheet materials. For all the thermal oxidation temperatures investigated, no significant increase in the D/G ratio was measured. If significant damage was done to the sidewall of the CNTs during the purification procedure, an increase in the D/G, as well as the D/G' ratios would be observed.

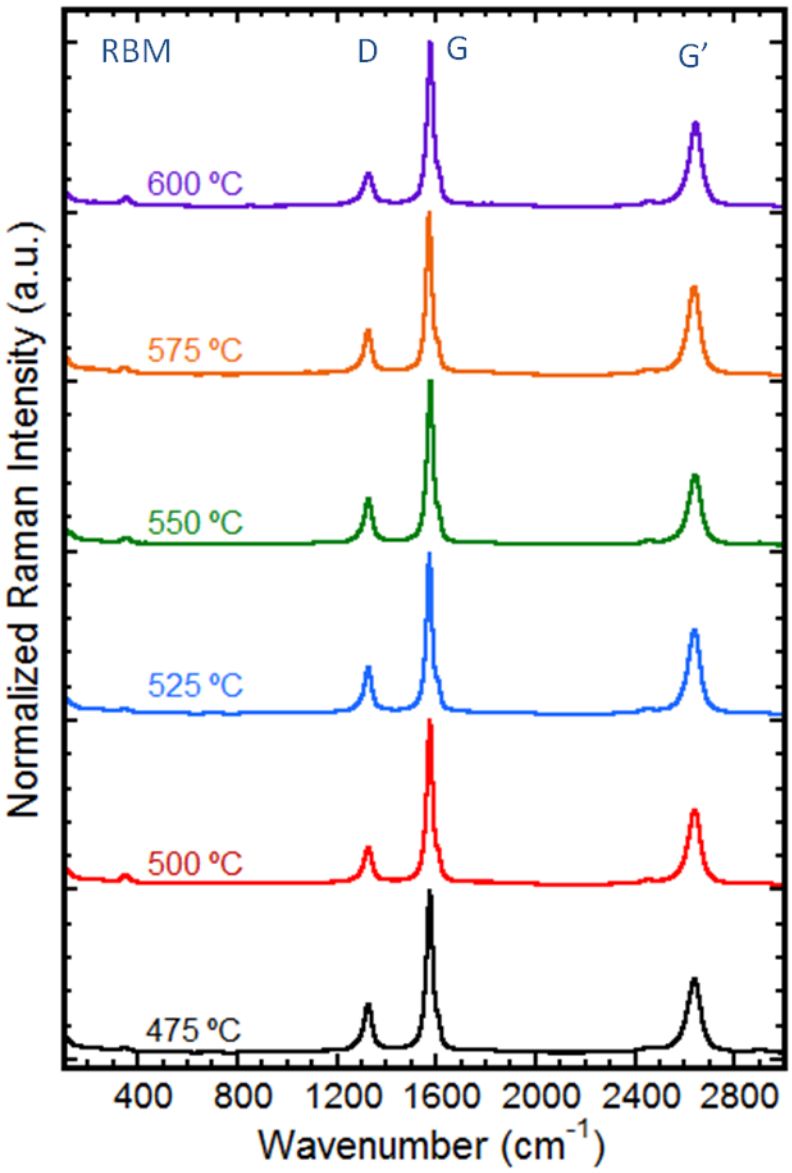

Figure 44. Normalized Raman spectra for Nanocomp carbon nanotube sheet materials as a function of thermal oxidation temperature. The plotted Raman data is a combination of three different measurement points taken on each sample, averaged, and baseline corrected. Original figure created by author, data taken by Anthony Sammarco

5.3 Results and Discussion

Figure 45 shows optical (Figure 45a) and scanning electron microscopy (Figure 45b) images of the ultrasonic weld interface between the copper and the CNTs ribbon segments. At the weld edge, a clear distinction between the two materials is visible. Small areas of CNTs are exposed

and lifted from the CNT network in several locations across the weld area and appear brighter in the SEM images (Figure 45b). The presence of these delaminated CNTs is attributed to roughening of the CNT network during the welding process. The ability to ultrasonically weld to different bulk CNT form factors including densified CNT wires (Figure 41c) and CNT ribbons (Figure 41d) have also been demonstrated. Although both form factors resulted in strong welds, the CNT ribbons were chosen for analysis due to the uniform weld area from sample to sample.

Of the ultrasonic welding parameters initially investigated, the most obvious impact on the quality of the weld was the choice of neural pattern in contact with the CNT surface. Highly textured knurl patterns such as pyramid or inverted pyramid designs cause severe abrasion and shredding of the 50 µm thick CNT conductor. In several cases, the use of a textured knurl pattern in contact results in very weak welds which failed before mechanical measurements could be taken (Figure 45). In contrast, when a smooth knurl pattern was used in contact with the CNT sheet materials, it provided a sufficient welding surface to make a strong ultrasonic bond with the copper foil.. Flat knurl patterns on both the Cu and CNT surfaces were did not effectively grip the welding materials get displaced during the ultrasonic welding. The choice of neural pattern in contact with the copper foil was much less sensitive but required a textured surface to hold it in place during welding At higher energies (> 160 J) however, the thin (20 µm) copper foil was prone to damage through work hardening and would stick to the welding head and fracture (Figure 41e).

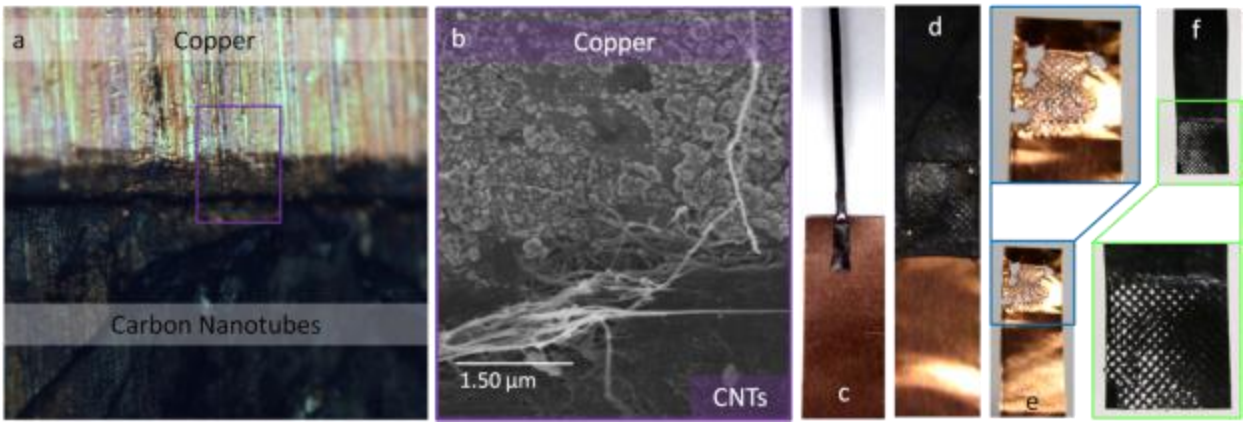

Figure 45. Optical microscope image (a) and scanning electron micrograph (b) of the ultrasonic weld interface between carbon nanotubes (CNTs) and copper. Photographs of a densified CNT wire ultrasonically welded to copper foil and a CNT ribbon ultrasonically welded to copper foil tab. Width of the copper tab is 0.5 cm. Photographs showing the impact of high energy work hardening and fusing of the copper foil to the welding head (e). Highly textured knurl patterns will perforate the CNT sheet (f). Original figure created by author.

Figure 46 summarizes the DMA testing performed on multiple CNT-copper ribbon segments under a high-low series of conditions. Of the three welding parameters investigated, the displacement of the welding horn has the most impact on the measured breaking strength of the weld. Low displacement amplitudes (12 µm) resulted in lower bond strengths (~400 g). Strength of the weld increased in strength (~900 g) with increasing displacement amplitude up to a maximum displacement amplitude of 18 µm for the ultrasonic welder. The breaking strength of the ultrasonic weld is relatively insensitive to both the welding pressure (Figure 46a) and total weld energy (Figure 46b) of the bond, and remained relatively constant within the measured error.

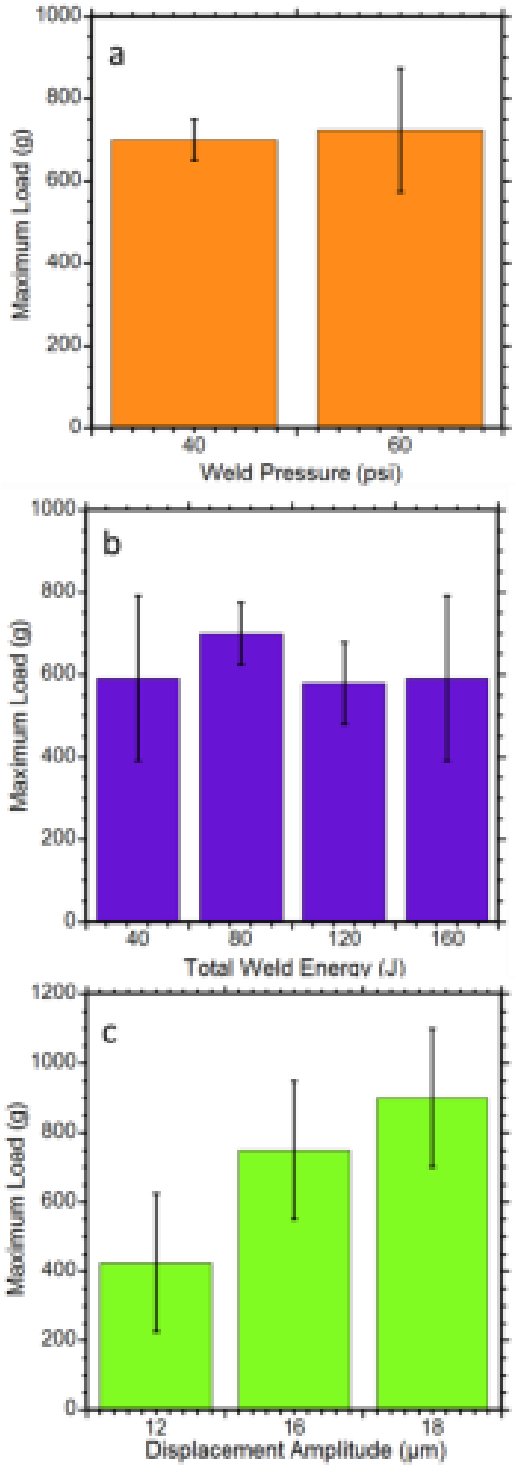

Figure 46. Dynamic mechanical analysis of the maximum load (g) before weld failure as a function of welding pressure (a), welding energy (b), and horn displacement amplitude (c). Error in the mechanical strength is represented by the standard deviation across 10 samples at each set of welding conditions. Original figure created by author, data taken by Jack Alvarenga.

In Raman spectroscopy of CNT materials, an increased ratio of the D and G peaks (D/G) is characteristic of increased damage to the sidewall of the CNTs. Raman analysis was performed to determine the extent of defect formation by analyzing the CNT sheet in multiple locations throughout the bond interface. the bottom most layer of CNTs in the network are actually bonded to the copper foil. The rest of the CNTs would be attached to the bottom most layer through Van der Wall forces, bundling, and network entanglement. To understand how the bottom most layer differs from the entangled surface CNTs surface CNTs were removed from the weld location through a combination of N,N,-dimethylacetamide (N,N,-DMA) solvent and an ultrasonic bath. During the cleaning procedure, a color change was visible in the N,N,-DMA solvent as CNTs were removed from the copper surface. Following 30 min in the ultrasonic bath, the copper foil was rinsed with N,N,-DMA to remove any CNTs material that was re-deposited onto the foil. The copper foil was then dried in a vacuum oven to remove any residual solvent and imaged using optical and scanning electron microscopy.

Following the ultrasonic cleaning procedure, areas of the copper foil surface still have carbon material attached. The optical microscope image in Figure 47f contains three different visible material morphologies on the copper foil. The three areas consisted of opaque deposits, semi-transparent films, and areas where copper foil appeared bright and reflective. Raman spectroscopy was performed on each of these three regions. The bright reflective areas had extremely low Raman signal intensity, and minimal characteristic CNTs peaks. The opaque areas maintain a strong Raman intensity as well as a high D/G ratio of approximately 2 (Figure 47Figure 47a purple curve).

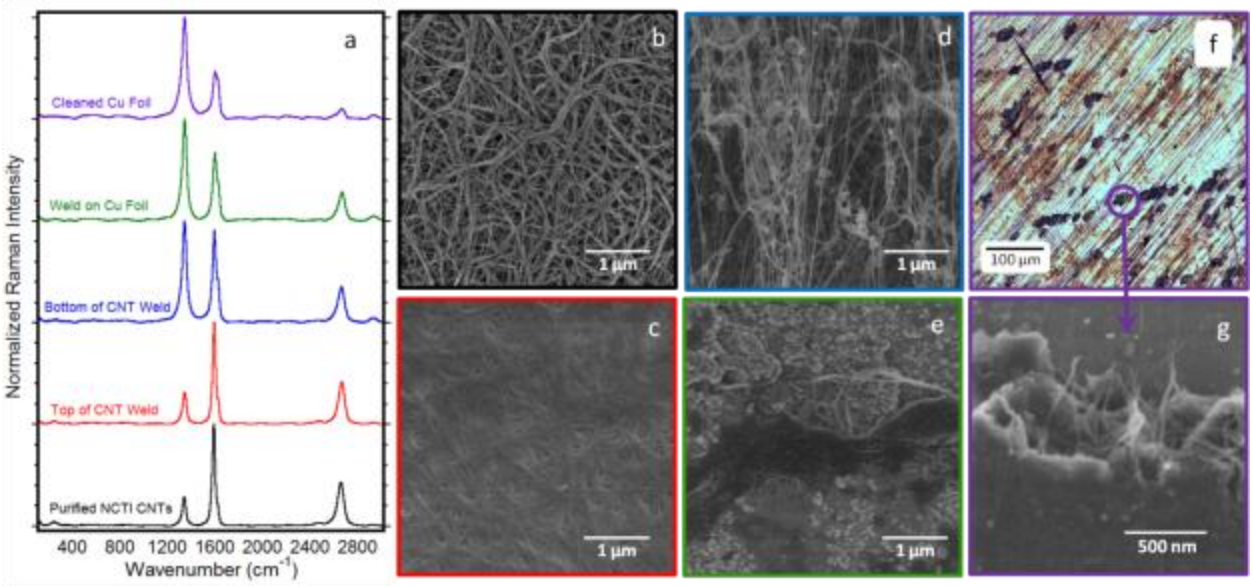

Figure 47. Optical microscopy images of copper foil (a) with ultrasonically welded carbon nanotube residues. Raman spectra of a copper foil location (b), a dark patch location (c), and a darker shadowed spot (d). The plotted Raman data is a combination of three different measurement points taken on each sample, averaged, and baseline corrected. Original figure created by author.

SEM images of the ultrasonic weld locations show networks of CNTs. The top of the ultrasonic weld surface show smooth entangled networks of CNTs mats with some amorphous carbon generation (Figure 47c). These locations appear more amorphous in structure which is consistent with the measured increase in the D/G Raman ratio. At the edges of these dark spots the tips of CNTs are clearly visible protruding from the mats (Figure 47g).

The change in CNT morphology at the metal interface observed in SEM images is consistent with SWCNTs welded to Ti electrodes.[80] The ability of these heavily damaged CNTs to remain adhered to the copper foil suggests that one ultrasonic welding mechanism is the formation of carbon metal bonds.[80] The formation of carbides would allow the heavily damaged CNTs to remain fixed to the metal surface throughout the ultrasonic bath cleaning procedure. Previous

studies used XPS analysis to show the evolution of carbon-titanium bonds at increasingly higher welding energies.[80]

A second proposed welding mechanism is the acoustic softening effect. During ultrasonic welding, CNTs can embedded themselves below the metal surface and provide the high mechanical strength and lower contact resistances.[81] Protruding CNT ends can then provide electrical contact points and mechanical rigidity to other CNTs in the network which are not directly welded to the metal contact. The ability for ultrasonic welding techniques to embed CNTs into the metal matrix has also been shown to lower the two-terminal electrical contact resistance between individual/small bundles of CNTs and the metal.[80] Although lower two terminal resistances have been measured for CNT based microelectronics it is unclear how those properties translate to bulk structures.

In the current work, a modified transmission line method (TLM) was used to determine the specific contact resistance of the ultrasonic weld between the CNTs and the copper foils. A series of ultrasonic welds were made at decreasing separation towards a reference contact. The measured two-point resistance was plotted as a function of the weld spacing in Figure 48. A linear fit was used to determine the y-axis intercept. The value of the y intercept is twice the contact resistance of an individual ultrasonic weld (an equal contribution from both ends of the TLM structure). Correcting for geometry, CNTs ultrasonically welded to copper have a measured specific contact resistance of 9.9 $m\Omega\text{-}cm^2$. An equivalent TLM measurement was performed using CNT materials treated with potassium tetrabromoaurate ($KAuBr_4$) as a chemical dopant. $KAuBr_4$ has previously been shown to reduce the contact resistance of mechanically formed electrical connections.[3] Following chemical doping, the specific contact resistance was reduced significantly to 4.3 $m\Omega\text{-}cm^2$. The ultrasonic welding values are nearly an order of

magnitude lower than contact resistances achieved through mechanical compression.[3] For comparison, specific contact resistances in other well characterized systems are 8 mΩcm^2 and 1 mΩcm^2 for ITO/silver and Si-PV/silver contacts respectively.[82]

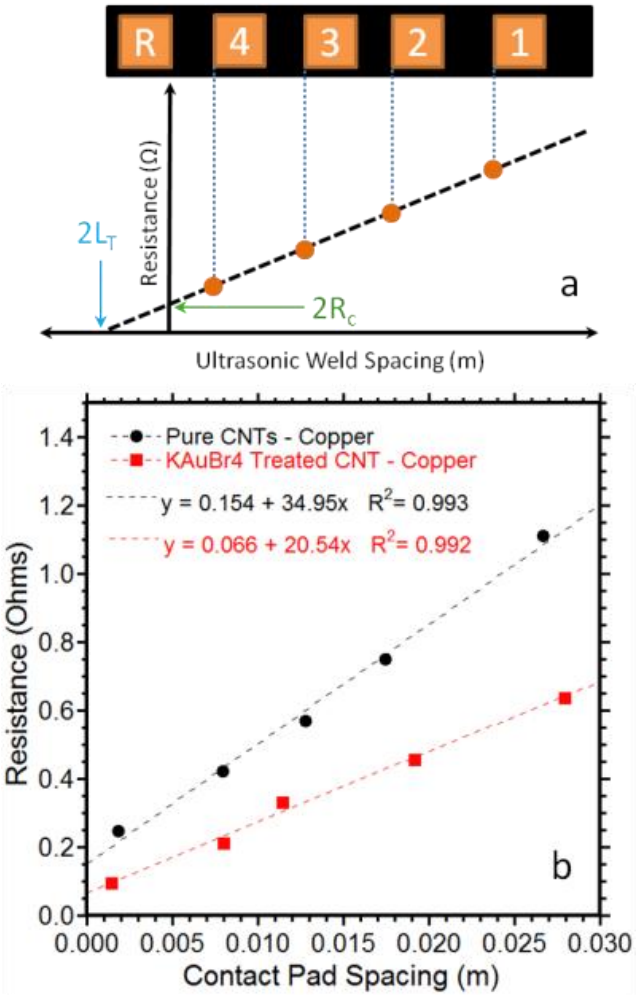

Figure 48. Two point resistance measurements as a function of copper pad spacing that have been ultrasonically welded to carbon nanotube sheet materials. Measurement error is within the data points. Original figure created by author.

The low contact resistance and the strong mechanical strength across the 0.5 x 0.5 cm weld area demonstrates the viability of ultrasonic welding for making reliable contacts between bulk CNT conductors and metallic interconnects.

5.4 Carbon Nanotube To Carbon Nanotube Welding

In addition to interconnects between bulk CNT and metal, ultrasonic welding can be used to form CNT-CNT bonds. Such an approach can be useful when attempting to bond or stitch one or more bulk CNT conductors end to end. Thus, the ultrasonic welding approach can eliminate the need for adhesives or bulky crimp connections. To demonstrate the ability of CNT-CNT welding, an applied force of 60 psi at 10 μm amplitude and 20 J of wild energy was used to bond two Nanocomp ribbon segments together. The strength of the weld was measured by dynamic mechanical analysis on the TA instruments Q800 DMA. Three different areas of bulk CNT-CNT overlap were investigated by increasing the number of ultrasonic welds from 2 to 4 to 6 as illustrated by the inset of Figure 49. Each individual weld area is 0.5 cm x 0.5 cm of the ribbon. The bulk CNT ribbon width was held constant at 1 cm and a total 5 samples were prepared for each of the overlapping weld area (2, 4, and 6 total weld spots) configurations. The static force required to break each bond is displayed in Figure 49. The strongest bond was achieved for the largest area of overlap (6 welds) at a maximum breaking strength of 80 lbs/ft width and 6% strain. The two smallest areas of overlap had roughly the same maximum braking force at 55 lbs/ft width.

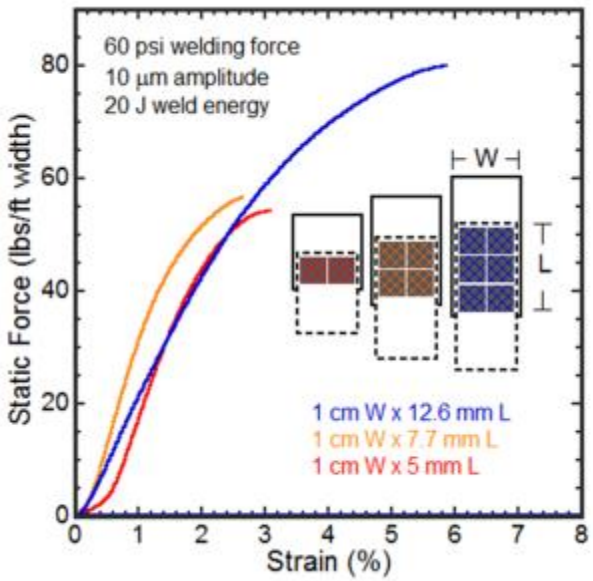

Figure 49. Stress-strain curves for carbon nanotube ribbon segments ultrasonically bonded together with increasing area of overlap. Measurement error is within the data points. Original figure created by author.

Similarly, another set of ribbon segments were prepared to investigate the impact of bulk CNT ribbon width on the strength of the ultrasonic bond. Ultrasonically welded CNT ribbon test strips were prepared using 0.5 cm wide CNT papers so that only one ultrasonic weld would fit across the test strip for comparison to the 1 c m wide ribbons (ultrasonic weld configurations are illustrated by the inset of Figure 50). The narrower width CNT ribbon segments performed comparably well to the wider 1 cm CNT ribbons (Figure 50). Under the present test conditions, similar maximum static forces of 50-60 pounds per foot width were achieved. In practice, ultrasonic welds could be made to stitch together bulk CNT papers of any width, mechanical testing in the present work is limited to ~1 cm wide test strips due to the size of the TA Q800 DMA.

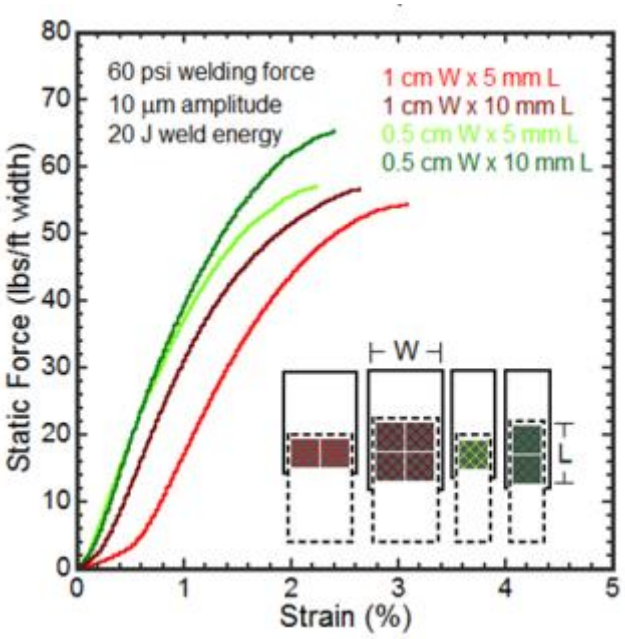

Figure 50. Stress-strain curves for carbon nanotube ribbon segments ultrasonically bonded together with two different linear widths of overlap. Measurement error is within the data points. Original figure created by author.

The resistance (Ω) of a densified CNT wire was monitored as a function of ultrasonic welding energy along its length. Separate ultrasonic welds were performed end-to-end along the CNT wire while 4-point resistance was monitored (Figure 51a). The resistance per length of the wire remained constant following all nine welds. After a full set of ultrasonic welds was made down the length of the wire, another full set of welds at increased energy, welding pressure and amplitude were performed. The electrical resistance was measured after each full set of welds (Figure 51b). After five weld sets electrical conductivity remained the same as the baseline value. This data suggests that the ultrasonic welding process, under the conditions tested, does not negatively impact the electrical conductivity of the wire. However, the ultrasonic bonding process does create mechanical deformations in the wire converting it from a cylindrical form factor to one more representative of a ribbon conductor.

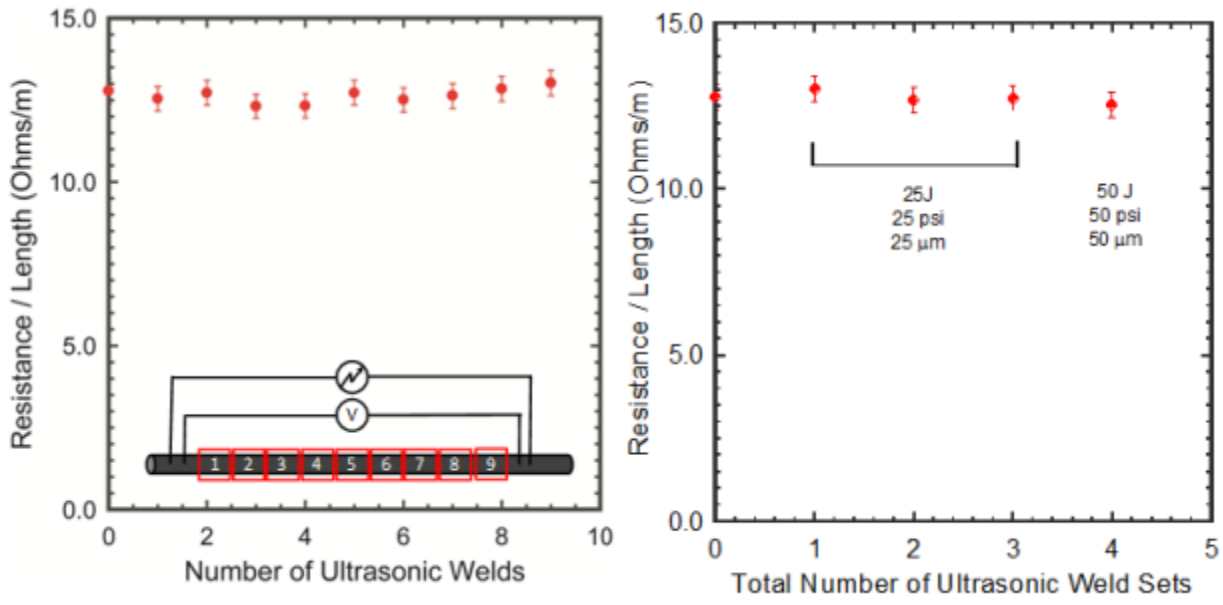

Figure 51. Resistance of a densified carbon nanotube wires as a function of ultrasonic welds (a) along its length and (b) total number of weld sets with increasing energy. Measurement error is provided. Original figure created by author.

The Raman spectra were taken (Figure 52) for SWCNT paper electrodes before and after repeated ultrasonic welding. Following repeated welding in the same location a slight decrease in the concentration of smaller diameter SWCNTs compared to larger diameter was observed, based on relative peak intensities in the radial breathing mode region (Figure 52b). Similarly, a slight increase in D-band intensity (Figure 52c), typically an indicator of defects in the SWCNTs is observed following ultrasonic welding, as well as a slight increase in the G' band peak intensity (Figure 52d). Although these changes in the Raman spectra are minimal, they do suggest that some damage to smaller diameter SWCNTs could be occurring during the ultrasonic welding process.

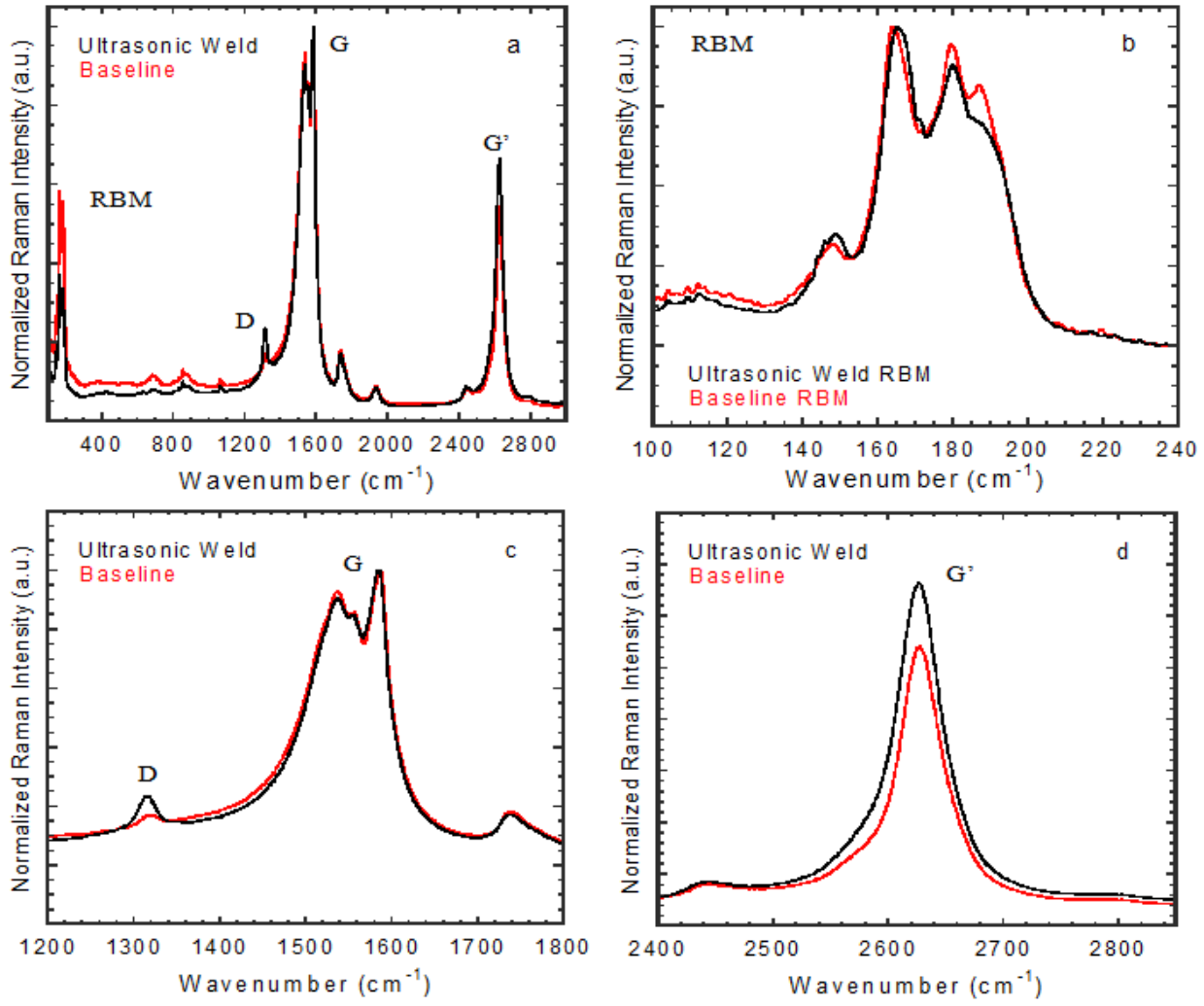

Figure 52. (a) Raman spectra of single-wall carbon nanotubes following repeated ultrasonic welds (25 welds) in the same location and compared to the same material without welding. Zoomed in regions of the (b) radial breathing modes (130-210 cm^{-1}), (c) D (1320 cm^{-1}) and G bands (1500-1600 cm^{-1}), and (d) the G' peak (2625 cm^{-1}) are provided for clairity. The plotted Raman data is a combination of three different measurement points taken on each sample, averaged, and baseline corrected. Original figure created by author.

5.5 Conclusions

Carbon nanotubes were ultrasonically welded to copper foils using a series of welding conditions. Flat knurl patterns on the CNT side of the weld provided a sufficient welding surface to make mechanical and electrical contact to the copper without abrasive destruction to the CNT

network. Displacement amplitude of the ultrasonic horn had the largest impact on the strength and quality of the weld. Larger displacement amplitudes (up to 18 μm) resulted in the strongest mechanical welds (~900 g breaking strength across the 0.5 x 0.5 cm weld) and lower displacement amplitudes (12 μm) reduced the strength of the welds (~400 g). Raman spectroscopy was taken on the ultrasonic weld locations and minimal damage to the CNT materials was measured based on the D/G of the spectra. Following a solvent cleaning procedure, the CNT materials that remained tightly bound to the copper foil have a significantly increased D/G >1, suggesting that breaking of the carbon-carbon bonds allows for possible mechanisms attributed to the formation of carbides and insertion of CNTs below the copper surface. Finally, the optimized carbon-copper weld also reduced the contact resistance of the weld to be 9.9 mΩ-cm^2, based upon a modified transmission line method. The contact resistance can be further reduced by a factor of 2x through the addition $KAuBr_4$ chemical dopant. Overall, ultrasonic welding has been demonstrated for the first time as a viable method for making electrical and mechanical contact between bulk CNT conductors and metallic interconnects.

There are several limitations to the work presented in this section. The mechanical and electrical properties of the ultrasonic welds could be expanded to a larger set of metals and interconnection morphologies. The automation potential of ultrasonic welding CNT interconnects should be investigated for commercial applications. Also, the ability to make ultrasonic welds should be revisited as the diameter of CNT wires and cables increases towards larger form factors.

5.6 Applications of Carbon Nanotube Electrical Conductors

The viability of CNT conductors was demonstrated for several wire and cable applications over the course of the dissertation research. Various CNT form factors were used to make cable demonstrations from flat large area electrodes to cylindrical conductive wires. Technology

demonstrations spanned the range of conductors from transparent thin films and electrodes to power and data transmission cables -- including antennas (summarized graphically in Figure 53).

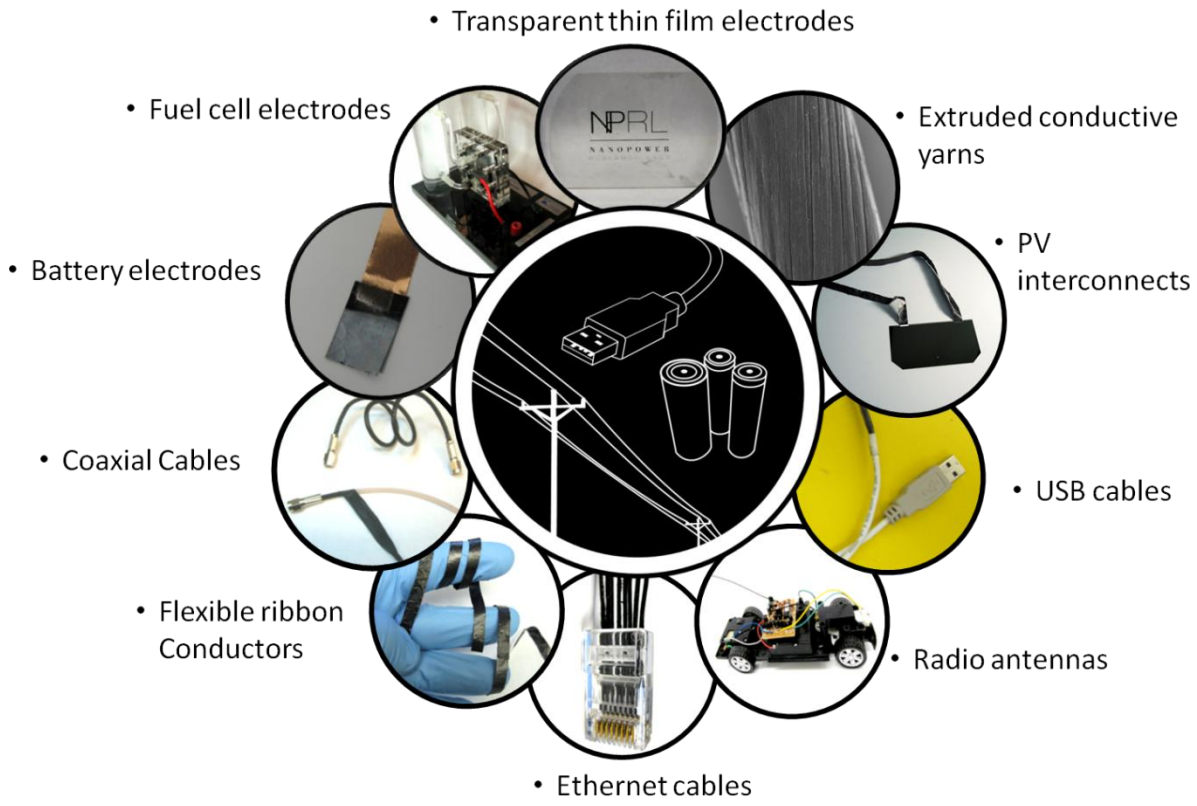

Figure 53. Graphical representation of carbon nanotube based electrical conductors developed during the course of the dissertation research. Original figure created by author.

The functional product demonstrations were fabricated using electrically insulated CNT conductors that were contacted (electrically and mechanically) to application specific interconnects (e.g. Ethernet and USB component contact pads). Electrical insulation was applied to the wires by threading the bare CNT conductors through polyolefin heat shrink tubing and using a heat gun to affix the polyolefin to the conductors (1. and 2. in Figure 54). Mechanical connections were made to each specific CNT connector per application. In the case of Ethernet and USB cables the corresponding male and female connection were purchased from Digi Key Inc, and the final CNT cable was insulated with an outer layer of heat shrink tubing.

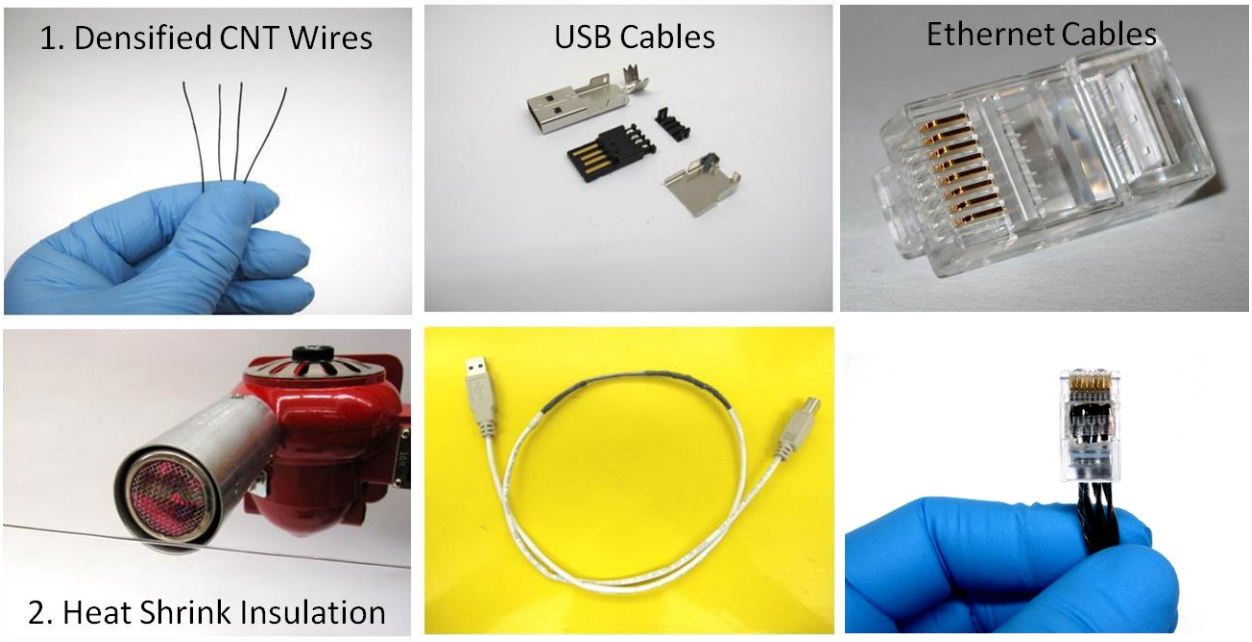

Figure 54. Basic steps required for the fabrication of functional conductors made from carbon nanotube conductors. Photographs and original figure created by author.

The performance of the Ethernet cables was measured by comparing the download and upload speed using an internet based application: http://www.speedtest.net. Data packets were transferred over a 100 Mbps connection between RIT and a server hosted in St. Catharines, Ontario, Canada. Five separate measurements were taken using each Ethernet Cable type and the average speeds are plotted in Figure 55. CNT based Ethernet cables performed at the same data transmission rates as the commercial copper based Ethernet cable. Additionally, the first CNT Ethernet cable was manufactured in 2010 and since then it has been successfully used as an active Ethernet cable on a laboratory work station computer without any loss in performance.

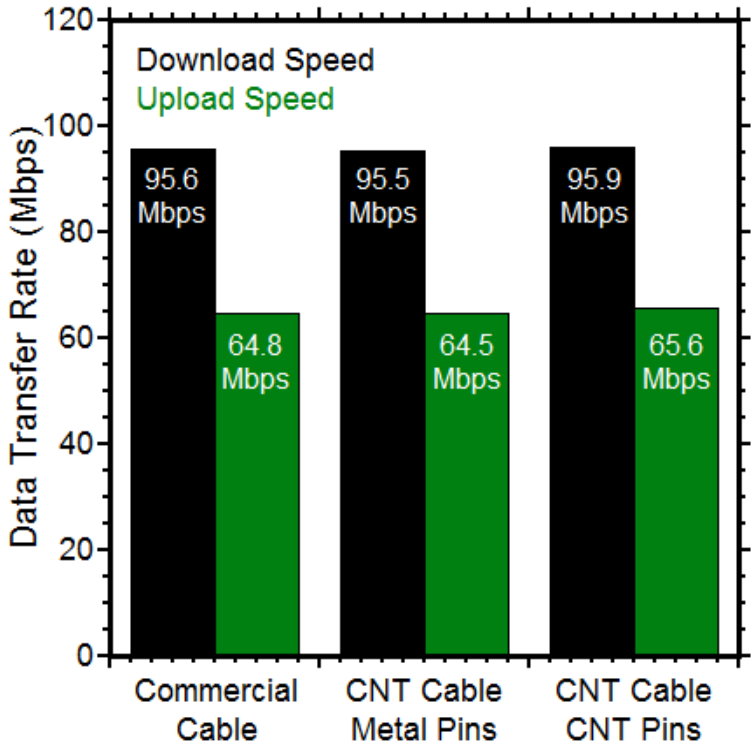

Figure 55. Data upload and download speeds using commercial copper based Ethernet cables compared to carbon nanotube based Ethernet cables. The plotted values are the average of three speed tests for each Ethernet cable design. Original figure created by author.

Chapter 6: Life Cycle of CNT Conductors: Recycling Single-Wall Carbon Nanotubes from End-of-Life Applications

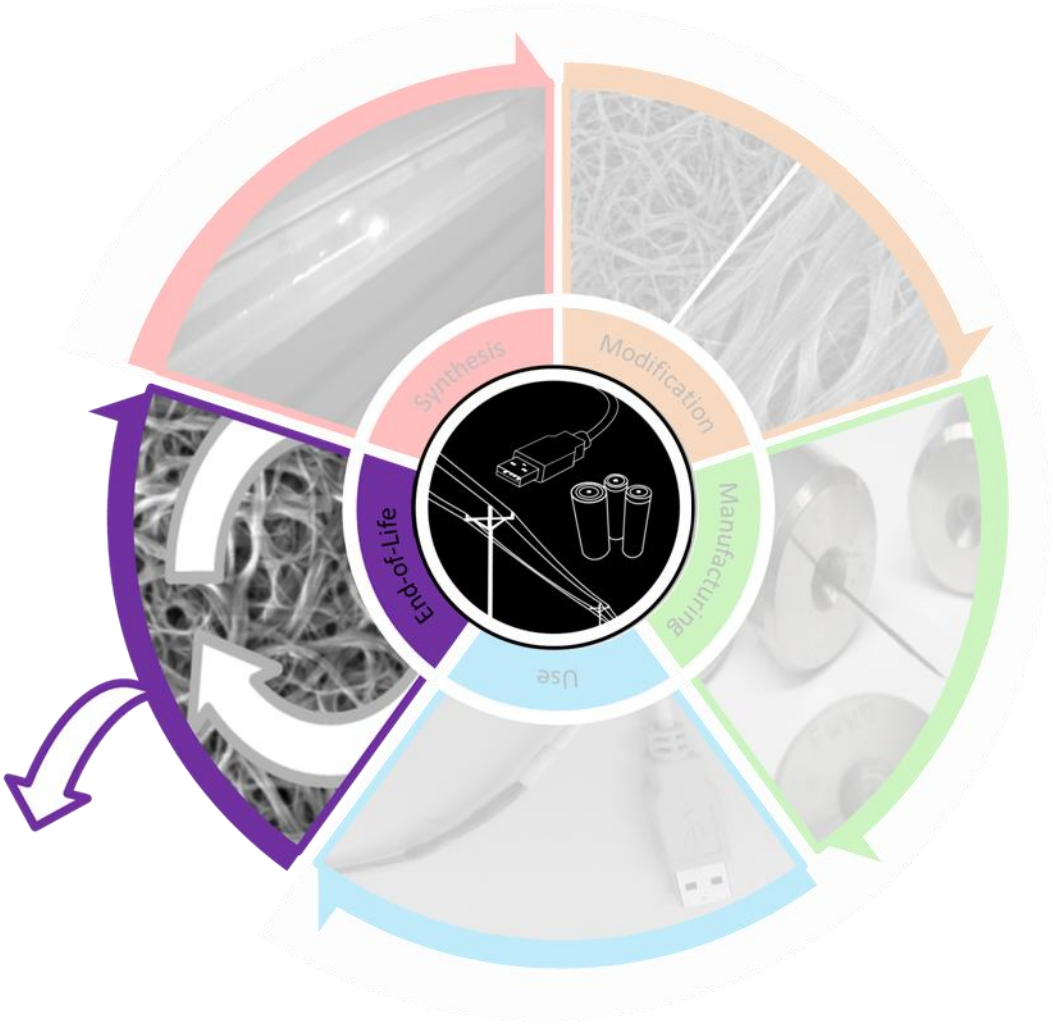

Figure 56.This chapter of the dissertation looks at end-of-life options such as refunctionalization for carbon nanotube based conductors. Original figure created by author.

Chapter 6 of the dissertation investigates the end-of-life stage of the CNT conductor life cycle. SWCNT end-of-life management options, such as recycling, are investigated for the first time as an alternative to land filling or incineration of CNT based conductors. There are a number of reasons for recovering and reusing SWCNTs at their end-of-life including: (1) the high cost

associated with the manufacture of CNT materials can be reduced through multiple use phases, (2) the high cumulative energy demand required to synthesize the material can be recovered and preserved through refunctionalization processes, (3) potential release of CNT waste into the environment can be minimized if CNTs are recycled instead of land filled, and (4) prevention of human exposure to CNTs during illegal third world electronic waste recycling practices.

This chapter will focus on a near-term application of SWCNTs materials as an electrical conductor in lithium ion battery anodes. Specifically, SWCNTs are used as both an electrode and as a lithium insertion material in the anode of a lithium ion battery. The battery was forced to an end-of-life state through extended cycling and recycling techniques were used to recover the SWCNT material and refunctionalize it to a reusable material. The refunctionalized SWCNTs were then incorporated into the anode of new lithium ion battery which performed as-well-as the virgin SWCNT materials with a reduced chemical and electrical footprint.

6.1 Introduction

There is considerable interest in developing lithium ion batteries that are capable of meeting the energy density demands of portable electronics, electric vehicles, and alternative energy storage systems. Their superior energy density over other rechargeable battery technologies allows for the fabrication of lighter, thinner, and higher capacity batteries. Research is ongoing for new chemistries and materials with improved properties over that of state-of-the-art. Such an effort requires a concerted development of both electrodes and electrolyte to improve battery capacity, cycle life, and charge–discharge rates while maintaining the highest degree of safety available. The unique electrochemical and mechanical properties of single-wall carbon nanotubes (SWCNTs) make them a candidate material for use in the next generation of high energy/high power density batteries.[12, 83] Theoretical calculations suggest that reversible capacities exceeding

a LiC_2 stoichiometry (>1116 mAh g^{-1}) is attainable for SWCNTs due to the diffusion of lithium ions into stable sites located on the nanotube surface, inside individual nanotubes, and between SWCNTs in the interstitial sites of close-packed bundles.[84, 85] Recently, purified SWCNT electrodes with titanium contacts have achieved a measured capacity of 1050 mAh/g,[86] representing a dramatic improvement over the conventional graphite LiC_6 limit (i.e. 372 mAh/g) for lithium intercalation.[87, 88] When used as an additive, the high aspect ratio of the SWCNTs allows formation of an electrical percolation network at significantly lower weight loading than conventional carbons, like carbon black and graphite.[89] In addition, SWCNTs have the capability to be assembled into free-standing electrodes (absent of any binder or current collector) as an active lithium ion storage material or as a physical support for ultra high capacity electrode materials like silicon or germanium.[86, 90-92] As battery technology continues to develop around these nanomaterials, SWCNTs could be used in large enough quantities to cause potential environmental and economic impacts, such as high energy demand, high cost of production, and EOL particulate risks, and to warrant proactive thinking about proper waste management and reclamation of the materials before they enter the waste stream.[18]

Although the ability to recycle carbonaceous materials such as carbon powders, carbon fibers, and graphite has been investigated for a few applications,[93-96] recycling of nano-carbons such as buckyballs and CNTs has not been widely considered. These nano-carbons represent a new generation of carbonaceous materials with high cost, high embodied energy, and uncertain environmental and human health impacts.[21-23, 97-99] Recycling SWCNTs could reduce their life cycle impacts and improve their energy profile if they can be recovered using a method that requires less energy and results in reduced costs in comparison to synthesizing new virgin

material.[18] Thus, the goal of this work is to demonstrate the feasibility of recycling SWCNTs without compromising their nanoscale properties and functionality.

6.2 Experimental

6.2.a Methods Overview

To quantify and compare production and recycling impacts, SWCNTs have been synthesized via laser vaporization, purified through a combination of acid reflux and thermal oxidation procedures, fabricated into SWCNT free standing papers, and cycled as electrodes in lithium ion battery pouch cells. The SWCNT-Li^+ pouch cells are then forced to their end-of-life though extended cycling. Upgrading technologies for recycling or *refunctionalizing* (defined as the recovery and removal of unwanted impurities introduced during the use phase, without damaging the properties and functionality of the material) EOL SWCNTs, consisting of acid and thermal treatments, are investigated to return the SWCNTs to their pre-cycling properties and functionality. The material is characterized through a combination of scanning electron microscopy (SEM), thermal gravimetric analysis (TGA), Raman spectroscopy, and optical absorption spectroscopy. The direct electricity and volumetric chemical consumption required to recycle the EOL-SWCNTs is measured and compared to values for producing virgin SWCNT material. A schematic flow diagram of the process is provided in **Fig. 1** and each step is described in detail below.

6.2.b SWCNT Laser Vaporization Synthesis and Purification

The SWCNTs in this study were synthesized via pulsed laser vaporization using a 1064 nm Nd:YAG laser under previously published conditions.[13, 69, 70] Briefly, SWCNT material was synthesized from a Ni (3 % w/w) and Co (3 % w/w) doped graphite flake target (1-2 μm pressed to 25,000 psi) in a 1150°C three-zone tube furnace, and 200 SCCM flowing argon at 760 ± 10 torr. Purification of the as-produced SWCNT material occurs through a series of acid and thermal treatments developed following established procedures.[12, 13, 69, 70] For example, 150 mg of as-produced SWCNT material is brought to reflux at 125 ºC in 3M nitric acid for 16 hours and then is vacuum-filtered onto 1 μm PTFE membrane filter papers with copious amounts of water to remove residual acid. The SWCNT paper from acid reflux was thermally oxidized in air at 525°C at a ramp rate of 10 °C/minute in a Lindberg BlueM 1200 furnace. SEM, TGA, optical absorption, and Raman spectroscopy analyses were conducted during the purification process to assure that the quality of the purification was > 95 % w/w SWCNTs. The abbreviation "pure-SWCNTs" will be used when referencing high purity SWCNT material (purified via the above method) prior to electrochemical cycling in a Li^+ battery coin cell for the remainder of the manuscript.

6.7.c Material Characterization

The SWCNT material was characterized via scanning electron microscopy (SEM), optical spectroscopy, thermogravimetric analysis (TGA), and Raman spectroscopy. SEM analysis was performed using a Hitachi S-900 field emission electron microscope with an accelerating voltage of 2 kV. Optical absorption spectroscopy is performed in N,N-dimethylacetamide (DMA) 99+ % spectro-photometric grade (Sigma Aldrich) with a Perkin-Elmer Lambda 900 spectrophotometer from 300 nm – 1600 nm. SWCNT carbonaceous purity (w/w %) was obtained from the peak

ratios of the absorption maxima at 650 nm (1.9 eV) and 950 nm (1.3 eV) using the previously reported method.[69] Raman spectroscopy is performed using a 1.96 eV He-Ne laser with a JY-Horiba Labram spectrophotometer over the range 100 cm^{-1} to 2800 cm^{-1}. TGA is performed up to 1000°C at 10 ^{o}C/min using a TGA Q5000IR from TA instruments on representative portions of the as-produced SWCNT material.

6.2.d Galvanostatic Testing and End-of-Life SWCNT Recovery

All SWCNT electrodes were galvanostatically cycled from 0.005 - 3V using an Arbin BT-2000 at 25°C versus lithium metal foil. The electrolyte was 1M $LiPF_6$ in ethylene carbonate (EC), propylene carbonate (PC), and diethyl carbonate (DEC) (Novelyte) at a ratio of 1:1:2 by volume, respectively. A specific capacity of 372 mAh/g was assumed to establish constant current C/t rates (where t is the time for a complete charge or discharge in hours), and the cells were charged-discharged at a C/10 rate. EOL-SWCNTs were produced by cycling 28 mg pure SWCNTs in a 3 cm x 4 cm pouch cell to ensure enough material to perform the recycling processes. The Li/SWCNT pouch cell was constructed by compressing lithium metal onto a nickel mesh (Dexmet) current collector, and SWCNTs were electrically contacted by ultrasonically bonding a 15 um copper foil tab (Fukuda) with an Amtek Ultraweld 40. The separator and electrolyte were kept the same as in the coin cell testing and the pouch cell material (Dai Nippon Printing) was sealed using a U-line H-161 impulse sealer. The pouch cell was galvanostatically cycled at a C/10 rate from 0.005 - 3V until the lithium ion extraction capacity from the SWCNT electrode reached 20% of the original capacity, which was deemed to be EOL in this study. The electrochemical performance of the recycled SWCNTs was compared to purified SWCNTs in a 2032 coin cell configuration with a Celgard 2325 separator.

The EOL-SWCNT electrode material was removed from the pouch cell inside a moisture- and oxygen-controlled glove box and placed into a scintillation vial with 50 mL of DEC electrolyte. A magnetic stir bar was added to the vial prior to removal from the inert environment. The EOL-SWCNT electrode was homogenized on a magnetic stir plate for 3 hours at room temperature before an additional 1 hour homogenization in an ultrasonic bath at 40 ˚C. The homogenized material was then recovered via vacuum filtration onto a 1 µm polytetraflouroethylene (PTFE) filter paper and dried in a vacuum oven at 100 °C for 2 hours. The homogenized-SWCNT anode material increased in mass to 56 mg and was divided into two equal segments, which were subsequently used to investigate two potential upgrading technologies.

6.2.e Single-Wall Carbon Nanotube Recycling

Two different methods of recycling EOL-SWCNTs recovered from Li^+ battery electrodes were investigated as depicted in **Fig. 1**, based on published SWCNT purification methods.[70, 100, 101] The first method uses a nitric acid reflux procedure followed by a thermal oxidation in air to remove the SEI layer, and the second method uses a concentrated HCl acid rinse followed by a thermal oxidation. The schematic flow diagram of the recycling methods is provided in **Fig. 1** as an overview and described in detail below.

6.2.f Acid Reflux Procedure (Acid Reflux)

An acid reflux was chosen as a recycling procedure due to its established use in purifying as-produced laser SWCNTs.[70, 100, 101] Specifically, half (28 mg) of the homogenized-SWCNT

electrode was refluxed for 16 hours consisting of 6 M nitric acid and 3 M HCl acid. The resulting acid reflux-SWCNT material was recovered via vacuum filtration onto a 1 μm PTFE filter paper. The acid reflux filtrate was discarded, and the SWCNT paper was rinsed with deionized water and acetone to remove intercalated acid. The acid reflux-SWCNT material was then dried in a vacuum oven for 2 hours at 100 °C. An initial low-temperature thermal oxidation was performed, in a Lindberg/Blue M tube furnace, to 500 °C at a temperature ramp rate of 10 °C/min under a gas flow rate of 0.200 L/min dry industrial air (Airgas Inc). A final high-temperature thermal oxidation was performed under similar conditions to a final temperature based on the temperature from the TGA 1st order derivative peak maximum of the acid reflux-SWCNTs to remove remaining impurities. EOL-SWCNT material recycled though this procedure will be referred to as "acid reflux" SWCNTs in the text and figures for the remainder of the article.

6.2.g HCl Acid Procedure (HCl Acid)

A hydrochloric acid rinsing procedure was developed as a simplified alternative to the acid reflux. In this procedure, concentrated hydrochloric acid (37 %) (Sigma Aldrich) was added to the remaining 28 mg of the homogenized EOL-SWCNT paper and magnetically stirred for 1 hour at room temperature. The HCl-SWCNT material was then placed in an ultrasonic bath for 15 minutes. The HCl-SWCNTs were recovered via vacuum filtration onto a 1 μm PTFE filter paper and rinsed with deionized water and acetone to remove intercalated acid, and dried at 100 °C in a vacuum oven for 2 hours. An initial low temperature thermal oxidation was performed, following the above conditions of the acid reflux-SWCNT procedure, to a final temperature of

500 °C and a final high temperature oxidation was performed under similar conditions based on the temperature from the TGA 1st order derivative peak maximum of the HCl acid-SWCNTs to remove remaining impurities. EOL-SWCNT material recycled though this procedure will be referred to as "HCl acid" SWCNTs in the text and figures for the remainder of the article.

7.2.h Direct Electricity Consumption and Chemical Waste Generation

The direct electricity (kWh) consumption of the equipment used for the synthesis, purification, and recycling procedures is measured using a Watts Up? Pro® digital power meter. The instantaneous power consumption is recorded at 1 second data intervals for the duration of each recycling step. The total direct electricity consumption of each recycling process is the sum of measured electricity inputs to all processing steps. The direct volumetric chemical waste generation during each step in the purification and recycling processes is also measured. All chemicals (e.g. deionized water, hydrochloric acid, nitric acid, and acetone) used in the processing and recycling steps are considered hazardous waste, which therefore requires proper disposal and treatment. In this report, the total volume of chemical waste generated is compared to the volumetric chemical waste generated from the synthesis and purification procedures. To make an accurate comparison of the direct electricity consumed and volumetric chemical waste generated it was assumed that the pure, acid reflux, and HCl acid SWCNT procedures are performed with equivalent SWCNT mass loading. Both recycling processes, if successful, will produce functionally equivalent materials as the pure SWCNTs.

\

6.3 Results and Discussion

TGA of the SWCNT material showed an increase in the non-combustible TGA residue (at 900 °C) from <4 % in the pure-SWCNT material to 49.5 % in the EOL-SWCNTs (see **Fig. 2**). This 45 % increase in the non-combustible mass fraction is attributed to the formation of the solid electrolyte interphase (SEI) layer. During the first cycle lithium insertion of the SWCNT/lithium battery, a portion of the lithium atoms react with the non-aqueous solvent at the electrode surface and form the SEI layer. This layer is necessary to facilitate interaction between lithium ions and the SWCNT electrode material.[102-104] This SEI layer consists of number of different lithium-containing compounds ($Li_x(solvent)_yC_z$) including $LiPF_6$, $LiCF_3SO_3$, $LiN(SO_2CF_3)_2$, and Li_2CO_3.[104, 105] Ultimately, the SEI layer can continue to grow until it negatively impacts the performance of the battery. The growth of the SEI is one of several mechanisms that occur with extended cycling leading to the failure of a lithium battery system. Disassembling the EOL battery and removing the SEI layer on the SWCNT electrode would be a critical step in the recycling of the SWCNT material. Initial attempts to remove the SEI layer using solvents (e.g. deionized water, N,N,-dimethylacetamide, ethanol, acetone) were not successful and motivated the investigation of acids to solubilize the SEI.

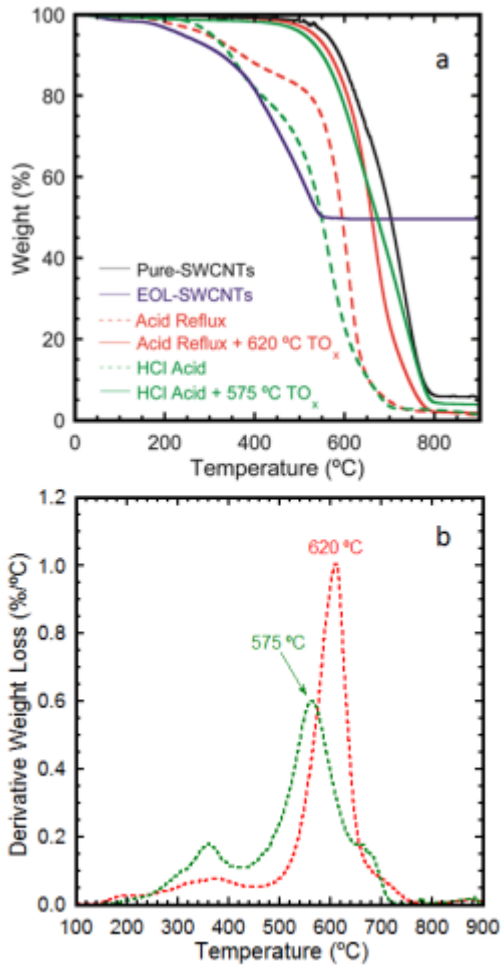

Figure 57. Thermo gravimetric analysis of (a) single-wall carbon nanotubes at each step in recycling process from free standing lithium ion battery electrodes and (b) the first order derivatives of acid-reflux and HCl treated SWCNTs prior to thermal oxidation, peak combustion temperatures are labeled. Original figure created by author and reproduced with permissions from Schauerman, C.M.; et al; "Recycling Single-Wall Carbon Nanotube Anodes from Lithium Ion Batteries." *J. Mater. Chem.*, 2012, *22*, 12008-12015 for use in dissertations.

Figure 57a illustrates that the non-combustible mass fraction is reduced to <1 % w/w following initial acid treatments for both the acid reflux-SWCNTs and HCl acid-SWCNT methods. However, residual combustible impurities still contribute to the pre-combustion of the acid reflux-SWCNT and HCl acid-SWCNT materials as is evident from the shift to lower combustion temperatures with decomposition of the SWCNT material starting at ~200 °C (dotted lines

Figure 57a). An initial low temperature oxidation was performed on both materials to 500 °C to remove the remaining combustible impurities and prevent the pre-combustion of the SWCNTs. The final thermal

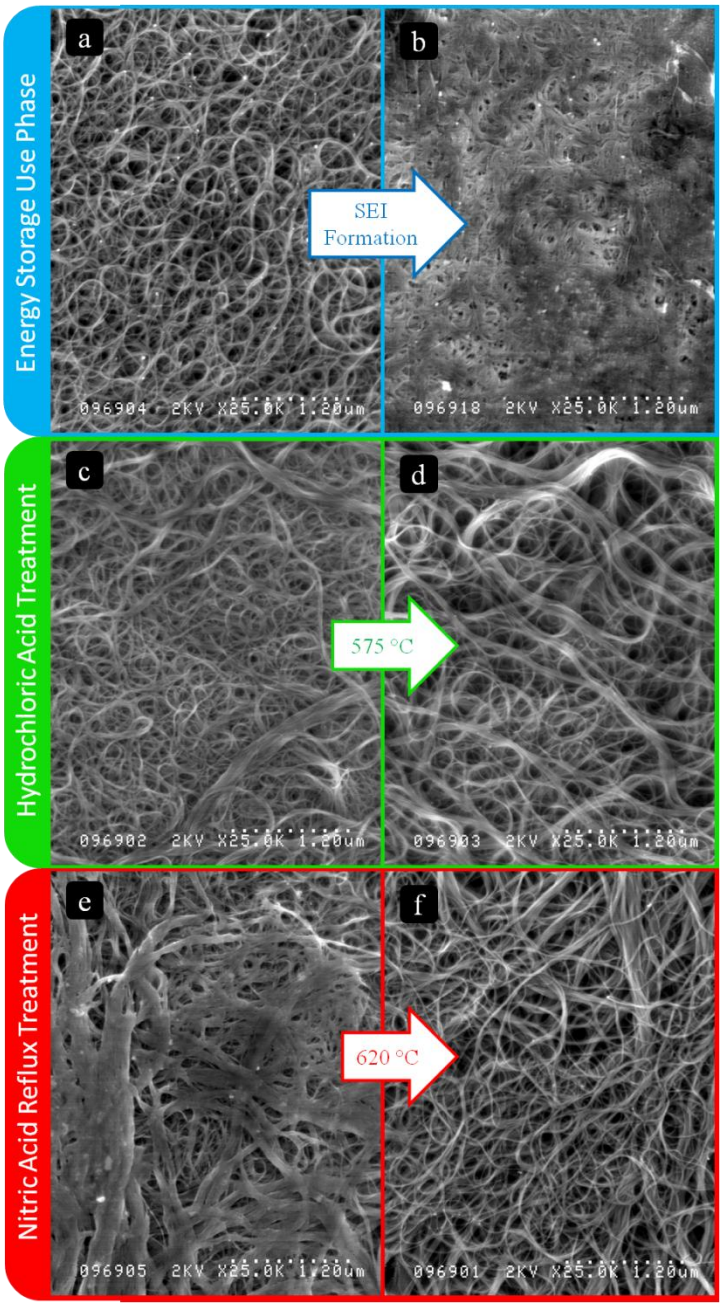

Figure 58. Scanning electron micrographs of a) high purity single-wall carbon nanotubes (SWCNTs) pre-electrochemical cycling, b) post-electrochemical cycling end-of-life SWCNTs with solid electrolyte interphase coatings, c) HCl acid treated EOL-SWCNTs, d) 575 °C thermal oxidation of HCl treated SWCNTs, e) nitric acid reflux treated EOL-SWCNTs, and f)

620 °C thermal oxidation of acid reflux SWCNTs. All images are at 25,000x magnification. Original figure created by author and reproduced with permissions from Schauerman, C.M.; et al; "Recycling Single-Wall Carbon Nanotube Anodes from Lithium Ion Batteries." *J. Mater. Chem.*, 2012, *22*, 12008-12015 for use in dissertations.

oxidation temperatures were chosen based on the peak combustion temperature of 1st order derivative (Figure 57b dotted lines) 620 °C for acid reflux-SWCNTs and 575 °C for HCl acid-SWCNTs. The peak combustion temperature was chosen instead of the onset of the main combustion peak to ensure high SWCNT purity in the recycling process, but likely negatively impacted the SWCNT material recovery efficiency.[100] The increased thermal oxidation temperature for the acid reflux-SWCNT in the recycling procedure is attributed to the increased combustible impurities on the surface of the SWCNTs. The thermal oxidation treatments, below the decomposition temperature of the pure-SWCNTs, were successful in removing the remaining combustible impurities and resulted in the recovery of the TGA curve morphology to that which is typical of pure-SWCNTs in Figure 57a.

Scanning electron micrographs of the pure-SWCNTs, EOL-SWCNTs, HCl acid-SWCNTs and acid reflux-SWCNTs are provided in Figure 58. Typical surface morphology for high purity laser produced SWCNTs is present in Figure 2a.[11, 13, 69, 70, 106] Following lithium ion testing, a build-up of the SEI layer on the bundled EOL-SWCNTs is clearly visible (**Fig. 3b**).Treatment of the EOL-SWCNTs with HCl acid reduced the SEI on the SWCNTs although some coatings are still visible in the micrograph image (Figure 58c). No evidence of residual SEI compounds is visible in micrographs of the thermally oxidized (575 °C) HCl acid-SWCNTs (Figure 58d). Coatings remain present in micrographs of the acid reflux-SWCNTs (Figure 58e) prior to thermal oxidation treatments. Higher purification temperature (620 °C) were therefore required to

adequately remove remaining impurities (Figure 58f). The surface morphology of both the acid reflux-SWCNTs and HCl-SWCNTs exhibited modest increases in SWCNT bundling, based upon SEM, following the recycling procedures in comparison to the pure-SWCNTs.

Further evidence of the removal of the SEI layer was obtained through Raman spectroscopy (see Figure 59) which measures the phonon interactions between side wall atoms of the SWCNTs. Little change in the normalized peak intensities was measured between the samples for each step in the SWCNT electrode life cycle, however shifts in the peak locations were observed in the EOL-SWCNTs. A clear Raman shift in the peak wavenumbers (5 cm^{-1}) is visible for the radial breathing modes (RBM ~200 cm^{-1}) as well as the G (~1600 cm^{-1}) and G' (~2600 cm^{-1}) peaks of the EOL-SWCNTs. RBMs are indicative of phonon scattering and molecular expansion and contraction in the radial dimension, and can be used to directly calculate the diameters of individual SWCNTs.[107] The shift in the RBM is likely the result of SEI films dampening radial oscillations of the nanotubes (Figure 59b) which is similar to the shift in the RBMs due to polymer wrapping of the SWCNTs.[108, 109] A recovery of the peak locations was achieved following the removal of the SEI layer through the acid and thermal treatments and the SWCNT RBM peaks returned to their pure-SWCNT values. It is important to note the retention of all SWCNT diameter peaks is observed throughout the coin cell testing and recycling process. If specific diameters were damaged, during any step of the process, it would be reflected by the absence of the

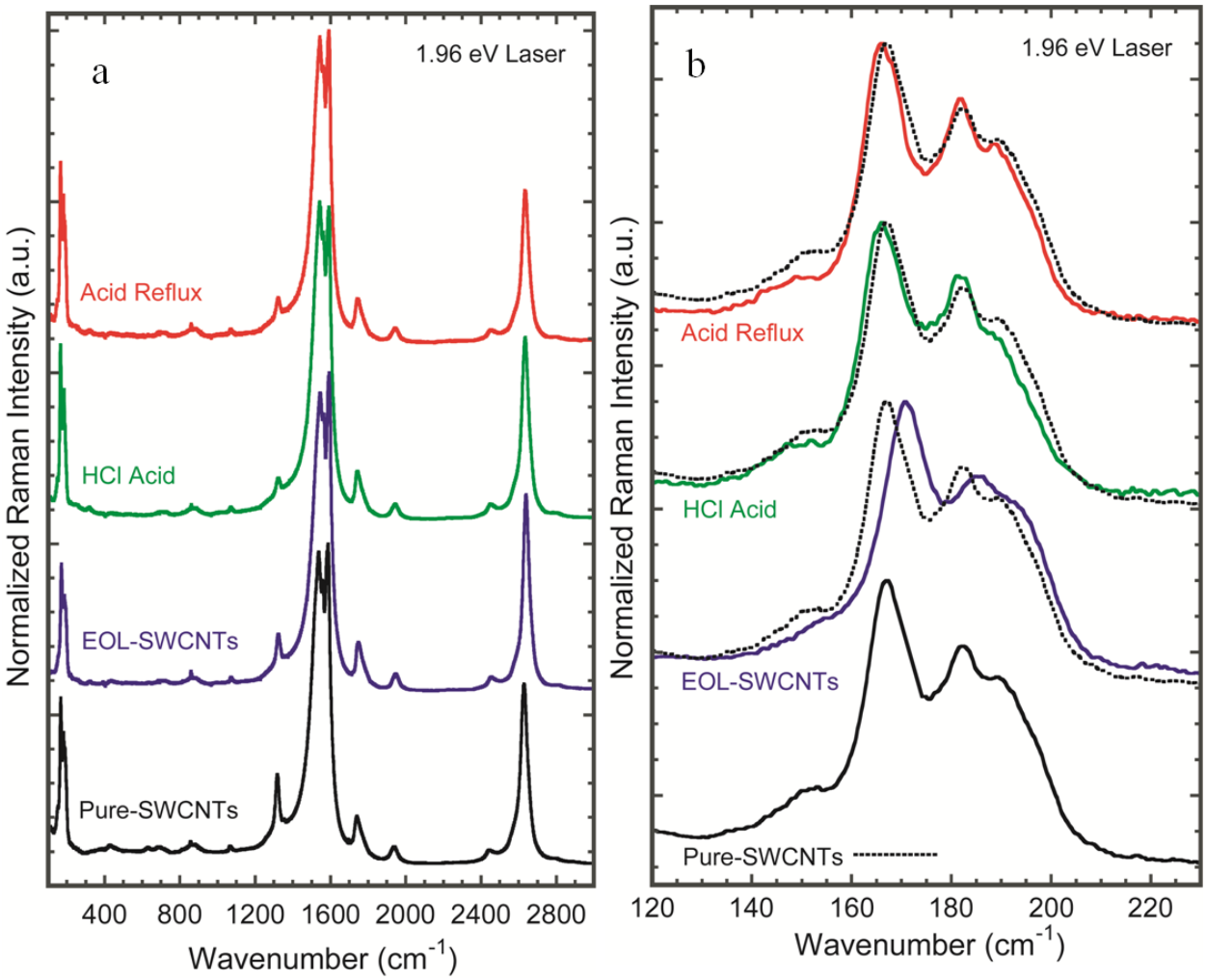

Figure 59. Normalized Raman spectra of high purity, end-of-life, and high purity recycled single-wall carbon nanotube (SWCNT) radial breathing modes (RBM). Curves are offset for clarity and high purity SWCNTs RBM overlays (dotted lines) are provided as a guide to the eye for comparison. The plotted Raman data is a combination of three different measurement points taken on each sample, averaged, and baseline corrected. Original figure created by author and reproduced with permissions from Schauerman, C.M.; et al; "Recycling Single-Wall Carbon Nanotube Anodes from Lithium Ion Batteries." *J. Mater. Chem.*, 2012, *22*, 12008-12015 for use in dissertations.

corresponding RBM peaks in the Raman spectra. Additionally, there is no enhancement of the D-band or suppression of the G' band for the Raman spectra suggesting that the structure of the SWCNTs is also maintained with increased processing.

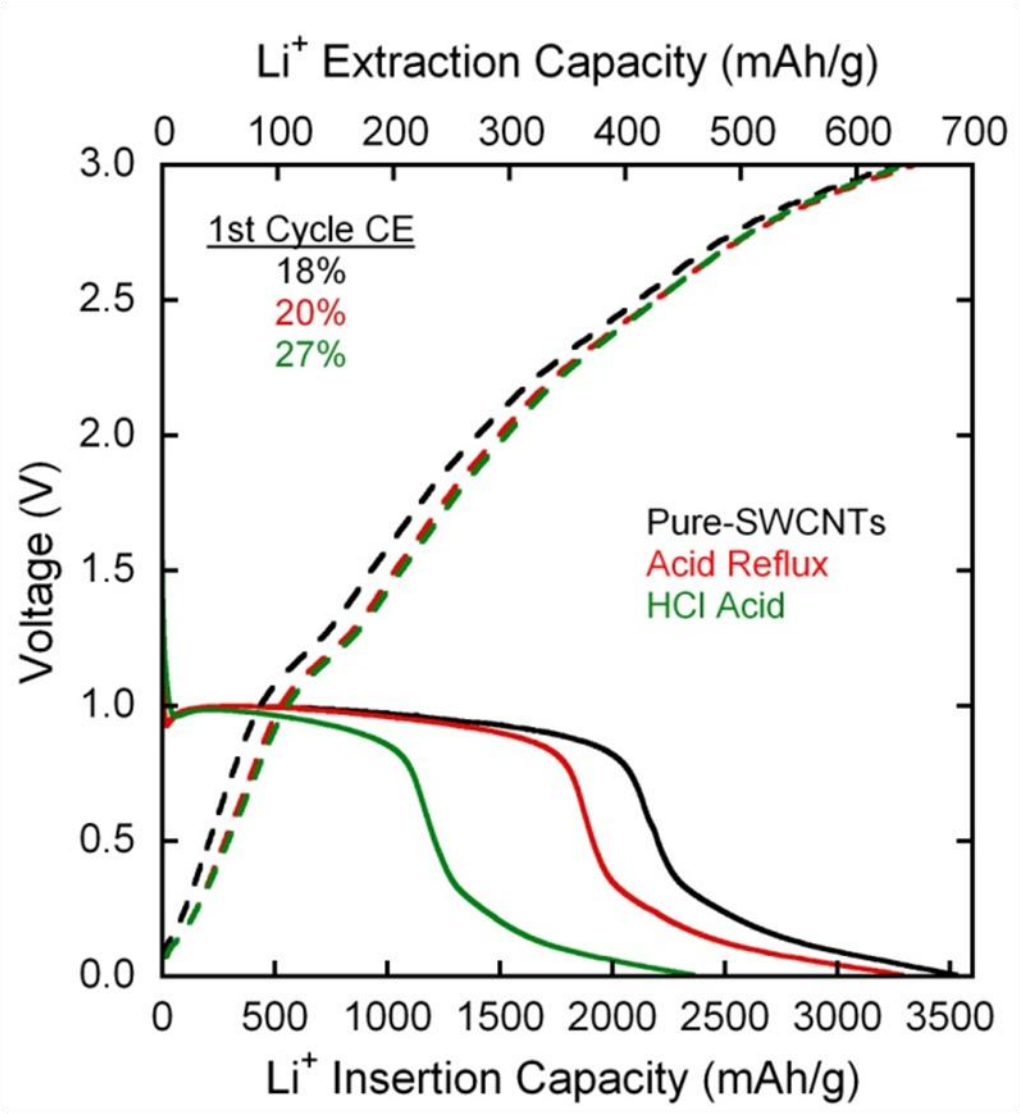

Figure 60. Lithium insertion capacity (solid lines) and lithium extraction capacity (dashed lines) for high purity single-wall carbon nanotube (SWCNT) electrodes, acid reflux recycled SWCNTs, and HCl acid recycled SWCNT electrodes. Original figure created by author and reproduced with permissions from Schauerman, C.M.; et al; "Recycling Single-Wall Carbon Nanotube Anodes from Lithium Ion Batteries." *J. Mater. Chem.*, 2012, *22*, 12008-12015 for use in dissertations.

Li^+ coin cells were fabricated from the free-standing acid reflux-SWCNT and HCl acid-SWCNT recycled material, and cycled using identical testing parameters as the pure-SWCNT electrodes.

Comparable extraction capacities (650 mAh/g) were measured for both recycled SWCNT electrodes (see Figure 60). The coulombic efficiency of the HCl-SWCNTs increased to 27 % compared to 18% coulombic efficiency in the pure-SWCNT materials. The coulombic efficiency of the coin cells is directly related to the formation of the SEI layer on the surface area of the electrode material during Li^+ cycling. Factors such as residual SEI material and graphitization of the SWCNTs could also contribute to the increase. However, graphitization was not observed in the battery cycling data of the recycled-SWCNT material where a voltage plateau would be present in the extraction voltage profiles (dotted lines Figure 60) at ~ 0.1 V indicative of electron insertion between graphene planes.[83] The lack of the voltage plateau feature suggests graphite is not forming during the recycling process. Additionally, graphite particles were not visible in any of the SEM micrographs of either recycled material. Therefore, increased bundling of the SWCNT networks, from the acid reflux and HCl acid purification process, may account for the increased coulombic efficiency.

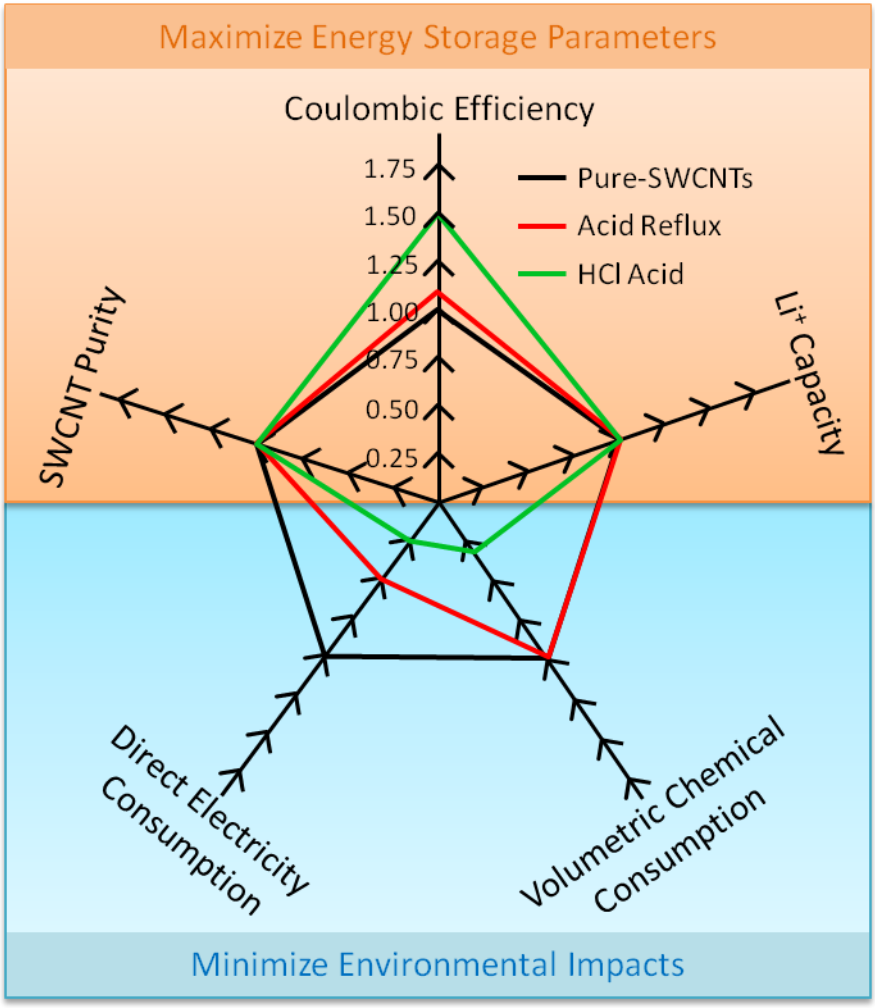

Figure 61. Change in relevant metrics following electrochemical cycling and SWCNT recycling. All data was normalized to pure-SWCNT values as the baseline. Data points further from the origin represent an increase over the baseline whereas data points closer to the origin represent a decrease relative to the baseline value. Original figure created by author and reproduced with permissions from Schauerman, C.M.; et al; "Recycling Single-Wall Carbon Nanotube Anodes from Lithium Ion Batteries." *J. Mater. Chem.*, 2012, *22*, 12008-12015 for use in dissertations.

The development of refunctionalization processes for nanomaterials requires a systems level view to evaluate the overall impact of each pathway. Relevant metrics are graphically represented in Figure 61 for both recycled SWCNT material types. Results are normalized to the production of new pure-SWCNTs as a baseline reference. Metrics to be maximized are

highlighted in the top half of Figure 61 and compare the SWCNT carbonaceous purity and lithium ion battery performance metrics of the SWCNT electrodes. UV-vis-NIR analysis was performed on the pure, acid reflux, HCl acid SWCNT materials, and all three have measured carbonaceous purities greater than 95%. The refunctionalized SWCNT material performs as good as or better than the pure-SWCNT material, demonstrating increased coulombic efficiency without a reduction in the material carbonaceous purity or extraction capacity. Metrics to be minimized are highlighted in the bottom half of Figure 61 and compare the environmental impacts for each recycling procedure. The measured electricity of refunctionalizing SWCNTS using the acid reflux and HCl treatments was 50% and 75%, respectively, of the total direct energy required to synthesize and purify pure-SWCNTs from primary materials. It is important to note that the acid reflux procedure used to refunctionalize the EOL-SWCNTs is the exact same procedure used to purify as-produced SWCNTs. Therefore, refunctionalizing SWCNTs with the acid reflux procedure will *always* result in less direct electricity than the synthesis and purification of new SWCNT material. Additionally, the simplified steps in the HCl procedure resulted in a 66 % reduction in the volumetric chemical waste generation. Because both procedures result in functionally equivalent materials, the reduced environmental impacts of the HCl acid procedure may make it a preferred method in comparison to the acid reflux procedure.

6.4 Conclusions

SWCNTs were successfully synthesized via laser vaporization synthesis, purified, and incorporated into a Li+ ion battery coin cell. The coin cells were galvanostatically cycled at high C-rates until failure. The EOL-SWCNT material was recovered from the Li+ battery electrodes and refunctionalized utilizing upgrading procedures originally developed for purifying as-

produced virgin SWCNT material. Conventional nitric acid reflux and hydrochloric acid treatments followed by thermal oxidation in air were successful in restoring EOL-SWCNT material to pre-cycling (pure-SWCNT) properties without destruction of their nanoscale structure and functionality. The recycled-SWCNT material was then successfully incorporated into new SWCNT electrode Li+ battery coin cells with comparable measured insertion and extraction capacities to the virgin pure-SWCNT electrodes. The recycled SWCNT materials demonstrated improved coulombic efficiencies over the cycling performance of the pure-SWCNT materials. The direct electricity of the recycling procedure and chemical waste generated was measured and compared to direct electricity and chemical waste generated when synthesizing and purifying new SWCNT materials. A 50 % (acid reflux SWCNTs) and 75 % (HCl acid SWCNTs) reduction in the direct processing electricity is achieved through recycling, as compared to the synthesis and purification of new virgin SWCNT material. The implications of this work are 1) it is possible to recover, refunctionalize, and reuse SWCNTs from an electrochemical application; 2) the recycling procedure of nanomaterials will likely be similar to purification steps relevant to the native material; and 3) preservation of the nanoscale dimensions and functionality of the SWCNT far outweigh elemental recycling of the carbonaceous base material for synthesizing new virgin SWCNTs. The initial results of this study also warrant further investigation of recycling multi-component samples, which require additional separation of waste streams and removal of other contaminants from the SWCNT networks. Overall, this study highlights the ability and importance of developing recycling procedures for emerging nanomaterials. As nanomaterials are increasingly adopted, forward thinking consideration of recycling, refunctionalization, and reuse will be necessary, to ensure these materials do not cause unforeseen negative environmental impacts.

There are some limitations to the results presented in this section. The ability to refunctionalize SWCNTs from lithium ion battery anodes in a controlled laboratory environment would need to be expanded to larger scale mixed waste streams. Policy would need to be developed to effectively collect distributed end-of-life CNT products for refunctionalization processes. The impact of collecting, refunctionalizing, and making new CNT products should be compared to the synthesis of virgin CNT products at industrial scales through a comprehensive LCA.

Chapter 6 Acknowledgements: I would like to acknowledge the assistance of Matthew J. Ganter in the assembly, half cell cycling, and disassembly of the SWCNT anode lithium ion half cells.

Chapter 7 Dissertation Summary and Conclusions

The entire life cycle of carbon-based conductors was investigated (Figure 62) starting from the laser vaporization synthesis of new SWCNTs to the refunctionalization of end-of-life SWCNTs. During the course of the sustainable production of CNT wires and cables several milestones were reached. A full glove box laser vaporization reactor enclosure was designed and constructed which isolates the researcher from as-produced SWCNT dust and nanoparticles. SWCNT were synthesized via laser vaporization using nanometal catalyst particles which increased the material yield by 50 % and simplified the purification steps to a thermal oxidation and HCl rinse. SWCNTS were modified at the nanoscale through the incorporation of chemical dopants, mechanical densification, and applied current alignment. Bulk electrical conductors were manufactured using two different techniques; drawing die densification and superacid extrusions with electrical conductivities as high as $4.9x10^6$ S/m. Functional conductors were fabricated and demonstrated their viability as USB cables, Ethernet cables, coaxial cables, and conductive electrodes for lithium ion batteries. At their end-of-life a new technique for restoring the conductive function of SWCNTs was developed for the first time and was demonstrated as a viable alternative to land filling end-of-life SWCNTs.

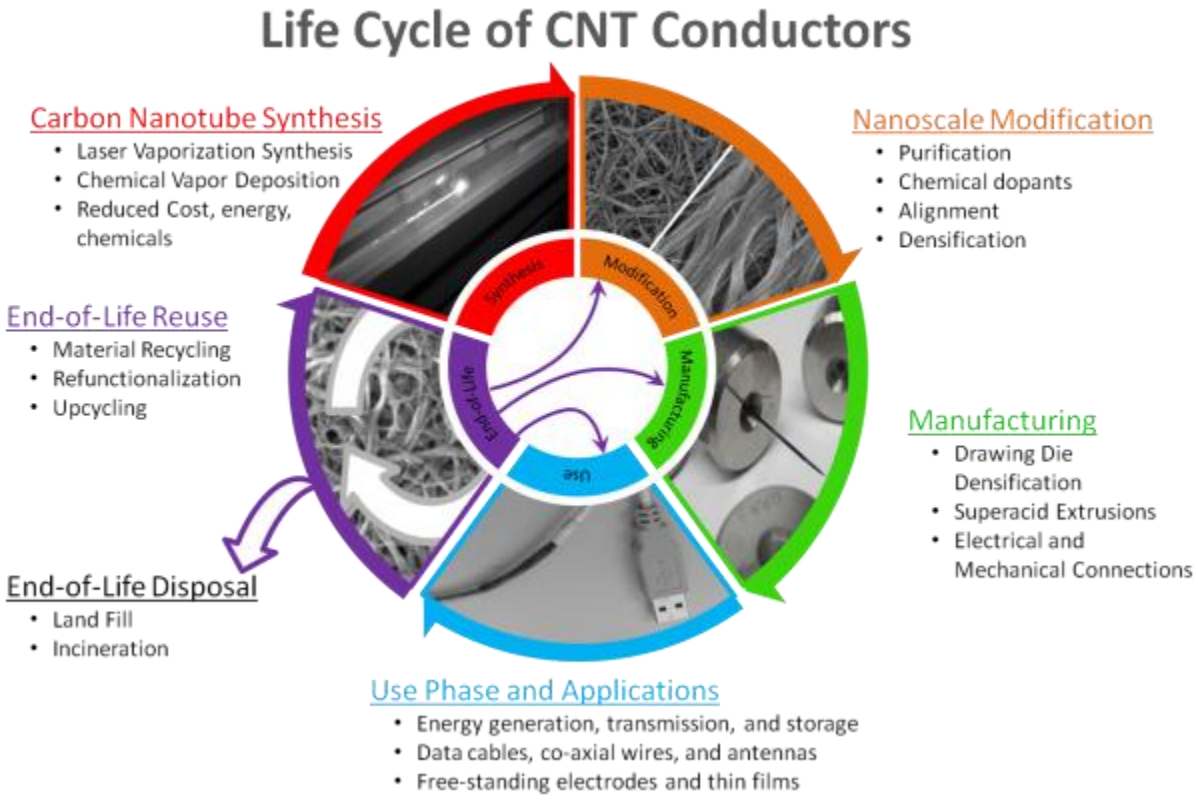

Figure 62. Life cycle of carbon nanotube based conductors with modified end-of-life path options for refunctionalizing carbon nanotubes for use in new products. Original figure created by author.

Limitations and New Research Areas

In addition to achieving parity with the electrical conductivity of copper, unresolved questions pertaining to the environmental and human health impacts of CNTs could affect the development and commercial adoption of these conductors. Because of the large cumulative energy demand and high cost associated with the manufacturing of CNTs, refunctionalization can potentially lessen some these impacts at end of life. There are however other impacts along the way to commercialization that should also be addressed. Therefore, sustainability-focused initiatives could address several open areas of research:

- Quantifying the environmental and human health impacts of all nanomaterials including SWCNT, DWCNT, and MWCNTs.
- Developing green chemistry approaches which reduce the chemicals, electricity, emissions, and cost of CNT manufacturing
- Quantify the impacts of the green synthesis of CNTs at industrial levels through a through life cycle assessment
- Develop a policy driven framework to govern the collection, disposal, and refunctionalization of CNT containing waste streams which minimized environmental and human health impacts

Sustainabilitists have the necessary tools required to address these questions and more as the field of nanotechnology continues to grow and evolve.

A synopsis of each chapter of the dissertation is discussed below with a conclusion sentence highlighting an important take away from the work.

Chapter 2:  Original figure created by author.	Chapter 3 of the dissertation demonstrated the advantages of using nanometer diameter catalyst particles for the synthesis of SWCNTs via laser vaporization. Specifically, nanometal catalysts enhanced the yield (both carbonaceous purity and rate of SWCNT growth). Increasing the production of SWCNTs through the use of more efficient catalyst will help lower the direct electricity consumption, per mass, of SWCNTs during the synthesis process. In addition, the use of nanometal catalyst reduced the purification steps necessary to achieve high purity free standing papers. The reduction in purification steps reduced the direct electricity consumption and chemical waste generation. **Major Result:** The use of nanometal catalyst increases the SWCNT yield and reduce the direct electricity consumption and chemical waste generation.
Chapter 3-1:  Original figure created by author.	Chapter 4 of the dissertation investigated a series of chemical treatment methods to increase the electrical conductivity in bulk networks of SWCNTs. Increasing the electrical properties of bulk SWCNT networks is a critical component of making functional devices out of the nanomaterials. Understanding how to properly control and modify the chemical environment around nanotubes to increase the electrical conductivity. **Major Result:** Chemical dopants such as $KAuCl_4$ and $KAuBr_4$ are able to increase the electrical conductivity of a bulk SWCNT conductor by an order of magnitude, however the delivery method is critical to maximizing the susceptibility response.
Chapter 3-2:	Because commercial sources of CNTs vary in synthesis method (e.g. HiPCO, CoMoCAT, CVD, arc, flame) they also vary in composition. Synthesis

 Original figure created by author.	methods like CVD will also produce SWCNTs, DWCNTs, and MWCNTs in varying quantities. Chapter 5 examined mixed systems of single-wall and multi walled carbon nanotubes and measured differences in the chemical doping susceptibility between the two CNT species. The chemical doping susceptibility of the mixed system (from 0 % w/w to 100 % w/w SWCNTs in MWCNTs) increased with increasing SWCNT content. The 100 % SWCNT paper showed the highest response to chemical dopants and has a correspondingly higher change in the Raman Spectra. **Major Result:** Moving to bulk CNT conductors that are comprised of predominately small diameter single or few walled carbon nanotubes will maximize the doping susceptibility and thus electrical conductivity.
Chapter 4:  Original figure created by author.	Chapter 6 of the dissertation builds off of the findings of chapter 5 and investigates methods of modifying the nanoscale morphology of SWCNTs and mixed species (SWCNTs, DWCNTs, and MWCNTs) of commercially produced CVD CNTs and laser produced SWCNTs. Superacids are used to dissolve CNTs at high weight loadings and reassemble them into highly dense aligned bundles. Applied heat, current, and extrusion methods are employed to increase the density and alignment of the individual CNTs within the bulk network, and from continuous bulk wire conductors with high conductivity. **Major Result:** Chlorosulfonic acid is a power tool for modifying CNT networks at the nanoscale, and through high weight loading dispersion can produce continuous CNT wires with very high electrical conductivity.
Chapter 5:	Chapter 7 Proposal Summary: Chapter 7 of the dissertation develops methods of contacting the bulk CNT conductors from previous chapters to real-world metallic contacts. Because carbon materials do not lend themselves to

 Original figure created by author.	conventional solder and welding techniques to make electrical contact another method bonding was investigated: ultrasonic welding. In this method ultrasonic energy is used to mechanically and electrically contact bulk CNT materials to metallic **Major Result:** Ultrasonic welding can be used as a viable method for forming both electrical and mechanical contacts to metallic interconnects.
Chapter 6:  Original figure created by author.	This chapter focused on a near-term applications of SWCNTs materials as a electrical conductor in lithium ion battery anodes. Specifically, SWCNTs were used as both an electrode and as a lithium insertion material in the anode of a lithium ion battery. The battery was forced to an end-of-life state through extended cycling and recycling techniques were used to recover the SWCNT material and refunctionalize it to a reusable material. The refunctionalized SWCNTs were then incorporated into the anode of new lithium ion battery which performed as-well-as the virgin SWCNT materials with a reduced chemical and electrical footprint. **Major Result:** Refunctionalization of SWCNT lithium ion battery anodes can reduce the direct electricity consumption and chemical waste generation while restoring the original functionality.

Figure 63 is a timeline representation of notable milestones in the development and manufacturing of carbon based conductors achieved during the course of this dissertation research.

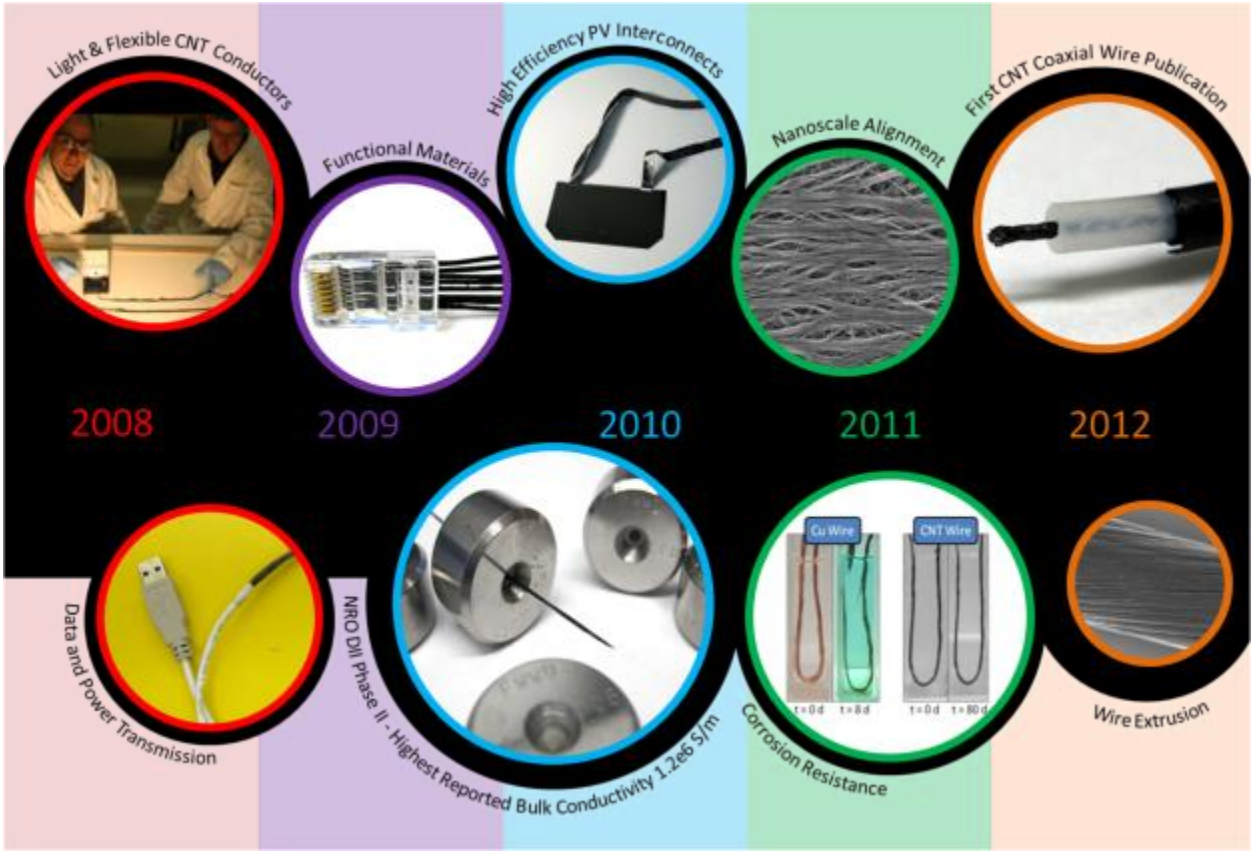

Figure 63. Carbon nanotube conductor developmental timeline from the start to finish of the PhD dissertation research. Original figure created by author.

List of Journal Publications, Conference Proceedings, and Conference Presentations

Journals Articles

(1) Forney, M.W.; R.A.; Raisanen, A.; **Schauerman**, C.M.; Staub, J.W.; Foringer, R.D.; Willis, S.M.; Ridgley, R.D. and Landi, B.J.; High capacity Si-carbon nanotube anodes for lithium-ion batteries. *JICRD 2013.*

(2) Jarosz, P.R.; Shaukat, A.; Mastrangelo, T.L.; **Schauerman, C.M.;** Cress, C.D.; Ridgley, R.D.; and Landi, B.J.; "Coaxial Cables with Single Wall Carbon Nanotube Outer Conductors Exhibiting Attenuation/Length within Specification." *IEEE Micro & Nano Letters*, **2012**, *In Press*.

(3) Rossi, J.E.; Cress, C.D.; Helenic, A.R.; **Schauerman, C.M.**; DiLeo, R.A; Cox, N.D.; Messenger, S.R.; Weaver, B.D.; Hubbard, S.M.; Landi, B.J.; "Ion Irradiation of Electronic-Type-Separated SWCNTs: A Model for Radiation Effects in Nanostructured Carbon." *Journal of Applied Physics*, 2012.

(4) **Schauerman**, **C.M.**; Ganter, M.J.; Gaustad, G.; Babbitt, C.; Raffaelle, R.P.; Landi**,** B.J.; "Recycling Single-Wall Carbon Nanotube Anodes from Lithium Ion Batteries." *J. Mater. Chem.*, **2012,** *22*, 12008-12015.

(5) Jarosz, P.R.; Shaukat, A.; **Schauerman**, **C.M.**; Cress, C.D.; Kladitis, P.E.; Ridgley, R.D.; Landi**,** B.J. "High Performance Lightweight Coaxial Cable from Carbon Nanotube Conductors." *ACS Applied Materials and Interfaces*, **2012**, *4*, 1103-1109.

(6) Jarosz, P.; **Schauerman, C.M.**; Alvarenga, J.; Moses, B.; Mastrangelo, T.; Raffaelle, R.; Ridgley, R.; Landi**,** B.; "Carbon Nanotube Wires and Cables: Near-Term Applications and Future Perspectives." *Nanoscale*, **2011**, *3* (11), 4542 - 4553.

(7) Ganter, M.J.; DiLeo, R.A.; **Schauerman**, **C.M.**; Rogers, R.E.; Raffaelle, R.P.; Landi**,** B.J.; "Differential scanning calorimetry analysis of an enhanced $LiNi_{0.8}Co_{0.2}O_2$ cathode with single wall carbon nanotube conductive additives." *Electrochimica Acta*, **2011**, *56*, 7272-7277.

(8) Alvarenga, J.; Jarosz, P.R.; **Schauerman**, **C.M.**; Moses, B.T.; Landi**,** B.J.; Cress, C.D.; Raffaelle, R.P.; "High conductivity carbon nanotube wires from radial densification and ionic doping." *Appl. Phys. Letters,* **2010**, *97*, 182106.

(9) Cress, C.D.; **Schauerman**, **C.M.**; Landi**,** B.J.; Messenger, S.R.; Raffaelle, R.P.; Walters, R.J.; "Radiation effects in single walled carbon nanotube papers." *J. Appl. Phys.* **2010**, *107*, 014316.

*(10)***Schauerman**, **C.M.**; Alvarenga, J.X.; Landi**,** B.J.; Cress, C.D.; Raffaelle, R.P. "Impact of nanometal catalysts on the laser vaporization synthesis of single wall carbon nanotubes." *Carbon* **2009**, *47*, 2431-2435.

(11)Ganter, M.J.; Landi**,** B.J.; Worman, J.J.; **Schauerman**, **C.M.**; Cress, C.D.; Raffaelle, R.P.; "Variation of Single Wall Carbon Nanotube Dispersion Properties with Alkyl Amide and Halogenated Aromatic Solvents." *Mater. Chem. & Physics* **2009**, *116*, 235-241.

(12)Landi**,** B.J., DiLeo, R.A., **Schauerman**, **C.M.**, Cress, C.D., Ganter, M.J., Raffaelle, R.P. "Multi-walled carbon nanotube paper anodes for lithium ion batteries." *J. Nanosci. and Nanotechnol.* **2009**, *9*, 3406–3410.

(13)Landi**,** B.J.; Ganter, M.J.; **Schauerman**, **C.M.**; Cress, C.D.; Raffaelle, R. P. "Lithium Ion Capacity of Single Wall Carbon Nanotube Paper Electrodes" *J. Phys. Chem. C.*, **2008**, *112*, 7509-7515.

Conference Proceedings

(1) Ganter, M.J.; DiLeo, R.A.; Doucett, A.; **Schauerman, C.M.**; Rogers, R.E.; Gaustad, G.; Landi, B.J.; "Electrochemical Performance and Safetey of Lithium Ion Battery Anodes Incorporating Single Wall Carbon Nanotubes" MRS Proceedings Spring, **2012.**

(2) **Schauerman, C.M.**; Ganter, M.J.; Raffaelle, R.P.; Landi, B.J. "End-of-life Strategies for the Reuse and Recycling of Nanomaterials to Reduce Life Cycles Impacts" In the 4S Summer Symposium on Sustainable Systems, Sannäs, Finland, 2010.

(3) Moses, B. T.; Jarosz, P. R.; **Schauerman, C. M.**; Alvarenga, J.; Landi, B.J.; Raffaelle, R. P. Dynamic mechanical analysis of bulk carbon nanotube materials. In *Materials Research Society Symposium Proceedings* 2009, 1204 (Nanotubes and Related Nanostructures), Paper #: 1204-K18-48.

(4) Ganter, M.J.; Seager, T.P.; **Schauerman, C.M.**; Landi, B.J.; Raffaelle, R.P.; "A life-cycle energy analysis of single wall carbon nanotubes produced through laser vaporization," 2009 IEEE International Symposium on Sustainable Systems and Technology (ISSST), 2009.

(5) **Schauerman, C.M.**; Alvarenga, J.; Ganter, M.J.; Seager, T.P.; Landi, B.J.; Raffaelle, R.P.; "Single wall carbon nanotubes for conductive wiring," 2009 IEEE International Symposium on Sustainable Systems and Technology (ISSST), 2009.
(6) Brandhorst, H.W.; **Schauerman, C.M.** ; Ganter, M.J.; Seager, T.; Raffaelle, R.P.; "Reexamination of the feasibility of a world-wide, photovoltaic energy grid." At the 34th IEEE Photovoltaic Specialists Conference, Philadelphia, PA, 2009.
(7) Raffaelle, R.P.; **Schauerman, C.M.**; Cress, C.D.; Landi, B.J.; Forbes, D.; Hubbard, S.; Bailey, S.G.; "Nanomaterials for Space Power." *Proc. 8th European Space Power Conference*, September 14 – 19, 2008, Konstanz, Germany
(8) **Schauerman, C.M.**; Cress, C.D.; Alvarenga, J.; Landi, B.J.; Raffaelle, R.P.; "Single Wall Carbon Nanotube Conductive Ribbons." In *American Institute of Aeronautics and Astronautics: 6th International Energy Conversion Engineering Conference*; Cleveland, OH July 28-30, 2008, AIAA-2008-5653.
(9) Landi, B.J.; Ganter, M.J.; **Schauerman, C.M.**; DiLeo, R.A.; Cress, C.D.; Raffaelle, R.P. "Single Wall Carbon Nanotube – $LiCoO_2$ Lithium Ion Batteries." In *Materials Research Society Symposium Proceedings* 2008, Paper #: 1127-T03-06.
(10) Raffaelle, R.P.; Landi, B.J.; Cress, C.D.; Hubbard, S.M.; DiLeo, R.A.; Bailey, C.; **Schauerman, C.M.**; Giarra, M.; Andersen, J. "Nanomaterials for Space Power," In the *Society for the Advancement of Material and Process Engineering Fall Symposium*: Cincinnati, OH, 2007.Landi**,** B.; Ruf, H.;
(11) **Schauerman, C.M.**; Raffaelle, R.; Harris, J.; Hepp, A. "Injection CVD Grown MWNTs for PEM Fuel Cells." In *American Institute of Aeronautics and Astronautics: 2nd International Energy Conversion Engineering Conference*; Providence, Rhode Island; August, 2004; 5550.

PROFESSIONAL PRESENTATIONS

Oral Presentations

(1) **Schauerman, C.M.**; Staub, J,; Forney, M.W.; Alvarenga, J.; Foringer, R.D.; Landi, B.J.; "Ultrasonic Welding of Bulk Carbon Nanotube Conductors to Metallic Interconnects." In the 142nd Annual *Minerals, Metals, and Materials Society* Meeting, San Antonio, TX, **2013,** *Accepted*.
(2) **Schauerman, C.M.**; Maher, T.P.; Jarosz, P.R.; Rossi, J.E.; Mastrangelo, T.L.; Landi, B.J.; "Physical and Electrical Characterization of Single and Multi Wall Carbon Nanotube Bulk Networks." *In the American Institute of Chemical Engineers Meeting*, Pittsburgh, PA, **2012,** *Accepted*.
(3) **Schauerman, C.M.**; Ganter, M.J.; Gaustad, G.; Babbitt, C.; Raffaelle, R.P.; Landi**,** B.J.**;** "Recycling and Reuse of Single-Wall Carbon Nanotubes from Portable Energy Storage Systems" In the *Materials Research Society Fall Meeting*, Boston, MA, **2011**; GG3.7.
(4) **Schauerman, C.M.**; Ganter, M.J.; Raffaelle, R.P.; Landi, B.J. "End-of-life Strategies for the Reuse and Recycling of Nanomaterials to Reduce Life Cycles Impacts" In the 4S Summer Symposium on Sustainable Systems, Sannäs, Finland, **2010**.
(5) **Schauerman, C.M.**; Cress, C.D.; Alvarenga, J.; Landi, B.J.; Raffaelle, R.P. "Single Wall Carbon Nanotube Conductive Ribbons." In *American Institute of Aeronautics and Astronautics: 6th International Energy Conversion Engineering Conference*; Cleveland, OH July 28-30, **2008**, AIAA-2008-5653.

References

1. Gordon, R. B.; Bertram, M.; Graedel, T. E. In *Metal stocks and sustainability*, Proceedings of the National Academy of Science, Clark, W. C., Ed. 2005; pp 1209-1214.
2. Alvarenga, J.; Jarosz, P. R.; Schauerman, C. M.; Moses, B. T.; Landi, B. J.; Cress, C. D.; Raffaelle, R. P., High conductivity carbon nanotube wires from radial densification and ionic doping. *Applied Physics Letters* 2010, In Press.
3. Jarosz, P.; Schauerman, C.; Alvarenga, J.; Moses, B.; Mastrangelo, T.; Raffaelle, R.; Ridgley, R.; Landi, B., Carbon nanotube wires and cables: Near-term applications and future perspectives. *Nanoscale* 2011, 3, 4542-4553.
4. Behabtu, N.; Young, C. C.; Tsentalovich, D. E.; Kleinerman, O.; Wang, X.; Ma, A. W.; Bengio, E. A.; ter Waarbeek, R. F.; de Jong, J. J.; Hoogerwerf, R. E., Strong, light, multifunctional fibers of carbon nanotubes with ultrahigh conductivity. *Science* 2013, 339, 182-186.
5. Ericson, L. M.; Fan, H.; Peng, H.; Davis, V. A.; Zhou, W.; Sulpizio, J.; Wang, Y.; Booker, R.; Vavro, J.; Guthy, C.; Parra-Vasquez, A. N. G.; Kim, M. J.; Ramesh, S.; Saini, R. K.; Kittrell, C.; Lavin, G.; Schmidt, H.; Adams, W. W.; Billups, W. E.; Pasquali, M.; Hwang, W.-F.; Hauge, R. H.; Fischer, J. E.; Smalley, R. E., Macroscopic, Neat, Single-Walled Carbon Nanotube Fibers. *Science* 2004, 305, 1447-1450.
6. Behabtu, N.; Green, M. J.; Pasquali, M., Carbon nanotube-based neat fibers. *Nano Today* 3, 24-34.
7. Gordon, R. B.; Bertram, M.; Graedel, T. E., Metal stocks and sustainability. *Proceedings of the National Academy of Sciences of the United States of America* 2006, 103, 1209-1214.
8. Iijima, S., Helical microtubules of graphitic carbon. *Nature* 1991, 354, 56-58.
9. Zhang, Z.; Peng, J.; Zhang, H., Low-temperature resistance of individual single-walled carbon nanotubes: a theoretical estimation. *Applied Physics Letters* 2001, 79, 3515-3517.
10. Zhang, M.; Atkinson, K. R.; Baughman, R. H., Multifunctional carbon nanotube yarns by downsizing an ancient technology. *Science* 2004, 306, 1358-1361.
11. Landi, B. J.; Raffaelle, R. P., Effects of Carrier Gas Dynamics on Single Wall Carbon Nanotube Chiral Distributions During Laser Vaporization Synthesis. *Journal of Nanoscience and Nanotechnology* 2007, 7, 1-8.
12. Raffaelle, R. P.; Landi, B. J.; Harris, J. D.; Bailey, S. G.; Hepp, A. F., Carbon Nanotubes For Power Applications. *Material Science and Engineering: B* 2005, 116, 233-243.
13. Landi, B. J.; Cress, C. D.; Evans, C. M.; Raffaelle, R. P., Thermal Oxidation Profiling of Single-Walled Carbon Nanotubes. *Chem. Mater.* 2005, 17, 6819-6834.
14. Landi, B. J.; Ganter, M. J.; Schauerman, C. M.; Cress, C. D.; Raffaelle, R. P., Lithium Ion Capacity of Single Wall Carbon Nanotube Paper Electrodes *Journal of Physical Chemistry C* 2008, 112, 7509-7515.
15. Pico, F.; Rojo, J. M.; Sanjuan, M. L.; Anson, A.; Benito, A. M.; Callejas, M. A.; Maser, W. K.; Martinez, M. T., Single-Walled Carbon Nanotubes as Electrodes in Supercapacitors. *Journal of the Electrochemical Society* 2004, 151, A831-A837.
16. Jarosz, P. R.; Shaukat, A.; Mastrangelo, T.; Schauerman, C. M.; Cress, C. D.; Ridgley, R. D.; Landi, B. J., Coaxial cables with single-wall carbon nanotube outer conductors exhibiting attenuation/length within specification. *Micro & Nano Letters, IET* 2012, 7, 959-961.

17. Jarosz, P. R.; Shaukat, A.; Schauerman, C. M.; Cress, C. D.; Kladitis, P. E.; Ridgley, R. D.; Landi, B. J., High Performance Lightweight Coaxial Cable from Carbon Nanotube Conductors. *ACS Applied Materials & Interfaces* 2012.
18. Köhler, A. R.; Som, C.; Helland, A.; Gottschalk, F., Studying the potential release of carbon nanotubes throughout the application life cycle. *Journal of Cleaner Production* 2008, 16, 927-937.
19. Grieger, K.; Baun, A.; Owen, R., Redefining risk research priorities for nanomaterials. *Journal of Nanoparticle Research* 2010, 12, 383-392.
20. Mueller, N. C.; Nowack, B., Exposure Modeling of Engineered Nanoparticles in the Environment. *Environmental Science & Technology* 2008, 42, 4447-4453.
21. Poland, C. A.; Duffin, R.; Kinloch, I.; Maynard, A.; Wallace, W.; Seaton, A.; Stone, V.; Brown, S.; Macnee, W.; Donaldson, K., Carbon nanotubes introduced into the abdominal cavity ofmice show asbestos-like pathogenicity in a pilot study. *Nature Nanotechnology* 2008, 3, 423-428.
22. Lam, C.-W.; James, J. T.; McCluskey, R.; Hunter, R. L., Pulmonary Toxicity of Single-Wall Carbon Nanotubes in Mice 7 and 90 Days After Intratracheal Instillation. *Toxicological Sciences* 2004, 77, 126-134.
23. Healy, M. L.; Dahlben, L. J.; Isaacs, J. A., Environmental Assessment of Single-Walled Carbon Nanotube Processes. *Journal of Industrial Ecology* 2008, 12, 1-18.
24. Ng, S. H.; Wang, J.; Guo, Z. P.; Chen, J.; Wang, G. X.; Liu, H. K., Single wall carbon nanotube paper as anode for lithium-ion battery. *Electrochim. Acta* 2005, 51, 23-28.
25. Raffaelle, R. P.; Landi, B. J.; Harris, J. D.; Bailey, S. G.; Hepp, A. F., Carbon nanotubes for power applications. *Mater. Sci. Eng. B* 2005, 116, 233-243.
26. Landi, B. J.; Raffaelle, R. P., Effects of carrier gas dynamics on single wall carbon nanotube chiral distributions during laser vaporization synthesis. *J. Nanosci. & Nanotech.* 2007, 7, 883-890.
27. Gorbunov, A.; Jost, O.; Pompe, W.; Graff, A., Role of catalyst particle size in the synthesis of single-wall carbon nanotubes. *Applied Surface Science* 2002, 197-198, 563-567.
28. Lebedkin, S.; Schweiss, P.; Renker, B.; Malik, S.; Hennrich, F.; Neumaier, M.; Stoermer, C.; Kappes, M. M., Single-wall carbon nanotubes with diameters approaching 6 nm obtained by laser vaporization. *Carbon* 2001, 40, 417-423.
29. Rummeli, M. H.; Borowiak-Palen, E.; Gemming, T.; Pichler, T.; Knupfer, M.; Kalbac, M.; Dunsch, L.; Jost, O.; Silva, S. R. P.; Pompe, W.; Buchner, B., Novel Catalysts, Room Temperature and the Importance of Oxygen for the Synthesis of Single-Walled Carbon Nanotubes. *NANO LETTERS* 2005, 5, 1209-1215.
30. Yudasaka, M.; Zhang, M.; Iijima, S., Porous target enhances production of single-wall carbon nanotubes by laser ablation. *Chemical Physics Letters* 2000, 323, 549-553.
31. Zhang, M.; Yudasaka, M.; Iijima, S., Production of Large-Diameter Single-Wall Carbon Nanotubes by Adding Fe to a NiCo Catalyst in Laser Ablation. *Journal of Physical Chemistry B* 2004, 108, 12757-12762.
32. Landi, B. J.; Ruf, H. J.; Worman, J. J.; Raffaelle, R. P., Effects of Alkyl Amide Solvents on the Dispersiono of Single Wall Carbon Nanotubes. *J. Phys. Chem. B* 2004, 108, 17089-17095.

33. Nikolaev, P.; Gorelik, O.; Allada, R. K.; Sosa, E.; Arepalli, S.; Yowell, L., Soft-Bake Purification of Single-Walled Carbon Nanotubes Produced by Pulsed Laser Vaporization. *Journal of Physical Chemistry C* 2007, 111, 17678-17683.
34. Jorio, A.; Dresselhaus, M. S.; Dresselhaus, G., *Carbon Nanotubes: Advanced Topics in the Synthesis, Structure, Properties and Applications*. 1 ed.; Springer: 2008; p 721.
35. Collins, P. G.; Avouris, P., Nanotubes For Electronics. *Scientific American* 2000, 283, 62-69.
36. McEuen, P. L.; Bockrath, M.; Cobden, D. H.; Yoon, Y.-G.; Louie, S. G., Disorder, Pseudospins, and Backscattering in Carbon Nanotubes. *Physical Review Letters* 1999, 83, 5098.
37. Gao, B.; Chen, Y. F.; Fuhrer, M. S.; Glattli, D. C.; Bachtold, A., Four-Point Resistance of Individual Single-Wall Carbon Nanotubes. *Physical Review Letters* 2005, 95, 196802.
38. Zhu, L.; Xu, J.; Xiu, Y.; Sun, Y.; Hess, D. W.; Wong, C. P., Growth and electrical characterization of high-aspect-ratio carbon nanotube arrays. *Carbon* 2006, 44, 253-258.
39. Deck, C. Carbon nanotubes: Synthesis, characterization, and applications. D., UNIVERSITY OF CALIFORNIA, SAN DIEGO, 2009.
40. Ishii, S.; Okutsu, T.; Ueda, S.; Takano, Y., Transport properties of multi-walled carbon nanotubes grown by boron addition method. *Solid State Physics C* 2007, 5, 31-34.
41. Sreekumar, T. V.; Liu, T.; Kumar, S., Single-Wall Carbon Nanotube Films. *Chem Mater.* 2003, 15, 175-178.
42. Zhang, X.; Sreekumar, T. V.; Liu, T.; Kumar, S., Properties and Structure of Nitric Acid Oxidized Single Wall Carbon Nanotube Films. *J. Phys. Chem. B* 2004, 108, 16435-16440.
43. Gaa´l, R.; Salvetat, J. P.; Forro, L., Pressure dependence of the resistivity of single-wall carbon nanotube ropes. *Physical Review B* 2000, 61, 7320-7323.
44. Kim, G. T.; Choi, E. S.; Kim, D. C.; Suh, D. S.; Park, Y. W.; Liu, K.; Duesberg, G.; Roth, S., Magnetoresistance of an entangled single-wall carbon-nanotube network. *Physical Review B* 1998, 58, 16064.
45. Shim, B. S.; Tang, Z.; Morabito, M. P.; Agarwal, A.; Hong, H.; Kotov, N. A., Integration of Conductivity, Transparency, and Mechanical Strength into Highly Homogeneous Layer-by-Layer Composites of Single-Walled Carbon Nanotubes for Optoelectronics *Chem Mater.* 2007, 19, 5467-5474.
46. Liu, G.; Zhao, Y.; Deng, K.; Liu, Z.; Chu, W.; Chen, J.; Yang, Y.; Zheng, K.; Huang, H.; Ma, W.; Song, L.; Yang, H.; Gu, C.; Rao, G.; Wang, C.; Xie, S.; Sun, L., Highly Dense and Perfectly Aligned Single-Walled Carbon Nanotubes Fabricated by Diamond Wire Drawing Dies. *Nano Letters* 2008, 8, 1071-1075.
47. Whitten, P. G.; Gestos, A. A.; Spinks, G. M.; Gilmore, K. J.; Wallace, G. G., Free standing carbon nanotube composite bio-electrodes. *Journal of Biomedical Materials Reserach B* 2007, 82, 37-43.
48. Skákalová, V.; Kaiser, A. B.; Woo, Y. S.; Roth, S., Electronic transport in carbon nanotubes: From individual nanotubes to thin and thick networks. *Physical Review B* 2006, 74.
49. Bekyarova, E.; Itkis, M. E.; Cabrera, N.; Zhao, B.; Yu, A.; Gao, J.; Haddon, R. C., Electronic Properties of Single-Walled Carbon Nanotube Networks. *Journal of the American Chemical Society* 2005, 127, 5990-5995.

50. Petit, P.; Jouguelet, E.; Fischer, J. E.; Rinzler, A. G.; Smalley, R. E., Electron spin resonance and microwave resistivity of single-wall carbon nanotubes. *Physical Review B* 1997, 56, 9275-9278.
51. Wei, B.; Spolenak, R.; Kohler-Redlich, P.; Ruhle, M.; Arzt, E., Electrical transport in pure and boron-doped carbon nanotubes. *Applied Physics Letters* 1999, 74, 3149-3151.
52. Gong, Q.-M.; Li, Z.; Wang, Y.; Wu, B.; Zhang, Z.; Liang, J., The effect of high-temperature annealing on the structure and electrical properties of well-aligned carbon nanotubes *Materials Research Bulletin* 2006, 42, 474-481.
53. Geng, H.-Z.; Kim, K. K.; So, K. P.; Lee, Y. S.; Chang, Y.; Lee, Y. H., Effect of Acid Treatment on Carbon Nanotube-Based Flexible Transparent Conducting Films. *Journal of the American Chemical Society* 2007, 129, 7758-7759.
54. Kaiser, A. B.; Park, Y. W., Current-Voltage Characteristics of Conducting Polmers and Carbon Nanotubes. *Synthetic Metals* 2005, 152, 181-184.
55. Hecht, D.; Hu, L.; Grüner, G., Conductivity scaling with bundle length and diameter in single walled carbon nanotube networks. *Applied Physics Letters* 2006, 89.
56. Skakalova, V.; Kaiser, A. B.; Dettlaff-Weglikowska, U.; Hrncarikova, K.; Roth, S., Effect of Chemical Treatment on Electrical Conductivity, Infrared Absorption, and Raman Spectra of Single-Walled Carbon Nanotubes. *Journal of Physical Chemistry B* 2005, 109, 7174-7181.
57. Pauw, L. J. v. d., A method of measuring specific resistivity and hall effect of discs of arbitrary shape. *Philips Research Reports* 1958, 13, 1-9.
58. Yoon, S.-M.; Kim, U. J.; Benayad, A.; Lee, I. H.; Son, H.; Shin, H.-J.; Choi, W. M.; Lee, Y. H.; Jin, Y. W.; Lee, E.-H.; Lee, S. Y.; Choi, J.-Y.; Kim, J. M., Thermal Conversion of Electronic and Electrical Properties of AuCl3-Doped Single-Walled Carbon Nanotubes. *ACS Nano* 2011, 5, 1353-1359.
59. Yang, S. B.; Kong, B.-S.; Kim, D.-W.; Baek, Y.-K.; Jung, H.-T., Effect of Au Doping and Defects on the Conductivity of Single-Walled Carbon Nanotube Transparent Conducting Network Films. *The Journal of Physical Chemistry C* 2010, 114, 9296-9300.
60. Kim, K. K.; Yoon, S. M.; Park, H. K.; Shin, H. J.; Kim, S. M.; Bae, J. J.; Cui, Y.; Kim, J. M.; Choi, J. Y.; Lee, Y. H., Doping strategy of carbon nanotubes with redox chemistry. *New Journal of Chemistry* 2010.
61. Duong, D. L.; Lee, I. H.; Kim, K. K.; Kong, J.; Lee, S. M.; Lee, Y. H., Carbon Nanotube Doping Mechanism in a Salt Solution and Hygroscopic Effect: Density Functional Theory. *ACS Nano* 2010, null-null.
62. Choi, H. C.; Shim, M.; Bangsaruntip, S.; Dai, H., Spontaneous Reduction of Metal Ions on the Sidewalls of Carbon Nanotubes. *Journal of the American Chemical Society* 2002, 124, 9058-9059.
63. Duclaux, L., Review of the doping of carbon nanotubes (multiwalled and single-walled). *Carbon* 2002, 40, 1751-1764.
64. Uma Sathyakam, P.; Mallick, P. S., Towards realization of mixed carbon nanotube bundles as VLSI interconnects: A review. *Nano Communication Networks*.
65. Tanachutiwat, S.; Wang, W., Modeling Resistance of Mixed Carbon Nanotube Bundles. *Journal of Nanoscience and Nanotechnology* 2009, 9, 857-861.

66. Shang, L.; Ming, L.; Tanachutiwat, S.; Wei, W. In *Analyzing mixed carbon nanotube bundles: A current density study*, Circuits and Systems, 2008. ISCAS 2008. IEEE International Symposium on, 18-21 May 2008; 2008; pp 173-176.
67. Haruehanroengra, S.; Wei, W., Analyzing Conductance of Mixed Carbon-Nanotube Bundles for Interconnect Applications. *Electron Device Letters, IEEE* 2007, 28, 756-759.
68. Jin Gyu, P.; Shu, L.; Richard, L.; Xinyu, F.; Chuck, Z.; Ben, W., The high current-carrying capacity of various carbon nanotube-based buckypapers. *Nanotechnology* 2008, 19, 185710.
69. Landi, B. J.; Ruf, H. J.; Evans, C. M.; Cress, C. D.; Raffaelle, R. P., Purity Assessment of Single-Wall Carbon Nanotubes, Using Optical Absorption Spectroscopy. *Journal of Physical Chemistry B* 2005, 109, 9952-9965.
70. Schauerman, C. M.; Alvarenga, J.; Landi, B. J.; Cress, C. D.; Raffaelle, R. P., Impact of Nanometal Catalyst On The Laser Vaporization Synthesis of Single Wall Carbon Nanotubes. *Carbon* 2009, 47, 2431-2435.
71. DiLeo, R. A.; Landi, B. J.; Raffaelle, R. P., Purity Assessment of Multiwalled Carbon Nanotubes by Raman Spectroscopy. *Journal of Applied Physics* 2007, 101, 064307.
72. Zhao, Y.; Wei, J.; Vajtai, R.; Ajayan, P. M.; Barrera, E. V., Iodine doped carbon nanotube cables exceeding specific electrical conductivity of metals. *Sci. Rep.* 2011, 1.
73. Zhou, W.; Xie, S.; Sun, L.; Tang, D.; Li, Y.; Liu, Z.; Ci, L.; Zou, X.; Wang, G.; Tan, P.; Dong, X.; Xu, B.; Zhao, B., Raman scattering and thermogravimetric analysis of iodine-doped multiwall carbon nanotubes. *Applied Physics Letters* 2002, 80, 2553-2555.
74. Michel, T.; Alvarez, L.; Sauvajol, J. L.; Almairac, R.; Aznar, R.; Mathon, O.; Bantignies, J. L.; Flahaut, E., Structural selective charge transfer in iodine-doped carbon nanotubes. *Journal of Physics and Chemistry of Solids* 2006, 67, 1190-1192.
75. Takenobu, T.; Takano, T.; Shiraishi, M.; Murakami, Y.; Ata, M.; Kataura, H.; Achiba, Y.; Iwasa, Y., Stable and controlled amphoteric doping by encapsulation of organic molecules inside carbon nanotubes. *Nat Mater* 2003, 2, 683-688.
76. Davis, V. A.; Parra-Vasquez, A. N. G.; Green, M. J.; Rai, P. K.; Behabtu, N.; Prieto, V.; Booker, R. D.; Schmidt, J.; Kesselman, E.; Zhou, W.; Fan, H.; Adams, W. W.; Hauge, R. H.; Fischer, J. E.; Cohen, Y.; Talmon, Y.; Smalley, R. E.; Pasquali, M., True solutions of single-walled carbon nanotubes for assembly into macroscopic materials. *Nat Nano* 2009, 4, 830-834.
77. Duque, J. G.; Parra-Vasquez, A. N. G.; Behabtu, N.; Green, M. J.; Higginbotham, A. L.; Price, B. K.; Leonard, A. D.; Schmidt, H. K.; Lounis, B.; Tour, J. M.; Doorn, S. K.; Cognet, L.; Pasquali, M., Diameter-Dependent Solubility of Single-Walled Carbon Nanotubes. *ACS Nano* 2010, 4, 3063-3072.
78. Kharisov, B. I.; Kharissova, O. V.; Leija Gutierrez, H.; Ortiz Méndez, U., Recent Advances on the Soluble Carbon Nanotubes. *Industrial & Engineering Chemistry Research* 2008, 48, 572-590.
79. Ramesh, S.; Ericson, L. M.; Davis, V. A.; Saini, R. K.; Kittrell, C.; Pasquali, M.; Billups, W. E.; Adams, W. W.; Hauge, R. H.; Smalley, R. E., Dissolution of Pristine Single Walled Carbon Nanotubes in Superacids by Direct Protonation. *The Journal of Physical Chemistry B* 2004, 108, 8794-8798.
80. Chen, C.; Yan, L.; Kong, E. S.-W.; Zhang, Y., Ultrasonic Nanowelding of Carbon Nanotubes to Metal Electrodes. *Nanotechnology* 2006, 17, 2192-2197.

81. Zhao, B.; Chen, C.; Yadian, B.; Liu, P.; Li, Z.; Xu, D.; Zhang, Y., Effects of welding head on the carbon nanotube field emission in ultrasonic nanowelding. *Thin Solid Films* 2009, 517, 2012-2015.
82. Jackson, R.; Graham, S., Specific contact resistance at metal/carbon nanotube interfaces. *Applied Physics Letters* 2009, 94, 012109-3.
83. Landi, B. J.; Ganter, M. J.; Cress, C. D.; DiLeo, R. A.; Raffaelle, R. P., Carbon nanotubes for lithium ion batteries. *Energy & Environmental Science* 2009, 2, 638-654.
84. Zhao, J.; Buldum, A.; Han, J.; Ping Lu, J., First-Principles Study of Li-Intercalated Carbon Nanotube Ropes. *Physical Review Letters* 2000, 85, 1706.
85. Meunier, V.; Kephart, J.; Roland, C.; Bernholc, J., Ab Initio Investigations of Lithium Diffusion in Carbon Nanotube Systems. *Physical Review Letters* 2002, 88, 075506.
86. DiLeo, R. A.; Castiglia, A.; Ganter, M. J.; Rogers, R. E.; Cress, C. D.; Raffaelle, R. P.; Landi, B. J., Enhanced Capacity and Rate Capability of Carbon Nanotube Based Anodes with Titanium Contacts for Lithium Ion Batteries. *ACS Nano* 2010, 4, 6121-6131.
87. Dahn, J. R., Phase diagram of LixC6. *Physical Review B* 1991, 44, 9170.
88. Satoh, A.; Takami, N.; Ohsaki, T., Electrochemical intercalation of lithium into graphitized carbons. *Solid State Ionics* 1995, 80, 291-298.
89. Ganter, M. J.; DiLeo, R. A.; Schauerman, C. M.; Rogers, R. E.; Raffaelle, R. P.; Landi, B. J., Differential scanning calorimetry analysis of an enhanced LiNi0.8Co0.2O2 cathode with single wall carbon nanotube conductive additives. *Electrochimica Acta* 2011, 56, 7272-7277.
90. Lee, J.; Bae, J.; Heo, J.; Han, I. T.; Cha, S. N.; Kim, D. K.; Yang, M.; Han, H. S.; Jeon, W. S.; Chung, J., Effect of Randomly Networked Carbon Nanotubes in Silicon-Based Anodes for Lithium-Ion Batteries. *Journal of The Electrochemical Society* 2009, 156, A905-A910.
91. Cui, L.-F.; Hu, L.; Choi, J. W.; Cui, Y., Light-Weight Free-Standing Carbon Nanotube-Silicon Films for Anodes of Lithium Ion Batteries. *ACS Nano* 2010, 4, 3671-3678.
92. DiLeo, R. A.; Ganter, M. J.; Landi, B. J.; Raffaelle, R. P., Germanium-Single-Wall Carbon Nanotube Anodes for Lithium Ion Batteries. *Journal of Materials Research* 2010, 25, 1441-1446.
93. Inagakl, M.; Konno, H.; Toyoda, M.; Moriya, K.; Kihara, T., Sorption and recovery of heavy oils by using exfoliated graphite Part II: Recovery of heavy oil and recycling of exfoliated graphite *Desalination* 2000, 128, 213-218.
94. Schinner, G.; Brandt, J.; Richter, H., Recycling Carbon-Fiber-Reinforced Thermoplastic Composites. *Journal of Thermoplastic Composite Materials* 1996, 9, 239-245.
95. Fukui, R.; Odai, T.; Zushi, H.; Osawa, I.; Uzawa, K.; Takahashi, J. In *Recycle of Carbon Fiber Reinfoced Plastics for Automotive Application*, The Ninth Japan International SAMPE symposium Japan, Japan, 2005.
96. McNally, T.; Boyd, P.; McClory, C.; Bien, D.; Moore, I.; Millar, B.; Davidson, J.; Carroll, T., Recycled Carbon Fiber Filled Polyethylene Composites. *Journal of Applied Polymer Science* 2008, 107, 2015–2021.
97. Healy, M. L.; Dahlben, L. J.; Isaacs, J. A. In *Economic and Environmental Tradeoffs in SWNT Production*, NSTI Nanotechnology Conference and Trade Show, Nano Science and Technology Institute: 2006.
98. Ganter, M. J.; Seager, T. P.; Schauerman, C. M.; Landi, B. J.; Raffaelle, R. P. In *A Life-Cycle Energy Analysis of Single Wall Carbon Nanotubes Produced Through Laser Vaporization*, IEEE -

International Symposium on Sustainable Science and Technology, Phoenix, AZ, Phoenix, AZ, 2009; pp 1-4.
99. Anctil, A.; Babbitt, C. W.; Raffaelle, R. P.; Landi, B. J., Material and Energy Intensity of Fullerene Production. *Environmental Science & Technology* 2011, 45, 2353-2359.
100. Landi, B. J.; Cress, C. D.; Evans, C. M.; Raffaelle, R. P., Thermal Oxidation Profiling of Single-Walled Carbon Nanotubes. *Chemistry of Materials* 2005, 17, 6819-6834.
101. Landi, B. J.; Ruf, H. J.; Evans, C. M.; Cress, C. D.; Raffaelle, R. P., Purity Assessment of Single-Wall Carbon Nanotubes, Using Optical Absorption Spectroscopy. *The Journal of Physical Chemistry B* 2005, 109, 9952-9965.
102. Yoshio, M.; Brodd, R. J., *Lithium-Ion Batteries*. First ed.; Springer: New York, NY, 2009; p 452.
103. Buiel, E.; Dahn, J. R., Li-Insertion in Hard Carbon Anode Materials for Li-Ion Batteries. *Electrochimica Acta* 1999, 45, 121-130.
104. Balakrishnan, P. G.; Ramesh, R.; Kumar, T. T., Safety Mechanisms in Lithium-Ion Batteries. *Journal of Power Sources* 2006, 155, 401-414.
105. Nazri, G.-A.; Pistoia, G., *Lithium Batteries*. First ed.; Springer: New York, NY, 2009; p 708.
106. Landi, B. J.; Ganter, M. J.; Schauerman, C. M.; Cress, C. D.; Raffaelle, R. P., Lithium Ion Capacity of Single Wall Carbon Nanotube Paper Electrodes. *Journal of Physical Chemistry C* 2008, 112, 7509-7515.
107. Rao, A. M.; Bandow, S.; Richter, E.; Eklund, P. C., Raman spectroscopy of pristine and doped single wall carbon nanotubes. *Thin Solid Films* 1998, 331, 141-147.
108. Bahr, J. L.; Yang, J.; Kosynkin, D. V.; Bronikowski, M. J.; Smalley, R. E.; Tour, J. M., Functionalization of Carbon Nanotubes by Electrochemical Reduction of Aryl Diazonium Salts: A Bucky Paper Electrode. *Journal of the American Chemical Society* 2001, 123, 6536-6542.
109. Gilmore, K. J.; Moulton, S. E.; Wallace, G. G., Incorporation of carbon nanotubes into the biomedical polymer poly(styrene-[beta]-isobutylene-[beta]-styrene). *Carbon* 2007, 45, 402-410.